Design, synthesis and analysis of multicomponent crystals of furosemide

By

Yamkela Nomnganga

214097188

Thesis submitted in fulfilment of the requirements for the degree

Master of Applied Science: Chemistry

in the Faculty of Applied Sciences

at the Cape Peninsula University of Technology

Supervisor: Associate Professor Nikoletta B. Báthori (CPUT)

Co-supervisor: Dr. David O. Oluwole (CPUT)

Bellville Campus

December 2021

The financial assistance of the National Research Foundation and CPUT towards this research is acknowledged. Opinions expressed in this thesis and the conclusions arrived at, are those of the author.

Declaration

I, YAMKELA NOMNGANGA, declare that the content of this dissertation represents my own unaided work, and that the dissertation has not previously been submitted for academic examination towards any qualification. Furthermore, it represents my own opinions and not necessarily those of Cape Peninsula University of Technology.

Signature Y.Nomnganga Date 07 February 2022

Abstract

Furosemide (4-chloro-2-[(2-furanylmethyl)-amino]-5-sulfamoylbenzoic acid, FUR) was used to form multicomponent crystals with pyridine and its derivatives. Five multicomponent crystals of FUR were formed with pyridine (FUR·PYRw), 3-methyl pyridine or 3-picoline (FUR·3PIC), 4-methyl pyridine or 4-picoline (FUR·4PIC), 2,3-dimethyl pyridine or 2,3-lutidine (FUR·23LUT), and 2,4-dimethyl pyridine or 2,4-lutidine (FUR·24LUTw) via slow evaporation crystallisation method. The crystals were analysed by single-crystal X-ray diffraction, and the drug:coformer ratios were found to be 1:1 in all five multicomponent crystals. Thermogravimetry was used to verify the solvent content of the crystals, and the results of the infrared analysis supported the protonation state of the components observed in the single-crystal structures. Differential scanning calorimetry was used to follow the behaviour of the crystals under a temperature program. Powder X-ray analysis of the bulk showed that the single crystal of FUR·3PIC and FUR·PYRw are good representations of the bulk material, while for the structures FUR·4PIC, FUR·23LUT and FUR·24LUTw, the bulk is different, and this is very likely the result of the rapid desolvation of the material.

The five multicomponent crystals were desolvated at ambient temperature and pressure to produce polymorphs of FUR in their pure forms. The crystals of FUR·3PIC showed excellent stability over at least six months under ambient conditions, and no disintegration of the crystals were observed. The desolvation of FUR·4PIC resulted in the physical mixture of forms I and III, while desolvation of crystals of FUR·23LUT, FUR·24LUTw, and FUR·PYRw resulted in three new solid forms. The complete identification of these new forms is a challenging task and will form the basis of another project.

Acknowledgement

I would like to express my appreciation to the following people :

- Associate Professor Nikoletta B. Báthori (my supervisor) for kindly nurturing this dissertation from conception to completion and teaching me humanity and kindness.
- My co-supervisor, Dr David O. Oluwole for his patience and commitment in assisting me.
- Pat Whelan, Kevin Whelan, Gina Hilzinger, Martin Hilzinger, Hans Kuhn, and Christina Kuhn for being supportive in all forms during my studies.
- To my family, my friends from the Rotaract Club of Hout Bay and Thatha iThuba Organization and everyone else who walked this journey with me, I appreciate your support.

Dedication

This is for my grandparents who always believed in me and gave me confidence to believe in myself. I still feel you and your connection. Lalani ngokuthula!

Nofezile Ndlovukazi Nomnganga & Mncedisi Nomnganga

Table of Contents

List of Figures

Appendix figures

List of Tables

List of Symbols and Acronyms

Å	Angstrom
a, *b*, *c*	unit cell axes (Å)
α	designates angle between unit cell *b* and *c* axes (°)
β	designates angle between unit cell *a* and *c* axes (°)
γ	designates angle between unit cell *a* and *b* axes (°)
τ	torsion angle (°)
ε	Dielectric constant
Δ	change in
ΔH	change in enthalpy
3PIC	3-picoline or 3-methylpyridine
4PIC	4-picoline or 4-methylpyridine
23LUT	2,3-lutidine or 2,3-dimethylpyridine
24LUT	2,4-lutidine or 2,4-dimethylpyridine
API	Active Pharmaceutical Ingredient
ASU	Asymmetric unit
BCS	Biopharmaceutical Classification System
CSD	Cambridge Structural Database
DSC	Differential Scanning Calorimetry
FTIR	Fourier Transform Infrared
FUR	Furosemide or 4-chloro-N-furfuryl-5-sulfamoylanthranilic acid or 5-(aminosulfonyl)-4-chloro-2-([2-furanylmethyl]amino)benzoic acid
GRAS	Generally Regarded As Safe
HBA	Hydrogen bond acceptor
HBD	Hydrogen bond donor
LAG	Liquid assisted grinding
LUT	Lutidine
MCC	Multicomponent crystals

PIC	Picoline
pKa	Acid dissociation constant
PYR	Pyridine
PXRD	Powder X-ray diffraction
SEC	Slow evaporation crystallisation
SCXRD	Single crystal X-ray diffraction
T_{onset}	Onset temperature (°C)
T_{peak}	Peak temperature (°C)
TGA	Thermogravimetric analysis
V	Unit cell volume ($Å^3$)
US FDA	United States Food and Drug Administration
WHO	World Health Organization
Z	Number of formula units per unit cell

Glossary/Key Terms

Active Pharmaceutical Ingredients	any substance(s) intended to be used in the manufacture of a drug product
Coformer	the compound that will interact with the active pharmaceutical ingredient to form a multicomponent crystal during crystallisation.
Crystal Engineering	is a technique that can be used to modify the physical properties of an existing drug in order to enhance properties such as solubility, bioavailability, and tabletability.
Polymorphs	the ability of a compound to crystallise in more than one crystal structure
Supramolecular Chemistry	the study of complex assemblies and molecular recognition via non-covalent bonding.
Supramolecular synthons	units that illustrate the fundamental properties of the crystal structure, more precisely how the units are assembled in response to the intermolecular interactions that occur.
Solubility	at a given temperature and pressure, the ability of a solid material to dissolve in a liquid.
Hydrate	the result of a crystal structure product containing water
Onset temperature	the temperature at which a solid substance begins to melt

Atom colour code

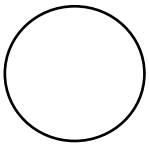

Hydrogen

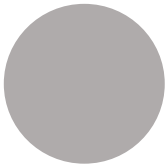

Carbon

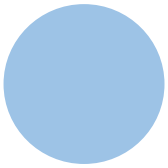

Nitrogen

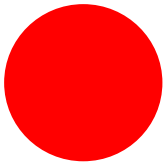

Oxygen

Sulfur

Chlorine

Chapter 1

Introduction

1.1 Background of the study

Poorly soluble drugs in pharmaceutical industry are great concern, causing some companies to evaluate their current drug target research and development strategies. Drug discovery and development is a time consuming and arduous process, taking over 12 years from target identification to regulatory approval with subsequent commercialisation and distribution (Pantziarka *et al*., 2007). Sadly, not all new chemical entities that passed through the different rigorous phases of clinical trials receive regulatory approval. This failure is often attributed to the undesired physical and chemical properties of the drugs and rarely the toxicology properties. It has been demonstrated that the development of a new molecular entity (small molecule compound) is capital intensive with an estimated cost of over 2.6 billion US dollars and an average of 1 billion US dollars (Mohs & Greig, 2017).

Due to the aforementioned challenges, pharmaceutical companies are sometimes reluctant to promote the traditional research and development of new chemical entities (Niazi, 2006). To minimise the exorbitant cost and long period for the development of new molecular entities, scientists have introduced alternative methods to modify the existing active pharmaceutical ingredients (APIs) and screen existing drugs for repurposing. Fast and affordable drug development is the vision of the pharma industry, however, current applied strategies are far from being rapid. It has been reported that usually, only one in ten drug molecules that make the clinical trials gets approved by the US FDA (United States Food and Drug Administration), and the rest of the new chemical entities are usually rejected due to unsatisfactory physicochemical properties (Pantziarka *et al*., 2007). It is estimated that in a year, only about 40 – 50 new drug molecules are approved by the US FDA. In 2020, the US FDA approved 53 new drug candidates (U.S. Food and Drug Administration, 2020).

The route of administration for a drug plays a vital role in eliciting a therapeutic response at the target sites of action, including enteral (orally), parenteral (injection), and topical (transdermal) administration (Niazi, 2006). For instance, most orally administered drugs are usually in solid dosage forms, including tablets and capsules; these orally administered drugs have to pass

through the gastrointestinal tract prior to reaching the bloodstream, where they can be transported to the receptors. For any drug to be absorbed in the site of its action, it needs to be present in the form of a solution, otherwise its bioavailability will be compromised (Savjani *et al*., 2012).

Using an oral route of administration, the chances of the drug not reaching its target sites are high when the drug is susceptible to solubility issues. However, in some cases, the solubility of the drug determines the route of administration. Nevertheless, most pharmaceutical companies prefer solid dosage forms because of safety, stability, cost and marketing considerations (Pantziarka *et al*., 2007). Regrettably, many oral drugs are associated with issues of poor solubility, hence bioavailability. Poor bioavailability is impacted by several factors that include drug permeability, dissolution rate, first-pass metabolism. Bioavailability is dependent on solubility and permeability with drug molecules that exhibit sparing solubility, and low permeability, sometimes accounts for poor bioavailability (Amidon *et al*., 1995).

Pharmaceutical drugs with low to sparing solubility often require high doses in order to obtain therapeutic plasma concentrations after oral administration. A drug with a high solubility has the highest dose strength soluble in 250 ml or less of aqueous media over the pH range of 1 to 7.5. The volume of 250 ml is derived from the common prescription of orally administered drugs to be taken with a glass of water (Amidon *et al*., 1995).

Drug design and synthesis of new crystalline solid-state pharmaceutical forms is a method of choice used towards improving the physicochemical properties of organic functional molecules with unsatisfactory chemical properties (Mazur *et al*., 2019). The crystalline form of a given compound plays an indispensable role in the properties of the material, such as melting point, mechanochemical behaviour, aqueous solubility, and dissolution rate (Aakeröy *et al*., 2012).

Crystal forms of drug molecules can exist as single-component or multicomponent crystals. Both crystal forms can be of great advantage in modifying drug candidates. Single-component crystals afford the opportunity to modulate the physicochemical properties of a compound but are limited to polymorph formation, which tends to show only small variance in physicochemical properties (Duggirala *et al*., 2016).

However, multicomponent crystals can be stoichiometric or non-stoichiometric and can exist as hydrates, solvates, salts, and cocrystals. In contrast to single-components, the development of multicomponent crystalline (MCC) drug substances presents additional challenges. For instance, physical stability can be an issue for solvates and hydrate compounds. For the longest time, salt formation has been a well-established method to improve physicochemical properties of novel solid forms; however, this approach is only applicable to APIs that contain ionisable moieties (Duggirala *et al*., 2016). Unlike cocrystal formation, which is applicable to most APIs, including those with ionisable and non–ionisable functionalities.

Over the years, modern approaches have been introduced and utilised by researchers to modify several solid-state pharmaceuticals. Amongst these, polymorph formation, solvation/hydration or amorphisation have been employed, and more recently, cocrystals were also considered; however, challenges can arise with some of these approaches (Babu & Nangia, 2011).

Cocrystallisation has proven to be a reliable and dependable modality for improving drugs with poor solubility (Kumar *et al*., 2018). In a study conducted by Shariare and co-workers, the *in vitro* dissolution and bioavailability of a furosemide nano-suspension was investigated. According to their findings, there was a significant increase in the solubility and bioavailability of furosemide; however, this method uses organic solvents, which are environmentally harmful and expensive, making it economically nonviable. Thus ultimately, an alternate route in pharmaceutical modification is to produce MCCs using methods that work efficiently and use a minimal amount of eco-friendly organic solvents (Shariare *et al*., 2019).

The Biopharmaceutics Classification System (BCS) categorises pharmaceutical compounds into four classes based on their aqueous solubility across the gastrointestinal pH range and permeability across the gastrointestinal mucosa (Niazi, 2006). The classes are as follows:

- BCS Class I- high solubility/high permeability.
- BCS Class II- low solubility/high permeability.
- BCS Class III- high solubility/low permeability; and
- BCS Class IV-low solubility/low permeability.

This classification takes into account the dose of the drug as well as its solubility. A drug with a greater absorption than 90% in humans is considered to be highly permeable. BCS class IV drugs

have low solubility and permeability; leading to poor absorption and oral bioavailability, and most diuretics, including furosemide, belong to this class.

The drugs and coformers that have been used for multicomponent crystal formation are mostly those that can form sustainable hydrogen bonds by accepting the proton from or donating the proton to the other molecule (Shariare *et al*., 2019). Hydrogen-bond propensity rules were introduced by Etter in her study on hydrogen-bonding patterns , and these rules are still relevant to the present studies (Etter, 1991). However, Etter mentioned that the first rule was developed by Donohue, who stated that all acidic hydrogens available in a molecule would be used for hydrogen bonding in the crystal structure of that compound.

Consequently, Etter developed a second rule complementary to the first: all good hydrogen-bond acceptors (HBA) will be used in hydrogen-bonding when there are available hydrogen-bond donors (HBD). The third rule, which is commonly applied in cocrystal design, states that the best hydrogen bond donor and the best hydrogen bond acceptor will preferably form hydrogen bonds with each other (Etter, 1991).

The other frequently observed feature in solid-state cocrystallisation is that MCCs are most likely to form between two components that have stronger hydrogen bonds to one another than to themselves. Strong hydrogen-bonds are N–H···O, O–H···O, N–H···N, and O–H···N, on the other hand, weak hydrogen bonds include like C–H···O–N or C–H···O=C, where a dash represents covalent bonds, and dots define intermolecular interactions. The co-existence of typical hydrogen bond donors, for instance, carboxylic acids, and receptors, e.g., amine or amide, are important factors for cocrystal formation.

1.2 Physicochemical properties of drugs

1.2.1. Solubility

Solubility, the phenomenon of the dissolution of a solute in a solvent to give a homogenous system, is one of the critical physicochemical properties sought after in drug development (Savjani *et al*., 2012). A desired concentration of the drug in the systemic circulation is important for the measurement of the efficacy of the drug. Ideally, for any drug to have a desired efficacy after absorption, it must be present in the form of solution at the site of absorption (Savjani *et al*., 2012).

In general chemistry, solubility is defined as the property of matter, called the solute, in solid, liquid, or gaseous state that is dissolved in a solid, liquid, or gaseous solvent to form a homogenous solution (Sharma *et al*., 2009). The solubility of the solute mainly depends on the solvent used, as well as the temperature and pressure under which the dissolution is carried out (Savjani *et al*., 2012).

Various models to determine or study the solubility of solid forms are available. Flory-Huggins solution theory describes the solubility of polymers. Hansen and Hildebrand solubility parameters are empirical methods for the prediction of solubility (Savjani *et al*., 2012). Moreover, solubility can also be predicted from other physical constants, such as the melting point (Savjani *et al*., 2012).

Intrinsic dissolution measures the rate of dissolution of a pure drug substance from a constant surface area, which is independent of formulation effects and measures the intrinsic properties of the drug as a function of dissolution media, e.g. pH, ionic strength and counter-ions (Qiao *et al*., 2011).

1.2.2. Permeability

Permeability is measured by the determination of partition coefficient (Log P); a measure of differential solubility of a compound in a hydrophobic solvent (*n*-octanol) and a hydrophilic solvent (water). In this approach, the logarithm values obtained from both the hydrophobic and hydrophilic experiments are then used to rank compounds in terms of hydrophobicity (Savjani *et*

al., 2012). Permeability across the biological membrane is important for the absorption and distribution of pharmaceutical drugs to sustain a good pharmacokinetic profile, including absorption, distribution, metabolism and excretion. The *n*-octanol/water partition coefficient is the attribute of permeability. The drug candidates with low solubility and low permeability are classified as BCS class IV drugs in which furosemide is one of the drug candidates. The improvement in the permeation of drugs by structural modification through crystal engineering is an alternative method to enhance the desired biopharmaceutical properties through the formation of cocrystals without changing the drug's structure (Bolla & Nangia, 2016). However, compared to solubility improvement, very few drug cocrystals, with the aim of improving their permeability, have been published (Bolla & Nangia, 2016). One of them is that of Desiraju and co-workers who demonstrated the use of cocrystallisations to enhance the permeability of BCS class IV drug, hydrochlorothiazide (HCT) (Sanphui *et al*., 2015). Cocrystals of HCT with nicotinic acid, nicotinamide, 4-aminobenzoic acid, succinimide, and resorcinol were prepared and analysed for solubility and permeability improvement. The results showed that the solubility of the HCT:nicotinic acid cocrystal is higher, and an improved permeability was also noted. The same trend was observed for all cocrystals except for HCT:succinic acid. It was then concluded that cocrystallisations could potentially enhance the permeability of HCT (Sanphui *et al*., 2015).

1.2.3. Bioavailability

In pharmacology, bioavailability is the rate and extent to which a pure drug reaches the circulatory system (Shargel, L., Yu, A.B., 1999). Overcoming the low oral bioavailability of APIs is a major challenge during the development of new chemical entities (NCE).

The bioavailability of a drug is extremely important in drug discovery as it influences the potency of the drug. Poor bioavailability is another major challenge of oral drugs influenced by several factors, including drug solubility and permeability, dissolution rate, first-pass metabolism, presystemic metabolism, and susceptibility to efflux mechanisms (Savjani *et al*., 2012). As mentioned earlier, most drug substances exist as solids, and therefore need to sufficiently dissolve in the body fluids before they can be absorbed.

1.2.4. Melting Point

The melting point of a substance is defined as the temperature at which the solid phase is in equilibrium with the liquid phase. This is a thermodynamic process in which the free energy is zero. Generally, a very high melting point for pharmaceutical drugs is undesirable; and it may contribute to low solubility and possibly hinder some moulding processes (Karagianni *et al*., 2018). Similarly, low melting points can hinder processing, drying and stability of a substance.

Melting point is one of the physical properties of solids used to determine the product's purity (Kumar & Nanda, 2017). The 'ideal' melting point of a solid demonstrates the thermodynamic stability of the new material. Subsequently, the thermal stability of an API can be modulated by selecting a coformer with a higher or lower melting point. Thermal analysis, such as differential scanning calorimetry (DSC) and thermal gravimetric analysis (TGA), is the most commonly used technique to determine the melting point of new cocrystal materials.

1.3 Supramolecular Chemistry

The philosophical root of supramolecular chemistry was first described by Fischer by his suggestion to interpret the enzyme–substrate interaction with the "lock and key model". Later on, this idea became the basic principle of molecular recognition and host–guest chemistry (Fischer, 1894). However, the application of this concept to synthetic systems was first achieved by Charles J Pedersen when he synthesised crown-ethers in 1960. Furthermore, Donald J Cram and Jean-Marie Lehn employed the same principle. As a result, the three of them were honoured for their work in supramolecular chemistry with a Nobel Prize in 1987 (Https://www.nobelprize.org/prizes/chemistry/1987/speedread/>, 1987). The chemical systems studied are broadly classified into two major categories: molecular recognition in solution is generally referred to as supramolecular chemistry, and organised self-assembly in the solid-state as crystal engineering. Both these streams have seen significant growth since their inception (Nangia, 2010).

Jean-Marie Lehn defined supramolecular chemistry as 'chemistry beyond the molecule', i.e., the chemistry of molecular compounds assembled via non-covalent interactions (Lehn, 1987). This

branch of chemistry has become popular and attracted many researchers in the field of science, encompassing ideas of physical and biological processes (Nangia, 2010). Supramolecular chemistry serves as an important area of chemistry that highlights the chemistry of molecular assemblies and that of intermolecular bonds (Daas *et al*., 2014). It focuses on investigating and understanding the compounds which contain more than one molecular assembly. It also aims to study the structure, function, and properties of these assemblies.

The understanding of molecular assemblies has enabled the design of new crystal structures via supramolecular synthon formation (Desiraju, 2005). In 1967, Corey was credited for introducing the concept of synthon in synthetic chemistry, and he described it as structural units in a molecule that are formed or assembled by established or conceptualised synthetic protocols (Corey, 1967). On the other hand, Desiraju introduced the concept of supramolecular synthon, which plays a pivotal role in crystal engineering. According to Desiraju, supramolecular synthons are structural units in supermolecules that are formed by known or conceived synthetic protocols through intermolecular interactions, including hydrogen bonding (Desiraju 2005).

Supermolecules are formed as a result of supramolecular synthons—repeating structural units in crystal structures that can be formed by known or conceivable synthetic operations (Desiraju, 1995). The ability to design and synthesise the desired supermolecule lies in the understanding and application of molecular recognition. As stated earlier, this is the basis of supramolecular synthesis and crystal engineering. Both phenomena employ non-covalent interactions to form robust new materials from molecules or ions, but not atoms (Aakeröy *et al*., 2002).

Supramolecular synthons help researchers produce tailored multicomponent crystals. Supramolecular synthons can be classified into two groups, homosynthons and heterosynthons (Fleischman *et al*., 2003). Supramolecular homosynthons are composed of identical complementary functional groups, usually referred to as dimers; examples of this are carboxylic acid dimers and amide dimers, Figure 1.1. In contrast, supramolecular heterosynthons consist of different but complementary functional groups, including carboxylic acid-aromatic nitrogen, carboxylic acid-amide, hydroxyl-aromatic nitrogen, etc., Figure 1.1 (Shattock *et al*., 2008). Supramolecular heterosynthons are of particular interest and most studied in cocrystal design

because the functional groups in different entities can stimulate the formation of a cocrystal (Kane *et al.*, 1995; Shan *et al*., 2002; Aakeröy *et al*., 2001; Reddy *et al*., 2006).

In order to enhance the possibility of forming multicomponent crystals or supramolecular synthons, analysing existing structural data detailed with laboratory experiments can serve as a proactive and smart approach (Bhattacharya *et al*., 2018b, Aakeröy & Sinha, 2018). This can be achieved using the Cambridge Structural Database (CSD), containing over one million crystal structures of organic and inorganic compounds (Groom *et al*., 2016). The CSD is a viable tool in achieving the statistics of existing supramolecular synthons and also aid the search for new supramolecular synthons. The higher the probability of the synthon in the CSD, the greater is its likelihood and predictability to occur in crystal structures.

The amide-pyridine-N-oxide heterosynthon has been identified to exhibit a higher occurrence probability of 80%. In contrast, the amide-pyridine synthon has <5% probability and low predictability in cocrystal synthesis, (Nangia, 2010). Allen *et.al* described the CSD as 'the systematic analysis of large numbers of related structures which is a powerful research technique, capable of yielding results that could not be obtained by any other method' (Taylor & Kennard, 1982). Although Fabian posited that 'synthons formation is controlled by the strength of hydrogen bond between the given molecule and the coformer as opposed to the number of hydrogen bond acceptors or donors present' (Fábián, 2009).

Knowing the hierarchy of homo- and heterosynthons probability becomes important in systematic cocrystal design and engineering. The synthons with higher probability have proved to be more reliable and robust in forming the expected hydrogen bond motif in the crystal structure . However, the issues of carboxylic acid and pyridine cocrystals on whether the product will be neutral or ionic is still unsolved (Duggirala *et al*., 2016).

Systematic investigation of supramolecular synthons usually involves the following:

i. The functionalities capable of forming supramolecular synthons are identified, with the possible diverse supramolecular synthons that can be formed via the intermolecular interactions between these functionalities.
ii. The CSD is searched for hits where a specific supramolecular synthon is available.
iii. The CSD is searched for hits where the specific supramolecular synthon is available in the absence of any competing moieties.

iv. A model compound experiment is designed to address the validity of the statistics obtained from the CSD analysis.

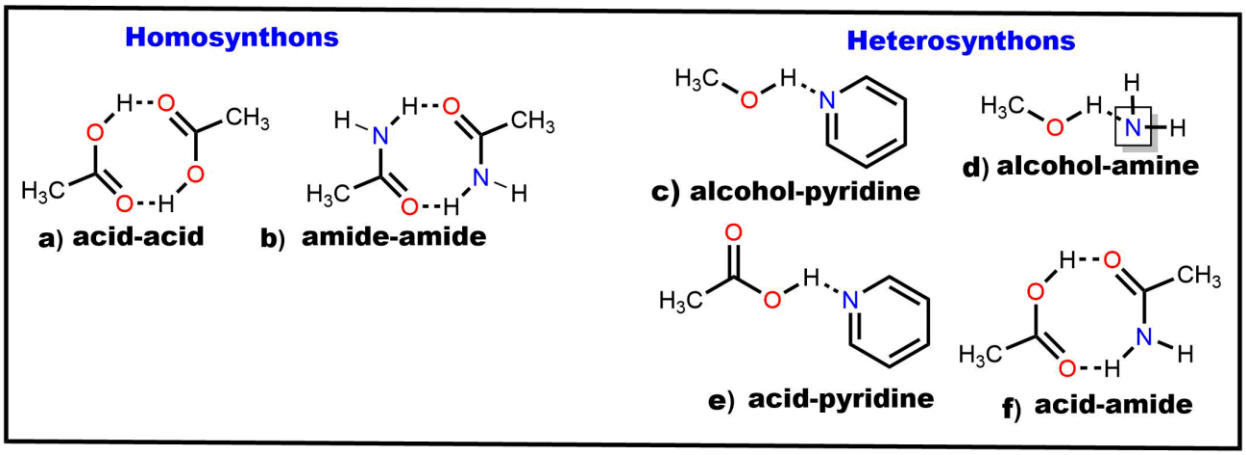

Figure 1.1: Supramolecular homosynthons: (a) carboxylic acid existing as a dimer, and (b) amide exhibiting a dimer configuration; supramolecular heterosynthons: (c) hydroxyl-aromatic nitrogen, (d) hydroxyl-amide, (e) carboxylic acid-pyridine, (f) carboxylic acid-amide.

Aakeröy (Aakeröy *et al*., 2002) and other scientists (Duggirala *et al*., 2016) have studied the behaviour of carboxylic acid functional groups as supramolecular synthons and proved that carboxylic acid is consistent in forming supramolecular heterosynthons with the best basic nitrogen. To study the interaction between the carboxylic acid and nitrogen containing groups, both groups looked at two nitrogen atoms with different basicity and observed how they interact with a carboxylic acid and a phenol moiety.

Aakeröy also conducted structural studies on twelve cocrystals of iso-nicotinamide with different carboxylic acids, in which a consistent pattern of hydrogen bond preference was revealed. It was noted that the crystal structures comprised of two dominant supramolecular synthons viz the heteromeric carboxylic acid···pyridine hydrogen bond and a self-complementary amide···amide synthon was dominant in the presence of widely differing chemical functionalities (Aakeröy *et al*., 2002).

Moreover, a study on carboxylic acid and alcohols hierarchy of supramolecular synthon formation with nitrogen acceptors was conducted (Shattock *et al*., 2008) and has shown that COOH···N supramolecular heterosynthon is the most dominant over the OH···N supramolecular heterosynthon. Furthermore, it was demonstrated that their respective COOH···COOH and

OH···OH supramolecular homosynthons are less favoured. Considering the aforementioned reports, it can be concluded that supramolecular heterosynthons are more likely to occur than supramolecular homosynthons (Aakeröy *et al*., 2002; Pauling & Brockway, 1934).

Studies on carboxylic acids and alcohols for their ability to form reliable and robust supramolecular heterosynthons are quite common in pharmaceutical research. This is because the majority of APIs contain these functional groups. Additionally, these functional groups are common in pharmaceutical excipients and inherently have become highly relevant as pharmaceutical cocrystal coformers.

1.4 Intermolecular Interactions

Intermolecular forces play a vital role in the formation of highly ordered crystalline materials because they dictate the way in which molecules interact with each other. The interactions take place between molecules, the molecules assemble and ultimately, the resulting solid material is defined in terms of its physical properties and reactivity (Aakeröy *et al*., 2002). This notion has again sparked an interest in the study and understanding of non-covalent interactions of molecules such as hydrogen bonds. In fact, the main intermolecular interactions used in crystal engineering are hydrogen bonds and van der Waals forces (Nangia & Desiraju, 2019). However, halogen bonding and C-H···π interactions are also emerging.

Among the non-covalent interactions, hydrogen bonding is regarded as the most widely applied intermolecular interaction in the formation of multicomponent crystals. Huggins developed the concept of hydrogen bond, and he presented it in a dissertation where he described the 'tautomerism' observed in acetoacetic esters (Huggins, 1936).

1.5 Solid-state forms

Multicomponent crystals (MCCs) are crystalline materials made up of two or more types of molecules in a stoichiometric ratio, which are linked by non-covalent intermolecular interactions. MCCs can exist in a number of crystalline forms, including salts, solvates/hydrates, cocrystals, or their combinations (Fig 1.2).

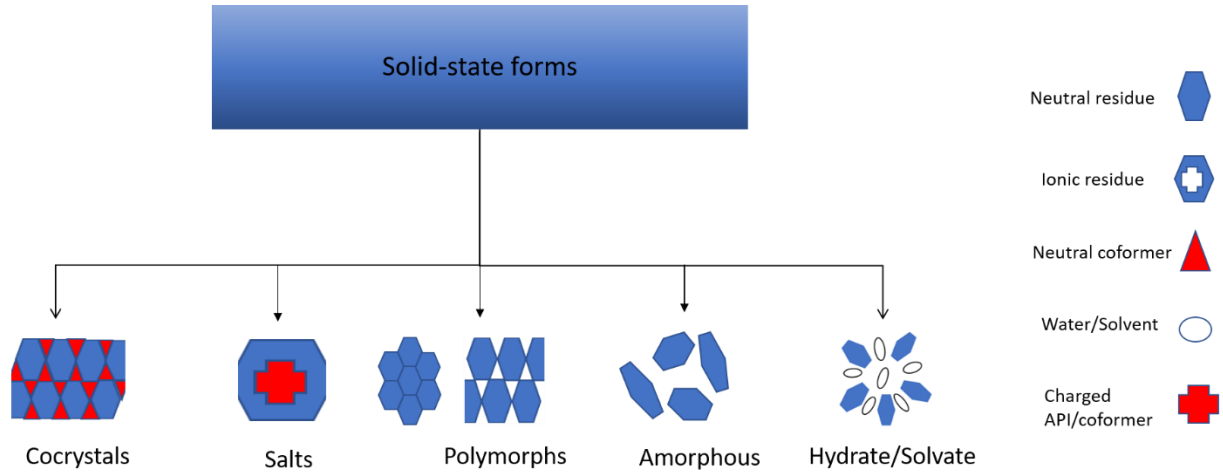

Figure 1.2: Graphical representation of different types of solid-state forms

1.5.1 Salts

At least 50% of orally administered pharmaceutical drugs are salt forms, and this is due to the improvement in the solubility and bioavailability often associated with this drug form (P.H.Stahl & C.G.Wermuth, 2003). A drug is considered a pharmaceutical salt when its formulation consists of an active pharmaceutical ingredient and ionic species, including cations or anions, Fig 1.3.

According to IUPAC, a salt is a ‘‘chemical compound comprising an assembly of cations and anions’’ (McNaught & Wilkinson, 1997). Salt formation occurs during a process of proton transfer from an acid to a base. Indeed, there is a link between cocrystals, and salts created by the extent to which the proton transfer occurs between the two components. During this reaction, if the proton sticks with the base, that signals a proton transfer and the resulting crystalline material is a salt, however, if the protons remain with the acid, then the resulting material is a cocrystal (Thakuria & Sarma, 2018). The degree to which the proton is transferred from an acidic compound to a basic compound is directly related to the pKa difference-the negative logarithm of the dissociation constant (Niazi, 2006). Therefore, the [ΔpKa = pKa (protonated base)-pKa (acid)] will decide the location of the transferrable proton between the acid-base medium reaction.

This rule of thumb of ΔpKa has been widely used to predict the formation of salt and/or cocrystals between crystallising acid-base pairs. Bhogala and co-workers studied the influence of pKa on a range of salts and cocrystals and observed that when the ΔpKa is more than 3.75, it is very likely that a salt will form. Likewise, a neutral cocrystal is expected to be formed when the ΔpKa is less

than 0. If the transition range falls between 0 and 3.75, the proton will have an intermediate H bond character, and this intermediate could lead to a salt or a cocrystal (Bhogala *et al*., 2005). Researchers in the crystal design field have correctly used this rule of thumb, and Cruz-Cabeza brought more meaning to it when she verified and quantified it in her recent work. She used the CSD data to collect crystal structures of acidic and basic compounds and determined their pKa values. The quantitave pKa rule revealed that if ΔpKa is below -1, the formation of cocrystals can be expected whereas, ΔpKa higher than 4 is most likely to result in salt formation. However, if the ΔpKa is between -1 and 4,the classification becomes a challenge and the so-called 'salt-cocrystal continuum' term is used (Cruz-Cabeza, 2012).

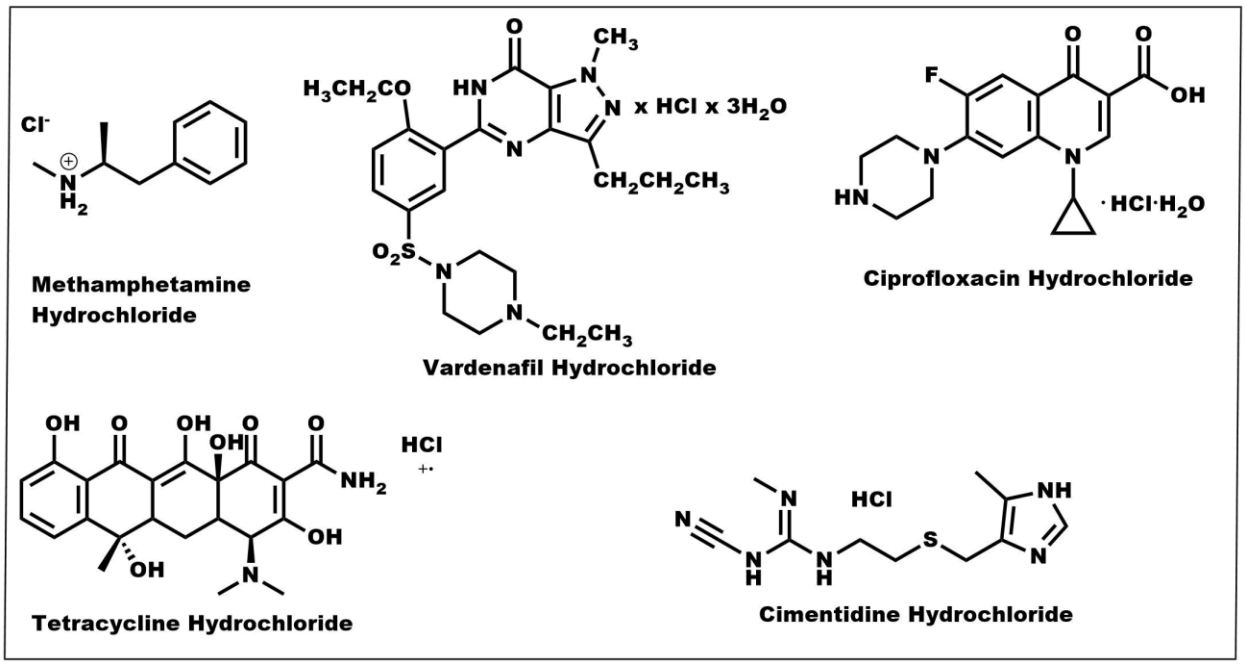

Figure 1.3: Structures of some commercially available pharmaceutical salts

1.5.2 Cocrystals

The emergence of cocrystals in the field of sciences dates back to the 1800s when the first cocrystal, quinhydrone (REF Code:QUIDON02 & QUIDON), was obtained when research on quinone was conducted (Wöhler, 1844). The components of the quinhydrone crystal structure were achieved only in 1958 due to the unavailability of the X-ray diffractometer at the time of discovery. The X-ray measurement showed that the quinhydrone is composed of quinone and hydroquinone in a 1:1 stoichiometric ratio. A number of cocrystals existed in the 1950s, but they

were broadly classified as molecular complexes, organic molecular compounds and solid-state complexes (Karagianni *et al*., 2018).

According to Karagianni and co-workers, the term cocrystal was suggested to describe a complex of hydrogen bonds formed between 9-methyl adenine and 1-methyl thymine (Karagianni *et al*., 2018). The term was subsequently employed by Margret Etter in her research on hydrogen bonding patterns of organic compounds (Etter, 1990).

In 2003, a significant number of researchers in the field of crystal engineering had a debate on the appropriate definition for cocrystals. This was instigated by Desiraju with a controversial letter explaining his preference for cocrystal to be known as “a multicomponent system held together by a non-covalent interaction” (Desiraju, 2003). A correspondence came from (Dunitz, 2003) who refuted the definition and pointed out that the term included solid solutions, encapsulated compounds or amorphous solids, making Desiraju’s preferred definition incomplete. Likewise, Aakeröy added and proposed strict compliance with three criteria for the definition of a cocrystal:

1. the neutrality of the ingredients,
2. the solid-state of the components in ambient conditions, and
3. the homogeneity of the crystalline material and the stoichiometry of the components.

Bond disputed criterion 2 and rather suggested the term “multicomponent molecular crystals” to describe a crystalline material whose components are either solid or liquid in ambient conditions (Bond, 2007). The Center of Drug Evaluation and Research (2018) intervened and proposed a universal definition for a cocrystal which is currently used by most researchers.

The US FDA Center of Drug Evaluation and Research (2018) stated that cocrystals are “solids which are crystalline materials composed of two or more molecules in the same crystal lattice”. Another generally accepted definition of pharmaceutical cocrystals was coined in the context of the Indo-US Bilateral Meeting on the Evolving Role of Solid-State Chemistry in Pharmaceutical Science (Aitipamula *et al*., 2012): "cocrystals are solids that are crystalline single-phase materials composed of two or more different molecular and/or ionic compounds generally in a stoichiometric ratio which are neither solvates nor simple salts".

The work of Grothe (Grothe *et al*., 2016) inspired by the work of Aitipamula (Aitipamula *et al*., 2012) proposed a universal classification and definitions of multicomponent crystals (the definitions of MCCs proposed by Grothe will be adopted in this work). The cocrystal is defined as a crystal with a coformer molecule incorporated with either another coformer or at least two ions. They went further to define the subclasses of cocrystals as a true cocrystal when the MCC contains only one coformer, cocrystal salt- one or more coformers, two or more ions, no solvents and cocrystal salt solvate contains one or more solvents, two or more ions, one or more coformers (Grothe *et al*., 2016).

Nonetheless, another dispute was raised as to whether cocrystals should be considered therapeutically equivalent to pure drugs as well as with regard to the necessary toxicity and efficacy studies. Despite the ongoing debates on the definition of cocrystals, cocrystals are known to be composed of two neutral components held together by non-covalent bonds with the possibility of intermediate states between salts and cocrystals.

The difference between cocrystals and other MCCs is clearly outlined by the FDA guidelines which state that "traditionally, solid state pharmaceutical forms of APIs are grouped either as polymorphs or as salts". However, cocrystals are distinct forms of these conventional pharmaceutical solid forms. Compared to polymorphs (the ability of a compound to crystallise in more than one crystal structure), cocrystals are composed of a coformer molecule with either another coformer or at least two ions in their crystal lattice. In comparison to salts, where the crystal's components are in an ionised state, the cocrystal components are in a neutral state and interact through non-ionic interactions (Grothe *et al*., 2016). Hence, one distinct difference between salts and cocrystals is that in salt formations there is a proton transfer and ionisation, while these do not appear in the cocrystals.

Studies on cocrystals are still ongoing, and new cocrystal structures are being published. This is evident from the gradual increase of cocrystal structures published in the Cambridge Structural Database (CCDC, 2019).

1.5.3 Solvates and Hydrates

Solvates are usually formed when solvent molecules are incorporated into the crystal lattice of a compound and can be regarded as molecular complexes formed between the host and the solvent molecules. Generally, solvates are unfavourable for use in the pharmaceutical industry because organic solvent residues are associated with toxicity (Censi & Di Martino, 2015).

When water is used as a solvent, and incorporated into the crystal, the resulting molecular complex is referred to as a hydrate. Hydrates are quite interesting forms of drug products since water is not associated with any safety concerns (Karagianni *et al*., 2018). Water molecules can also be incorporated in different ways into the crystal lattice. Morris and Rodriguez-Hornedo classified hydrates as channel or isolated site hydrates based on the nature of intermolecular forces demonstrated by water molecules in their crystal lattice. In the first case, the water molecules form interactions with other water molecules while they are in channels, and in the second case, the water molecules interact mostly with the so-called host compound. Interestingly, the two classes of hydrates could be either stoichiometric or non-stoichiometric because their crystal packing is mostly determined by the host molecules (Aakeröy & Sinha, 2018, Stokes *et al*., 2014, Bajpai *et al*., 2016).

Generally, at least 30% of crystalline drug forms exist as hydrates through changes in temperature, pressure, or relative humidity, which result in significant changes in physical properties and create severe problems during storage. Furthermore, hydrates may offer a faster or slower dissolution rate than the anhydrous form. It is assumed that the latter is due to the fact that there are fewer sites of the drug molecule available for interaction with more water molecules during dissolution. An interesting example is the dissolution is theophylline anhydrate, which dissolves faster than its hydrate form. In some cases, the hydrate form shows a more rapid dissolution rate than its anhydrous form. A good example for the latter is erythromycin dihydrate which exhibits a significant faster dissolution rate than that of the monohydrate and anhydrous forms (Shan & Zaworotko, 2010).

1.5.4 Polymorphism

Pharmaceutical drug candidates often exist in more than one crystalline solid-form with the same chemical composition, but different internal crystal structures leading to the forms with different physicochemical properties (Vippagunta *et al*., 2001) due to their different crystal structures and/or different molecular conformations. This is termed polymorphism (Savjani *et al*., 2012) and this solid-state behaviour is usually observed in organic molecules (Brittain, 2007).

Polymorphism offers both an advantage and a disadvantage in the pharmaceutical research. The lack of reliability of manufacturing as well as physical instability offered by a given polymorph can cause problems in the drug discovery and formulation process (Almarsson & Zaworotko, 2004). At the same time, a novel polymorph can provide an opportunity for generic pharmaceutical drug formulation. Moreover, their thermodynamic stability and improved physicochemical properties are sometimes promising for the improvement of the original solid form (Censi & Di Martino, 2015).

A demonstration made by various researchers has shown that the solubility differences between two or more polymorphic forms of the same compound are generally lower than a factor of 2 (Pudipeddi & Serajuddin, 2005) and rarely of 5. In essence, this indicates that one form may possess promising solubility than the original form, however, this could be futile since it is less stable than the original form; as a result, there may be no use in favouring this polymorph (Censi & Di Martino, 2015). To respond to the issue of polymorphs, several strategies have been developed to improve the screening of drugs for polymorphism (Fleischman *et al*., 2003).

Polymorphs are usually named in their chronological order as they are being discovered, and their naming is not associated with their thermodynamical stability. Common conventions are forms A, B, C or forms I, II, III, and forms α, β and γ (Crafts, 2007).

Polymorphism exists in three types; namely packing polymorphism, conformational polymorphism, and synthon polymorphism. Packing polymorphism is described as the ability of rigid molecules, from a conformational perspective, to pack themselves into different three-dimensional structures (Elder *et al*., 2015). An example of this form includes the tetramorphs of carbamazepine, as shown in Figure 1.4.

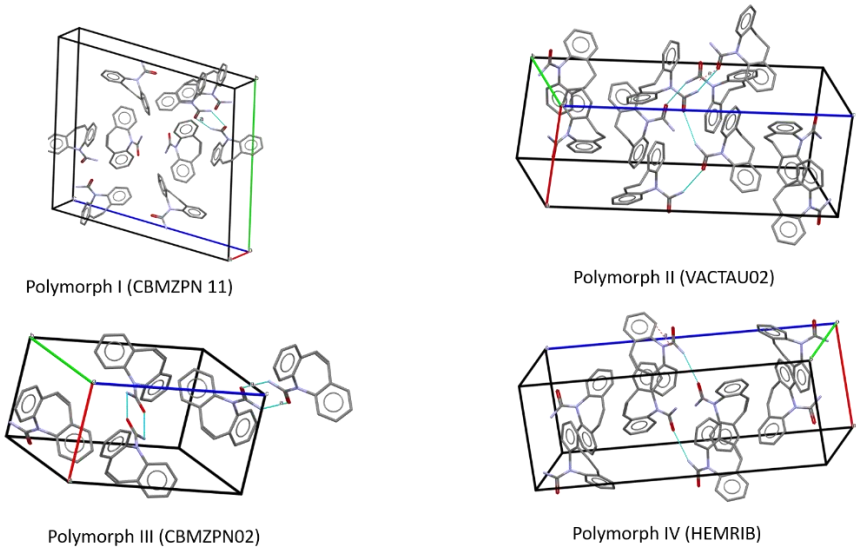

Figure 1.4: Carbamazepine polymorphs

In contrast, the conformational polymorphism is where flexible molecules are positioned into different conformations that pack into different shapes (Babu *et al*., 2010a). A common example of this type is the two polymorphs of ritonavir, shown in Fig 1.5 (Bauer *et al*., 2001). Bauer and co-workers extensively studied ritonavir polymorphs as the example of conformational polymorphism, where they demonstrated the molecular structures of both polymorphs and further elucidated why polymorph II of ritonavir is the more stable polymorph.

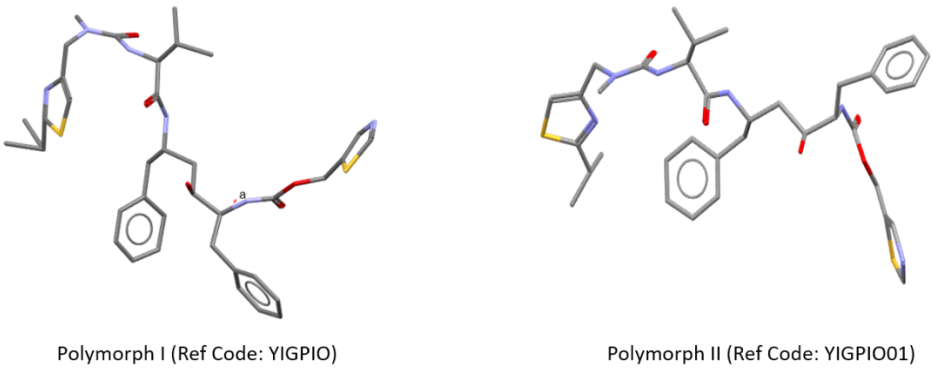

Figure 1.5: Ritonavir polymorphs

The third type of polymorphism, which is the most common, is the synthon polymorphism. It occurs when there is a difference in crystal structures of the same compound due to the difference in hydrogen bonding or the formed supramolecular synthon. Examples of this would be differences in carboxylic acid, carboxamide or sulfonamide motifs of furosemide (Fig 1.6). Though these three types are different in conformation, hydrogen bonding, packing, and unit cell parameters, or their lattice energy difference is usually very small, about 0.5-3.0 kcal (Nangia, 2008).

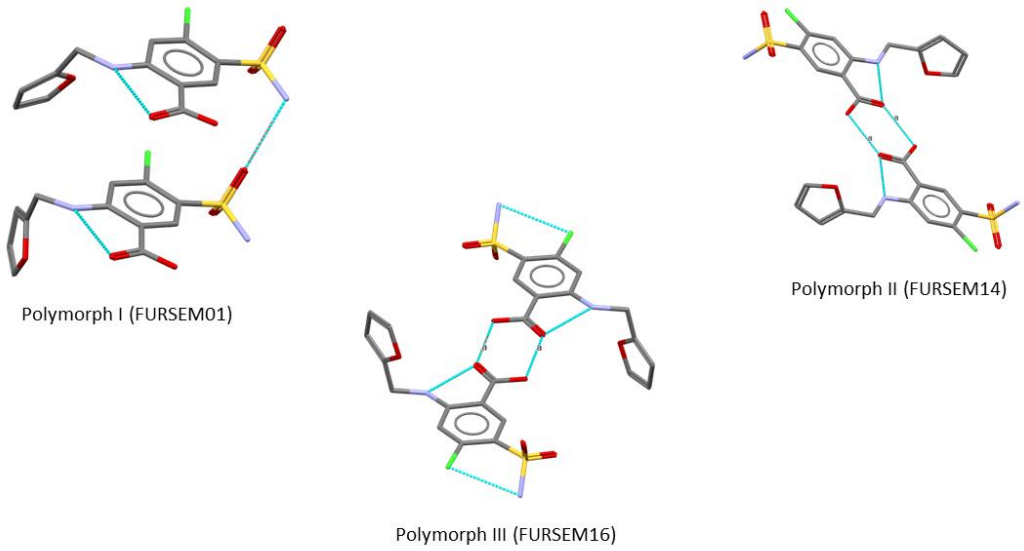

Figure 1.6: Furosemide polymorphs

The different types of polymorphs can coexist in one system, for example, conformational and synthon polymorphism or synthon and packing polymorphism (Babu *et al.*, 2010a). Though these three types are different in conformation, hydrogen bonding, packing, and unit cell parameters, their lattice energy difference is usually very small, about 0.5-3.0 kcal (Nangia, 2008).

Sometimes, it is a challenge and a rigorous task to identify new polymorphic forms of drug substances because both thermodynamic and kinetic processes must be considered (Otto & De Villiers, 2016). Unfortunately, new polymorphs can be discovered after the approval of a form of a pharmaceutical drug. The most commonly known example is that of ritonavir, an Abbott Pharmaceutical product marketed as Norvir that was approved by the FDA in 1996, and administered as both a liquid and semisolid capsule dosage forms (Crafts, 2007). Ritonavir is used for the treatment of the Human Immunodeficiency Virus (HIV). However, within two years of its

breakthrough, a testing laboratory in the United States observed failure in dissolution tests of the semisolid capsules. They later discovered that the failure was caused by the precipitation of the drug product out of the solution. Consequently, a new polymorphic form of ritonavir was extracted and believed to adversely affect the in-vivo exposure and the manufacturability of the dosage form of the original ritonavir (Crafts, 2007). The new polymorph was characterised as polymorph II, a stable orthorhombic form with a CSD refcode YIGP1001 (CDS version 5.42.2020).

Based on the literature, polymorphs have been observed to have monotropic or enantiotropic relationships (Figure. 1.7). Polymorphs are monotropic when one of the polymorphs is stable and expresses a higher solubility over the entire temperature range (Figure 1.7A). In contrast, two polymorphs exhibit an enantiotropic relationship if their stability changes and their solubility curve crosses at a given temperature (Figure 1.7B). In monotropic systems, the stable form at room temperature can be obtained by heating the metastable form at any temperature. (Lee, 2014).

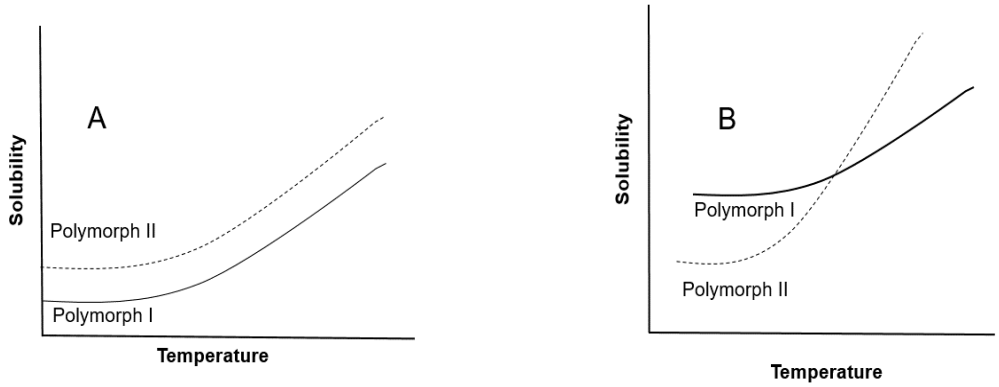

Figure 1.7 (A) Monotropic behaviour between two polymorphs (B) Enantiotropic behaviour between two polymorphs (Crafts,2007).

A recent comprehensive study on polymorphism was done by Cruz-Cabeza and Bernstein (Cruz-Cabeza *et al*., 2015) where they addressed several fundamental aspects of polymorphism. In this work, they went as far as correcting some of the misconceptions reported in the polymorphism literature, which seem to base conclusions on “chemical intuition rather than specific evidence”.

In most instances, polymorphism is attributed to the flexibility and size of a molecule, with the belief that flexible molecules are likely to occur in different crystal packing (conformational polymorphs). However, Cruz and Bernstein noted that there is no correlation between the flexibility and/or size of a molecule to form polymorphs. They also observed that achiral

compounds are more likely to form polymorphs than their chiral counterparts. Moreover, compounds that can form a hydrogen bond show a slightly higher tendency to polymorph formation than those which do not. Usually, the energy difference between polymorphs of the same compound is less than 1 kcal mol^{-1}, but conformational polymorphs tend to differ by larger values of up to 2.5 kcal mol^{-1}.

1.5.5 Amorphous forms

Amorphous forms are non-crystalline solids that lack long-range order. In the drug discovery field, this type of solid form has been viewed as less attractive than crystalline forms, as they are generally less stable both chemically and from a solid-state perspective. Conversely, amorphous solids can still be useful in pharma innovation because of their inherently higher solubility and other valuable properties. Amorphous solids exhibit higher solubility and fast dissolution rate because the energy barrier within molecules is lower when the solid changes to the solution state. The interest in understanding amorphous materials has increased, and engineering technologies have been used to control the stability of amorphous materials (Vippagunta *et al*., 2001; Engers *et al*., 2010; Murdande *et al*., 2011).

The advent of cocrystals has played a huge role in the transformation of an amorphous or hard-to-crystallise API into a readily stable crystalline solid. Although amorphous APIs are normally used and also form as part of the increasing number of dosage forms, crystalline products are still considered to be better due to their easier and more reproducible characterisation and greater chemical stability (Steed, 2013).

1.6 Crystal Engineering

In order to comprehensively understand the principle behind solid-state forms, such as cocrystals, it is imperative to discuss crystal engineering. The concept of crystal engineering explores the synthesis and design of pharmaceutical cocrystals by intermolecular interactions in a competitive hydrogen bond environment (Aakeröy *et al*., 2002). Through the work of Desiraju and co-workers, Aakeröy and others were able to contribute extensively on this evolving subject.

In crystal engineering, the crystal structures are viewed as if they are connected by a series of supramolecular interactions, therefore understanding the interactions that sustains the crystal packing is of utmost importance.

Almarsson and Zaworotko define crystal engineering as an application of supramolecular chemistry to the solid-state with an emphasis on the idea that crystalline solids are in reality, manifestations of self-assembly (Almarsson & Zaworotko, 2004). Therefore, crystal structures can be considered as the products of a series of weak but directional molecular recognition events.

Crystal engineering made its first remark in academic research as early as in the 1930s when Pauling defined the chemical bond in covalent and non-covalent terms (Pauling & Brockway, 1934). However, the term "crystal engineering" was invented in 1955 by R. Pepinsky (Pepinsky, 1955) but was not implemented until Schmidt studied a series of solid-state reactions in crystalline solids. As a result, most of the literature associates it with G.M.J. Schmidt, who related the solid-state reactivity of a large number of photodimerizable compounds with their crystal structures (Schmidt, 1971).

Once again, Schmidt attempted to answer the question of how to link a molecular property to a crystal property. Unfortunately, his research never materialised as he realised that real progress could not be made until it was possible to obtain a three-dimensional crystal structure of a molecular solid. It was through this realisation of a crystal structure knowledge that the term "crystal engineering" was born (Desiraju, 2013).

Despite the fact that crystalline solids are favoured in pharmaceutics, and also afford physicochemical stability which makes the crystalline solids even more attractive (Almarsson & Zaworotko, 2004), they can still present problems that are related to poor solubility properties and polymorphism. These problems have caused the approved crystalline forms to be limited to polymorphs, salts and stoichiometric solvates (Shattock *et al*., 2008). However, crystal engineering offers a new avenue for the development of pharmaceutical cocrystals, which serve as the main focus of this research. Over the years, crystal engineering has flourished, especially in terms of organic solids and metal-organic structures, and this can be seen from the large amount of published papers based on this particular field (Desiraju,2013; Goodman,2001).

Additionally, crystal engineering is based on the development of reliable supramolecular reactions, where the success and effectiveness of a reaction can be judged by the frequent occurrence of desired intermolecular interactions (Aakeröy *et al*., 2002). The number of times that a certain motif appears in a crystalline lattice is in many ways a measure of the yield of a supramolecular reaction. The same way that a covalent synthetic chemist searches for ways in which a specific reaction can be improved or prevented is the same way a supramolecular chemist tries to identify the experimental regime where a supramolecular synthon becomes dominant despite competition from other non-covalent forces. In fact, crystal engineering was gradually introduced into the field of organic chemistry by using the supramolecular synthon- a repeating structural unit in crystal structures that stimulates the design of supramolecular architectures based on a small number of recurring hydrogen bond patterns (Nangia, 2010).

As much as it is important to acknowledge that every intermolecular force will have some influence on the outcome of a crystallisation process, it is also evident that some non-covalent forces are more significant than others. Indeed, the foundation of crystal engineering lies in the concept of supramolecular chemistry. It is evident that both supramolecular chemistry and crystal engineering aim to understand the correlation between the structure-property relationships of crystalline materials and use that understanding to identify optimised material for a particular application.

Nangia and Desiraju recently published an outlook on the future of crystal engineering, and based on their findings, it can be seen that crystal engineering has a very promising future as more research questions keep rising (Nangia & Desiraju, 2019). As it stands currently, crystal engineering is witnessing increasing popularity as an independent field. Moreover, it is evident that both crystal engineering and supramolecular chemistry define a meeting point for organic, inorganic, physical, and computational chemists along with biologists and materials scientists (Nangia, 2010).

1.7 Pharmaceutical cocrystals

Pharmaceutical cocrystals have been proven to adopt a simple, straightforward regime to dramatically influence the solid-state properties of a drug substance, particularly its solubility and hence bioavailability (Steed, 2013). Kumar and co-workers have presented how

pharmaceutical cocrystals can enhance the physicochemical properties of APIs (Kumar & Nanda, 2017). As a result, their findings led to the development of new solid forms of drug molecules. Over 200 studies of pharmaceutical cocrystals have demonstrated improved solubility and/or dissolution rates (Duggirala *et al*., 2016).

Pharmaceutical cocrystals are a subclass of cocrystals, composed of at least a pharmaceutically acceptable coformer and an active pharmaceutical ingredient (API) which are held by non–covalent bonds in a fixed or variable stoichiometric ratio (Steed, 2013). It is strictly mandatory that the coformer molecule should be non-toxic with no adverse effects. Preferably, the coformer should be included on the list of Generally Recognised As Safe (GRAS) (U.S. Food and Drug Administration, 2019) compounds, which consists of over 3000 approved compounds (Trask, 2007).

At least 80% of pharmaceutical drug substances that are in circulation have been identified to have poor solubility (Karagianni *et al*., 2018). Estimates suggest that fewer than 1% of candidate drugs eventually reach the market (Aakeröy *et al*., 2009).

Using pharmaceutical cocrystal formation, Aakeröy. (Aakeröy *et al*., 2009) increased the solubility and melting point of the anticancer drug hexamethylenebisacetamide by modifying the chain length of the dicarboxylic acid coformer, resulting in an increase of up to a factor of 2.5 in aqueous solubility. The design or discovery of new useful solid-state forms opens up new avenues for intellectual property exploitation. As a result, there are now a number of patents covering pharmaceutical cocrystals. For example, stavudine forms patented cocrystals with melamine, 2-amino pyridine, and N-methyl-2-pyrrolidinone (Steed, 2013).

Another successful pharmaceutical cocrystal known is Entresto, composed of sacubitril-valsartan active drug ingredients. Entresto is a stable cocrystal with no polymorphs reported at the time of this research. It is used to treat symptomatic chronic heart failure with reduced ejection fraction in adult patients (Agency, 2015).

1.8 Furosemide

Furosemide (Fig 1.8), FUR, 4-chloro-2-[(2-furanylmethyl)-amino]-5-sulfamoylbenzoic acid, an anthranilic acid derivative, marketed as Lasix, is a loop diuretic pharmaceutical drug synthesised for the treatment of oedema and hypertension linked to congestive heart failure, cirrhosis of the

liver and renal disease (http://www.drugbank.ca/drugs/DB00695). This pharmaceutical compound was used as an API of interest in this research due to its propensity to form hydrogen bonds with the selected basic coformers.

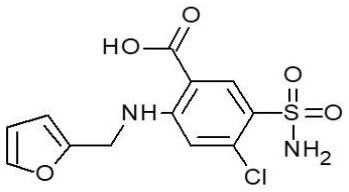

Figure 1.8. Furosemide (FUR)

Furosemide, also referred to as frusemide historically, is a small molecule with a molecular weight of 330.75 g mol^{-1} and a fairly low lipophilicity (logP=2.03) (Hardman,2001). This drug is well known for its low water solubility and low permeability,and is thus classified as the BCS group IV drug. The mechanism of action of furosemide is that it halts the reabsorption of excess water back into the body. It is administered orally as a solid tablet form and as a solution to be injected into the body (http://www.nhs.uk/medicine-guides). However, for intravenous administration, the solubility can be modified by formulating the drug in weakly basic buffer solution (pH 8) to yield a concentration of 10 mg mL^{-1} solution.

Furosemide is a versatile drug available almost in all countries around the world; it is cost-effective and has been extensively investigated for various therapeutic purposes. A series of studies have shown that furosemide could provide potential aid in resurrecting infected lungs when administered by inhalation. A recent study done by Waskiw-Ford has proved furosemide to be effective in lung infections when administered by inhalation (Waskiw-Ford *et al.*, 2018). Similarly, a study conducted by Yuengsrigul (Yuengsrigul *et al*., 1999) investigated furosemide as an alternative drug in reducing the bronchial inflammation of asthma. Subsequently (Prandota, 2002) replicated a similar study that showed that furosemide could significantly reduce bronchial inflammation of asthma.

Recently, furosemide was explored as a potential repurposing drug for COVID-19 treatment. The authors developed a screening strategy for identifying a compound with potential broad-spectrum anti-inflammatory activity targeting relevant cytokines of the pulmonary innate immune system (Wang *et al*., 2020). Furosemide was then identified as a small molecule

candidate with the properties: broad-spectrum anti-inflammatory mechanism of action targeting cytokine of innate immunity; low toxicity; and excellent safety profile; easily administered; inexpensive and can be easily manufactured worldwide. This was done by the use of in silico studies.

Generally, high doses or prolonged use of pharmaceutical drugs by patients are undesirable as this can cause addiction and severe side effects. Similarly, high doses of furosemide usually lead to fluid and electrolyte imbalance which can cause headaches, cramping, thirst, and weakness (Granero *et al*., 2010). It is because of this reason that the improvement of furosemide solubility, and subsequently the bioavailability is important.

Furosemide contains strong hydrogen bond donor and acceptor groups: carboxylic acid (-COOH), amine (-NH), hydroxyl (-OH), and sulfonamide ($-SO_2NH_2$), it can also form halogen bonding via the chlorine atom. These functional groups when reacted with other complementary molecules have been shown to exhibit robust heterosynthons via O–H···O and N–H···O hydrogen bonds forming a wide range of stable supramolecular structures.

Disorder of the whole SO_2NH_2 sulfonamide group is not commonly observed in FUR crystal forms, presumably because this group is usually involved in hydrogen bonding networks, as evidenced by a systematic study of aromatic primary sulfonamide pyridine-N-oxides synthons (Goud *et al*., 2011). It has been noted, that the NH_2 of the sulfonamide can adopt different orientations through rotations about the S–N bond in furosemide and furosemide cocrystals, indicating that there is conformational flexibility (Babu *et al*., 2010b).

Furosemide is known to be susceptible to the formation of polymorphs; at least three polymorphs of furosemide are known and reported by Babu (Babu *et al*., 2010b). The formation of polymorphs by FUR should not be attributed to its molecular flexibility (Cruz-Cabeza et al., 2015), as earlier suggested by Babu (Babu *et al*., 2010a). However, the structural flexibility of FUR makes it an interesting pharmaceutical drug in the field of supramolecular chemistry because of the variety of hydrogen bonds formed with various coformers and the observation of the various conformations in the FUR crystals.

Additional effort has been made toward the formation of FUR polymorphs via desolvation of FUR solvates. Boldyreva's (Minkov *et al*., 2014) work demonstrates how furosemide solvates can be used as precursors for the formation of various polymorphs of pure furosemide upon heating.

Salt formation of furosemide with sodium hydroxide and potassium hydroxide has been studied by Khandavilli *et al* (2014) in an attempt to optimise the physical properties of the furosemide drug.

The salt hydrates of furosemide were investigated, and it was discovered that the salt hydrates had superior solubility and stability as compared to the pure furosemide drug. The salt stability was established through the use of PXRD, which revealed no evidence of solidification over extended periods of time (Rao Khandavilli *et al*., 2014).

Formation of furosemide cocrystals with caffeine and cytosine as coformers have resulted in solubility improvement of the drug by 6 to 11 times. (Rao Khandavilli *et al*., 2014; Sangtani *et al*., 2015; Goud *et al*., 2012; Teraoka *et al*., 2019)

1.9 Research Problems

Knowing the stability of a pharmaceutical drug and its propensity to form polymorphs is an added advantage to drug design. In this research, the formation of polymorphs via desolvation of furosemide solvates was investigated. Under controlled conditions, the MCCs of furosemide were gently desolvated to produce polymorphs. The rationale for using solvates to create selected polymorphs is well reasoned. Due to the close proximity of the lattice energies of pairs of polymorphs (on the order of 1 $KJ.mol^{-1}$) (Price, 2013), the environmental conditions required to form the different forms can be very similar.

Furosemide (FUR) is a polymorphic drug with three known polymorphs best represented by the Cambridge Structural Database (CSD) structures FURSEM03, FURSEM14, and FURSEM16: form I, form II, and form III, respectively (Babu *et al*., 2010). It is in the interest of this work to investigate whether more furosemide polymorphs exist; consequently, this work shows an excellent illustration of the difficulties inherent in the directed formation of a polymorph's pure form.

1.10 Objective of the Research

This research aims to investigate whether furosemide can form stable multicomponent crystals with the selected coformers as suggested by the screening of the Cambridge Structural Database, furthermore, to determine if solvates of FUR can form desired FUR polymorphs via a gentle desolvation process under ambient conditions.

1.11 Research Hypothesis

- Furosemide and coformers including pyridine, picolines, and lutidines will be reacted via hydrogen bond formation to yield MCCs with enhanced physicochemical properties.
- Furosemide, as a weak acid can behave as a hydrogen bond donor or hydrogen bond acceptor depending on the coformer and conditions of the reaction.
- Upon slow drying or exposure to the atmosphere, one pure form of a polymorph of FUR will be obtained.
- Furosemide solvates can serve as precursors of desired polymorphs of the pure drug.

1.12 Research Outline/Plan

- Synthesis of multicomponent crystals via selected crystallisation methods.
- Characterisation of the obtained MCCs.
- Analysis of the results.

References

Aakeröy, C.B.& & Sinha, A.S. 2018. *Co-crystals : preparation, characterization and applications*. London ; Royal Society of Chemistry,.

Aakeroy, C.B., Beatty, A.M. & Helfrich, B.A. 2001. 'Total synthesis' supramolecular style: Design and hydrogen-bond-directed assembly of ternary supermolecules. *Angewandte Chemie - International Edition*, 40(17): 3240–3242.

Aakeröy, C.B., Forbes, S. & Desper, J. 2009. Using cocrystals to systematically modulate aqueous solubility and melting behavior of an anticancer drug. *Journal of the American Chemical Society*, 131(47): 17048–17049. https://pubs.acs.org/sharingguidelines.

Ambrogi, V., Perioli, L., Pagano, C., Marmottini, F., Ricci, M., Sagnella, A. & Rossi, C. 2012. Use of SBA-15 for furosemide oral delivery enhancement. *European Journal of Pharmaceutical Sciences*, 46(1–2): 43–48. http://dx.doi.org/10.1016/j.ejps.2012.02.004.

Babu, N.J., Cherukuvada, S., Thakuria, R. & Nangia, A. 2010a. Conformational and synthon polymorphism in furosemide (Lasix). *Crystal Growth and Design*, 10(4): 1979–1989. https://pubs.acs.org/sharingguidelines 20 October 2020.

Babu, N.J., Cherukuvada, S., Thakuria, R. & Nangia, A. 2010b. Conformational and synthon polymorphism in furosemide (Lasix). *Crystal Growth and Design*, 10(4): 1979–1989.

Bajpai, A., Scott, H.S., Pham, T., Chen, K.J., Space, B., Lusi, M., Perry, M.L. & Zaworotko, M.J. 2016. Towards an understanding of the propensity for crystalline hydrate formation by molecular compounds. *IUCrJ*, 3: 430–439. http://dx.doi.org/10.1107/S2052252516015633www.iucrj.org.

Banik, M., Gopi, S.P., Ganguly, S. & Desiraju, G.R. 2016. Cocrystal and salt forms of furosemide: Solubility and diffusion variations. *Crystal Growth and Design*, 16(9): 5418–5428.

Bauer, J., Spanton, S., Henry, R., Quick, J., Dziki, W., Porter, W. & Morris, J. 2001. Ritonavir: An extraordinary example of conformational polymorphism. *Pharmaceutical Research*, 18(6): 859–866.

Bhattacharya, S., Peraka, K.S. & Zaworotko, M.J. 2018a. Chapter 2: The Role of Hydrogen Bonding in Co-crystals. In *Monographs in Supramolecular Chemistry*. Royal Society of Chemistry: 33–79.

https://pubs.rsc.org/en/content/chapter/bk9781788011150-00033/978-1-78801-115-0 14 April 2021.

Bhattacharya, S., Peraka, K.S. & Zaworotko, M.J. 2018b. Chapter 2:The Role of Hydrogen Bonding in Co-crystals. In *Co-crystals: Preparation, Characterization and Applications*. https://pubs.rsc.org/en/content/ebook/978-1-78801-115-0 14 April 2021.

Bolla, G. & Nangia, A. 2016. Pharmaceutical cocrystals: Walking the talk. *Chemical Communications*, 52(54): 8342–8360. www.ncl-india.org. 6 April 2021.

Brittain, H.G. 2007. Polymorphism and solvatomorphism 2005. *Journal of Pharmaceutical Sciences*, 96(4): 705–728.

Censi, R. & Di Martino, P. 2015. Polymorph impact on the bioavailability and stability of poorly soluble drugs. *Molecules*, 20(10): 18759–18776.

Crafts, P. 2007. A tale of Disappering Polymorphs-Ritonavir. In *Chemical Product Design,Toward a Perspective through Case Studies.* 23–85.

Cruz-Cabeza, A.J., Reutzel-Edens, S.M. & Bernstein, J. 2015. Facts and fictions about polymorphism. *Chemical Society Reviews*, 44(23): 8619–8635. www.rsc.org/chemsocrev.

Cullity, B.D. and & Stock, S.R. 2014. *Elements of X-Ray Diffraction Third Edition*. Third Edit.http://doi.wiley.com/10.1016/0014-5793%2879%2980596-7.

Duggirala, N.K., Perry, M.L., Almarsson, Ö. & Zaworotko, M.J. 2016. Pharmaceutical cocrystals: Along the path to improved medicines. *Chemical Communications*, 52(4): 640–655.

Elder, D.P., Patterson, J.E. & Holm, R. 2015. The solid-state continuum: A perspective on the interrelationships between different solid-state forms in drug substance and drug product. *Journal of Pharmacy and Pharmacology*, 67(6): 757–772.

Fábián, L. 2009. Cambridge structural database analysis of molecular complementarity in cocrystals. *Crystal Growth and Design*, 9(3): 1436–1443. https://pubs.acs.org/sharingguidelines.

Goud, N.R. & Nangia, A. 2013. Synthon polymorphs of sulfacetamide-acetamide cocrystal based on N-H···OS and N-H···OC hydrogen bonding. *CrystEngComm*, 15(37): 7456–7461. www.rsc.org/crystengcomm 10 May 2021.

Granero, G.E., Longhi, M.R., Mora, M.J., Junginger, H.E., Midha, K.K., Shah, V.P., Stavchansky, S., Dressman, J.B. & Barends, D.M. 2010. Biowaiver monographs for immediate release solid oral dosage forms: Furosemide. *Journal of Pharmaceutical Sciences*, 99(6): 2544–2556.

Groom, C.R., Bruno, I.J., Lightfoot, M.P. & Ward, S.C. 2016. The Cambridge structural database. *Acta Crystallographica Section B: Structural Science, Crystal Engineering and Materials*, 72(2): 171–179. http://dx.doi.org/10.1107/S2052520616003954171.

Hardman JG, Goodman LS, G.A. 2001. *Goodman & Gilman's the pharmacological basis of therapeutics*.

Harold M. Schmeck Jr. 1987. Chemistry and Physics Nobels Hail Discoveries on Life and Superconductors; Three Share Prize for Synthesis of Vital Enzymes - The New York Times. *The New York Times*. https://www.nytimes.com/1987/10/15/us/chemistry-physics-nobels-hail-discoveries-life-superconductors-three-share-prize.html 23 September 2021.

Kane, J.J., Liac, R.F., Lauher, J.W. & Fowler, F.W. 1995. Preparation of Layered Diacetylenes as a Demonstration of Strategies for Supramolecular Synthesis. *Journal of the American Chemical Society*, 117(48): 12003–12004. https://pubs.acs.org/doi/abs/10.1021/ja00153a026.

Khandavalli,R., Gangavaram,S., Goud,R.N.,Cherukuvada,S.,Raghavender,S., Nangia,A.,Manjunatha,S.G., Nambiar,S. & Pal,S. 2014. High solubility crystalline hydrates of Na and K furosemide salts. *Crystal Engineering Communications*,16(22): 4842-4852. DOI:10.1039/c3ce42347f.

Kumar, A., Kumar, S. & Nanda, A. 2018. A review about regulatory status and recent patents of pharmaceutical co-crystals. *Advanced Pharmaceutical Bulletin*, 8(3): 355–363. http://apb.tbzmed.ac.ir 6 June 2020.

Lee, E.H. 2014. A practical guide to pharmaceutical polymorph screening & selection. *Asian Journal of Pharmaceutical Sciences*, 9(4): 163–175. http://dx.doi.org/10.1016/j.ajps.2014.05.002.

McNaught, A.D. & Wilkinson, A. 1997. IUPAC compendium of chemical terminology. *Choice Reviews Online*, 40(12): 40Sup-0262-40Sup – 0262. https://www.scirp.org/(S(i43dyn45teexjx455qlt3d2q))/reference/ReferencesPapers.aspx?ReferenceID=1286994 14 April 2021.

Nangia, A. 2008. Conformational polymorphism in organic crystals. *Accounts of Chemical Research*, 41(5): 595–604. https://pubs.acs.org/sharingguidelines 20 October 2020.

Nangia, A. 2010. Supramolecular chemistry and crystal engineering. *Journal of Chemical Sciences*, 122(3): 295–310.

Otto, D.P. & De Villiers, M.M. 2016. *Solid State Concerns During Drug Discovery and Development: Thermodynamic and Kinetic Aspects of Crystal Polymorphism and the Special Cases of Concomitant Polymorphs, Co-Crystals and Glasses*.

Pauling, L. & Brockway, L.O. 1934. The Structure of the Carboxyl Group: I. The Investigation of FormicAcid by the Diffraction of Electrons. *Proceedings of the National Academy of Sciences*, 20(6): 336–340.

Pepinsky, R. 1955. Crystal Engineering: a new concept in crystallography. *Phys. Rev.*, 100(3): 971.

Prandota, J. 2002. Furosemide: progress in understanding its diuretic, anti-inflammatory, and bronchodilating mechanism of action, and use in the treatment of respiratory tract diseases. *American journal of therapeutics*, 9(4): 317–328. https://pubmed.ncbi.nlm.nih.gov/12115021/ 13 April 2021.

Pudipeddi, M. & Serajuddin, A.T.M. 2005. Trends in solubility of polymorphs. *Journal of Pharmaceutical Sciences*, 94(5): 929–939.

Qiao, N., Li, M., Schlindwein, W., Malek, N., Davies, A. & Trappitt, G. 2011. Pharmaceutical cocrystals: An overview. *International Journal of Pharmaceutics*, 419(1–2): 1–11.

Rajesh Goud, N., Jagadeesh Babu, N. & Nangia, A. 2011. Sulfonamide-pyridine-N-oxide cocrystals. *Crystal Growth and Design*, 11(5): 1930–1939. https://pubs.acs.org/sharingguidelines 9 April 2021.

Reddy, L.S., Babu, N.J. & Nangia, A. 2006. Carboxamide-pyridine N-oxide heterosynthon for crystal engineering and pharmaceutical cocrystals. *Chemical Communications*, (13): 1369–1371.

Sanphui, P., Devi, V.K., Clara, D., Malviya, N., Ganguly, S. & Desiraju, G.R. 2015. Cocrystals of hydrochlorothiazide: Solubility and diffusion/permeability enhancements through drug-coformer interactions. *Molecular Pharmaceutics*, 12(5): 1615–1622. https://pubs.acs.org/sharingguidelines.

Savjani, K.T., Gajjar, A.K. & Savjani, J.K. 2012. Drug Solubility: Importance and Enhancement Techniques. *ISRN Pharmaceutics*, 2012(October 2018): 1–10.

Shan, N., Bond, A.D. & Jones, W. 2002. Crystal engineering using 4,4'-bipyridyl with di- and tricarboxylic acids. *Crystal Engineering*, 5(1): 9–24.

Shariare, M.H., Altamimi, M.A., Marzan, A.L., Tabassum, R., Jahan, B., Reza, H.M., Rahman, M., Ahsan, G.U. & Kazi, M. 2019. In vitro dissolution and bioavailability study of furosemide nanosuspension prepared using design of experiment (DoE). *Saudi Pharmaceutical Journal*, 27(1): 96–105. https://doi.org/10.1016/j.jsps.2018.09.002.

Sharma, D., Soni, M., Kumar, S. & Gupta, G. 2009. Solubility Enhancement – Eminent Role in Poorly Soluble Drugs. *Research Journal of Pharmacy and Technology*, 2(2): 220–224.

Shattock, T.R., Arora, K.K., Vishweshwar, P. & Zaworotko, M.J. 2008. Hierarchy of supramolecular synthons: Persistent carboxylic acid···pyridine hydrogen bonds in cocrystals that also contain a hydroxyl moiety. *Crystal Growth and Design*, 8(12): 4533–4545.

Steed, J.W. 2013. The role of co-crystals in pharmaceutical design. *Trends in Pharmacological Sciences*, 34(3): 185–193.

Stokes, S.P., Seaton, C.C., Eccles, K.S., Maguire, A.R. & Lawrence, S.E. 2014. Insight into the mechanism of formation of channel hydrates via templating. *Crystal Growth and Design*, 14(3): 1158–1166.

Taylor, R. & Kennard, O. 1982. Molecular Structures of Nucleosides and Nucleotides. 2. Orthogonal Coordinates for Standard Nucleic Acid Base Residues. *Journal of the American Chemical Society*, 104(11): 3209–3212. https://pubs.acs.org/sharingguidelines.

Trask, A. V. 2007. An Overview of Pharmaceutical Cocrystals as Intellectual Property †. https://pubs.acs.org/sharingguidelines 4 February 2021.

U.S. Food and Drug Administration. 2019. Generally Recognized as Safe (GRAS) | FDA. *Official website of the United States Government*. https://www.fda.gov/food/food-ingredients-packaging/generally-recognized-safe-gras 14 April 2021.

Vippagunta, S.R., Brittain, H.G. & Grant, D.J.W. 2001. Crystalline solids. *Advanced Drug Delivery Reviews*, 48(1): 3–26.

Wang, Z., Wang, Y., Vilekar, P., Yang, S.P., Gupta, M., Oh, M.I., Meek, A., Doyle, L., Villar, L., Brennecke, A., Liyanage, I., Reed, M., Barden, C. & Weaver, D.F. 2020. Small molecule therapeutics for COVID-19: Repurposing of inhaled furosemide. *PeerJ*, 2020(7): 1–21.

Yuengsrigul, A., Chin, T.W. & Nussbaum, E. 1999. Immunosuppressive and cytotoxic effects of furosemide on human peripheral blood mononuclear cells. *Annals of Allergy, Asthma and Immunology*, 83(6 I): 559–566.

Chapter 2

Experimental Section

2.1 Materials

2.1.1 Solvents and chemicals

Furosemide (FUR) drug was purchased in its pure form from Sigma Aldrich® and used without any further purifications. The supplementary coformers used for the multicomponent crystals (MCCs) formation experiments were also purchased from Sigma Aldrich® in an analytical grade and were used without further purification (Fig 2.1 and 2.2).

The selected coformers have functional groups that complement the API of choice (furosemide) for the formation of MCCs assembled via hydrogen bonds. A knowledge-based approach (hydrogen-bond propensity, synthon engineering, and supramolecular compatibility) by Cambridge Structural Database (CSD) was applied in this research to select coformers. Based on the screening results of furosemide, it was observed that the coformers (pyridine: PYR, 3-picoline: 3PIC, 4-picoline: 4PIC, 2,3-lutidine: 23LUT, and 2,4-lutidine: 24LUT) had the potential to cocrystallise with furosemide. The molecular structure of furosemide and the selected coformers are shown in Figures 2.1 and 2.2, and the properties of the compounds are summarised in Tables 2.1 and 2.2.

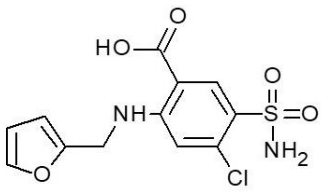

Figure 2. 1 Line diagram of furosemide

Table 2. 1 Properties of furosemide

API Name	Molecular Formula	Mr (g/mol)	pKa	Experimental Melting point °C	Solubility in H_2O @30°C mg/L
Furosemide (FUR)	$C_{12}H_{11}ClN_2O_5S$	330.75	4.25	220	73.1

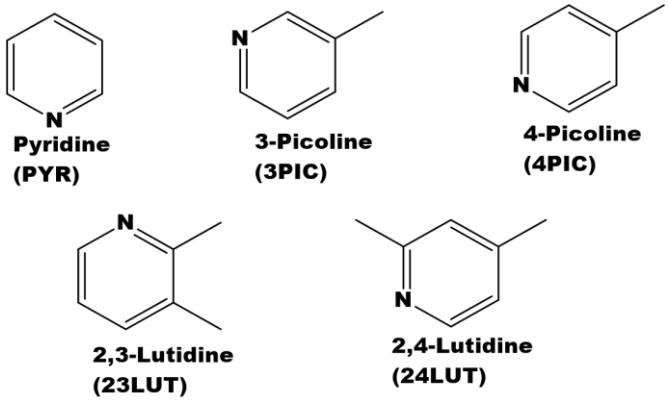

Figure 2. 2 Line diagrams of selected coformers

Table 2. 2 Properties of selected coformers

Chemical Name	Chemical Formula	Molecular Mass g/mol	Boiling Point °C	pKa*
Pyridine (PYR)	C_5H_5N	79.10	115.4	5.12
3-Picoline (3PIC)	C_6H_7N	93.13	144	5.63
4-Picoline (4PIC)	C_6H_7N	93.13	145	5.85
2,3-Lutidine (23LUT)	C_7H_9N	107.15	163	6.28
2,4-Lutidine (24LUT)	C_7H_9N	107.15	158.5	6.58

* Calculator Plugins were used for structure-property prediction and calculation. Marvin 16.4.25.0, 2016.

2.2 Multicomponent crystal formation

2.2.1 Mechanochemical method

The grinding method was utilised in the screening for a potential hit between the API and coformers. This is a versatile approach that researchers in the supramolecular and pharmaceutical field have widely used to screen and synthesise multicomponent crystals. Two grinding methods exist, namely liquid assisted and solid-state grinding, also known as neat grinding. Liquid assisted grinding (LAG) was the primary method employed in this work to screen the possibility of forming multicomponent crystals of the API with the selected coformers. This

method is cost-effective, rapid, and environmentally friendly. It can afford cocrystals more reliably than neat grinding, which often gives poor quality cocrystals, i.e. with low crystallinity.

Furosemide (0.05 g – 0.1 g) was weighed into a mortar and crushed with a pestle, and mixed with 2–3 ml of each of the liquid coformers. A paste was formed and ground for at least 30 minutes to ensure that the desired reaction between the API and the coformer occurred. The resultant product was then transferred into a vial and analysed by different analytical techniques, including FTIR, DSC, TGA, and PXRD. The obtained data from each technique were compared with the pristine API. The difference in the phase of the API with the coformers and the pristine API infers a successful formation of a new product.

2.2.2 Slow evaporation crystallisation

The following MCCs were isolated and characterised in this research, codified as follows: FUR·PYRw, FUR·3PIC, FUR·4PIC, FUR·23LUT and FUR·24LUTw. The API was weighed (0.1-0.2 g) into a vial, and a liquid coformer of a stoichiometric ratio was added to the vial. This mixture was then stirred on a hot plate at 40-60 °C to obtain a homogeneous solution. Afterwards, the homogenised solution was left to cool to ambient temperature, and the mixture was sealed with a perforated parafilm to foster slow evaporation of the solvent. After two to four weeks, needle-like or block-like crystals were observed in the different vials. Varying sizes of the vials were used to determine any differences between the crystals formed in a smaller or bigger surface area. As a result, it was observed that high-quality crystals suitable for single crystal X-ray analysis (SCXRD) were formed in the small vials, however, some crystals from larger vials could also be analysed by SCXRD.

Table 2.3: Coformers and the drug quantities used for synthesis of the MCCs.

Drug:Coformer	Mass (g)	Amount (ml)
FUR:PYR	0.0388	2
FUR:3PIC	0.0534	2
FUR:4PIC	0.1657	2
FUR:2,3LUT	0.1003	2
FUR:2,4LUT	0.1959	2

This technique involves nucleation and growth of a cocrystal from a saturated solution of both the coformer and API followed by allowing the process of evaporation to take place. It is also important to ensure that complete dissolution occurs between the two components, and failure to achieve this could result in precipitation of one of the components without achieving a suitable crystal for diffraction studies.

It should also be noted that this technique comes with various disadvantages. Obtaining crystals could take up to 6 months, and obviously, this hinders the progress of the research project. This issue was noted with FUR·24LUTw, which occurred only after two months after preparation. However, there are proven ways, which can be applied to accelerate the rate of evaporation, like changing the environment in which the reaction is conducted, but this does not always work. Ideally,elevated temperatures afford an increased rate at which the crystals can be formed. Sugandha and co-workers showed this by carrying out evaporation of methanol from a stoichiometric solution of ezetimibe and methyl paraben in methanol at 35 °C using a water bath. A powder cocrystal sample was obtained by evaporating (to dryness) an unidentified organic solvent from a solution of curcumin and phloroglucinol under vacuum using a rotary evaporator at 60 °C (Sugandha *et al*.,2014).

2.3 Analytical techniques for characterisation

2.3.1 Thermal Analysis

Thermal analytical techniques are some of the general techniques used in supramolecular chemistry and provide vital information for characterisation of amorphous and crystalline forms like crystals, cocrystals, polymorphs, solvates, and hydrates (Beyer *et al*.,2000).

Thermogravimetric analysis (TGA) was used to monitor the physical behaviour, specifically the mass of a material when exposed to a controlled temperature program in a set environment. TGA was used to quantify water or solvent content and losses. The thermal analysis data were acquired on a Perkin Elmer Pyris 6 thermogravimetric analyser equipped with nitrogen gas as a purge gas at a flow rate of 20 ml/min was used with the programmed temperature set from 30° C to 350°C at a ramp rate of 10°C /min during sample analysis.

The solid crystalline material was scooped from the vial and ground to small particles in a mortar and pestle. The solid material was reduced to fine particles because the results are influenced by the size, purge gas flow rate and sample heating rate. The ground sample of 3-5 mg for each analysis was inserted in the sample holder using a spatula. TGA was used to measure the sample mass loss during heating over a controlled temperature range. The onset temperature was used to determine sample decomposition and, in this case, the loss of a volatile component. The quantitation of the mass loss of the volatile coformer was used to confirm the stoichiometry.

Differential Scanning Calorimetry (DSC) was used to obtain accurate melting temperatures of the MCCs or any other enthalpy associated phase changes. The difference between the sample and reference heat flow rate were measured under a controlled temperature program. Crystalline samples of pure furosemide and each MCC of about (2-3 mg) were weighed individually using the ventilated aluminium pans: the same empty pan was used as a reference. The samples were analysed using the DSC 6000 from Perkin Elmer heated at a temperature of 30 °C to 250 °C at a heating rate of 10 °C /min. Nitrogen gas with a flow rate of 20 ml/min was applied to maintain the inert atmosphere.

DSC plays an important role in characterisation of crystal structures, as it provides accurate value for melting-onset temperature of solid forms. Additionally, this information can be used to confirm the formation of a multicomponent crystal by determining the differences in the phase changes such as melting point or polymorphic transition. The loss of volatile cocrystal components is also readily evident in this process. Herein, this technique was used to evaluate the melting point, purity and phase transition of the MCCs.

2.3.2 Fourier transform infrared spectroscopy

Spectroscopic techniques are usually considered as complementary techniques to X-ray based diffraction techniques. X-ray diffraction-based methods explicitly show the detailed structural information of materials, whereas spectroscopic methods are limited and only reveal the functional groups or atoms present in a structure. Fourier transform infrared spectroscopy (FTIR) is particularly useful to confirm protonation states of molecules, i.e. comparing salts vs. cocrystal compounds. A Perkin Elmer Attenuated Total Reflectance Two FTIR in the wavelength range of

400-4000 cm^{-1} was used to give a characteristic fingerprint of the obtained crystalline forms. A sufficient amount of the material was scooped with a spatula and placed on the diamond sample holder, and pressed using the gauge handle with a foot fixated on it.

The functional groups that were of interest in this research were the carbonyl group, hydroxyl group, the sulfonamide group, and the primary and secondary amine groups. Studying the changes in these moieties helped in the verification of the type of MCC (solvate, hydrate, cocrystal or salt) formed. The bulk material of the MCC obtained was analysed to evaluate any significant changes that occurred in the group frequency and fingerprint region. The spectra of the pure API and that of the synthesised MCC were superimposed to identify any changes in their moieties.

2.3.3 Diffraction methods

X-ray diffractometry techniques such as powder X-ray diffraction (PXRD) and single crystal X-ray diffraction (SCXRD) are powerful techniques for the identification and stoichiometric determination of crystals.

2.3.3.1 Powder x-ray diffraction (PXRD)

Powder X–ray diffraction analysis (PXRD) was used to identify crystalline forms. This is a common technique usually used together with SCXRD, and it is mainly used for the screening and determination of multicomponent crystal structures after they have been identified using SCXRD. Usually, the PXRD method is considered a reliable method for screening polymorphs however, it often fails to distinguish between true polymorphs (Healy *et al*., 2017). For this reason, it is necessary to use other techniques like the FTIR to validate the MCCs further, as was done herein. Particularly, this technique does not require high-quality single crystals to conduct the analysis.

The crystalline sample representing the bulk material was ground in a mortar and pestle to form a fine solid. This microcrystalline material was placed in a zero-background sample holder and spread evenly. The PXRD patterns were recorded on a Bruker® D2 Phaser X-ray powder diffractometer equipped with a LynxEye® detector (proportional counter), using Cu Kα radiation (λ = 1.5405 Å, nickel filter). XRD data were obtained at a scanning rate of 1° min^{-1} with a filter

time–constant of 2.5 s per step and a slit width of 6.0 mm. Samples were placed on a zero-background silicon wafer slide at an angular range of 2θ = 5°- 40° with the voltage and current tubes at 30 kV and 10 mA, respectively. The XRD data were processed using EVA® (evaluation curve fitting) software. Baseline corrections were performed on each diffraction pattern if it was necessary.

2.3.3.2 Single crystal x-ray diffraction (SCXRD)

Single crystal x-ray diffraction is an analytical technique that is used to determine with certainty the actual arrangement of atoms and/or ions within a crystal structure (Campana & Corporation, 2015). In general, this is done by scattering X-rays on electrons to extract structure factors from reflection densities as well as their Fourier transform data to calculate electron density maps. The SCXRD gives information on intermolecular interactions and interatomic distances, extending to the geometrical structure of molecules and molecular solids.

The SCXRD data were collected using a Bruker® DUO APEX II diffractometer with a graphite-monochromated Mo Kα radiation (λ= 0.71073 Å) at 173 K using Oxford Cryostream 700. A single crystal was scooped from the vial with the bulk material and analysed at 173 or 100K.

To ensure that the single crystal is representative of all the crystals in the bulk material, the diffraction pattern generated from the SCXRD and that from the PXRD was superimposed to identify similarities or differences.

2.3.4 Crystal structure determination

The crystal structures were solved using SHELXS-2016 (Sheldrick, 2015a)which employs a conventional structure-factor summation with complex scattering factors to perform full-matrix, blocked full-matrix, or conjugate-gradient least-squares refinement. SHELXL can be used to refine both small molecule and inorganic structures (Sheldrick, 2008). SHELXL-2016 was run under a graphical user interface, X-Seed (Sheldrick, 2015b; Barbour, 2001). The space groups were determined by collecting the intensities and predefined cell parameters inputs into the XPREP program (Poleti *et al*., 2003). SHELXL-2016 was used to directly solve all crystal structures and to refine them using full-matrix least-squares against F^2 for unique reflection.

$$\sum w(F_0^2 - kF_c^2)^2 \qquad \text{Eq. 1}$$

The residual index R was used to monitor the agreement between the observed structure factors (F_o) and the calculated structure factors (F_c). The residual index R_1 represents the agreement between observed and calculated structure factors when F is used, whereas the residual index R_2 represents the agreement when F^2 is used.

$$R_1 = \frac{\sum||F_o| - |F_C||}{\sum|F_o|} \qquad \text{Eq. 2}$$

$$R_2 = \left[\frac{\sum w\left(F_o^2 - F_c^2\right)^2}{\sum w(F_o^2)^2}\right]^{1/2} \qquad \text{Eq. 3}$$

The weighing scheme *w* was used to generate a constant distribution in terms of *a* and *b*, which was then refined further during the structure refinement final cycles.

$$w = \frac{1}{\sigma^2\left(F_0^2\right) + (aP)^2 + bP} \qquad \text{Eq. 4}$$

Where:

$$P = \frac{\max\left(o, F_0^2\right) + 2F_c^2}{3} \qquad \text{Eq. 5}$$

SHELXL-2016 refines against F^2, which results in a greater deviation from unity in the Goodness of fit (S) than refinement against F. The Goodness of fit (GoF) expression is:

$$S = \left[\frac{\sum w(|F_o|^2 - |F_c|^2)^2}{\left(N - n_p\right)^2}\right]^{\frac{1}{2}} \qquad \text{Eq. 6}$$

Hydrogen atoms bound to carbon atoms were idealised and refined as riding atoms with **Uiso (H)** = 1.2 Ueq (Ar-H, CH_2) or 1.5 Ueq (CH_3) of the carbon atom to which the H is bound. If possible, the hydrogen atoms bonded to carboxylic acids and amines were located in the difference electron density map and their coordinates refined freely, but their isotropic displacement parameters were fixed (Uiso (H) = 1.2 Ueq (O) or Ueq (N) as needed.

Calculated X-ray powder patterns were compared to experimental powder patterns for crystallisation using LAZY PULVERIX. POV-RAY was used to generate all of the crystal diagrams. The program LAYER was used to examine systematic absences and the symmetry of space groups. SHELXL-2016, LAZY PUVERIX, POV-RAY, and LAYER all used X-Seed as their graphical user interface (Barbour, 1999; Yvon *et al*., 1977).

2.4 Computational methods

2.4.1 Cambridge Structural Database (CSD)

The Cambridge Structural Database (CSD) is used to deposit crystal structures once they are reviewed. It is the largest repository of small molecule crystal structures where information related to the crystal structures is recorded as well as the crystallographic information for organic and organometallic compounds (Groom *et al.*, 2016). In addition, the structures of single crystals and powder diffraction studies that yield 3D atomic coordinates are captured in the CSD. Herein the CSD was used to search for the hits of furosemide MCCs available, and it was also used to find and select the suitable coformers for MCC synthesis.

2.4.2 Mercury

Analysis software Mercury includes features for investigating and analysing crystal structures. It can be used to import data such as chemical bond types and two-dimensional connection tables and present them in a three-dimensional illustration. It generates packing diagrams, defines and visualises Millers planes, and takes any direction of a slice through a crystal. Additionally, it displays space group symmetry elements, calculates voids based on either the contact surface or the solvent-accessible surface, and intermolecular potentials, as well as performing basic gas phase calculations (MacRae *et al*., 2020).

2.5 Computing components

Conquest: the primary program for advanced structure searching and information retrieval in the Cambridge Structural Database (CSD) (Bruno *et al*., 2002; Groom *et al*., 2016).

SADABS: an APEX application used to scale and correct data collected on a Bruker AXS area detector for absorption. The program is designed to exploit data redundancy and to correct errors caused by the variation in the volume of crystal, absorption by the crystal support and crystal decay during the measurement

XPREP: this program is used to analyse and manipulate data. It determines the space group and reads the raw data file (.raw) and the parameter file (.p4p) generated by the diffractometer control program. Additionally, it creates an instruction file (.ins) and data for reflection (hkl) (Barbour, 2001; Sheldrick, 2015b)

Pov-Ray: a program that generates three-dimensional high-resolution images (Cason *et al*., 2013).

References

Aitipamula, S., Banerjee, R., Bansal, A.K., Biradha, K., Cheney, M.L., Choudhury, A.R., Desiraju, G.R., Dikundwar, A.G., Dubey, R., Duggirala, N., Ghogale, P.P., Ghosh, S., Goswami, P.K., Goud, N.R., Jetti, R.R.K.R., Karpinski, P., Kaushik, P., Kumar, D., Kumar, V., Moulton, B., Mukherjee, A., Mukherjee, G., Myerson, A.S., Puri, V., Ramanan, A., Rajamannar, T., Reddy, C.M., Rodriguez-Hornedo, N., Rogers, R.D., Row, T.N.G., Sanphui, P., Shan, N., Shete, G., Singh, A., Sun, C.C., Swift, J.A., Thaimattam, R., Thakur, T.S., Kumar Thaper, R., Thomas, S.P., Tothadi, S., Vangala, V.R., Variankaval, N., Vishweshwar, P., Weyna, D.R. & Zaworotko, M.J. 2012. Polymorphs, salts, and cocrystals: What's in a name? *Crystal Growth and Design*, 12(5): 2147–2152. https://pubs.acs.org/sharingguidelines.

Beyers,H., Malan,S.F., van der Watt,J.G. & de Villiers,M.M. 2000. Structure-Solubility Relationship and Thermal Decomposition of Furosemide. Drug Development and Industrial Pharmacy,26(10):1077-1083.

Barbour, L.J. 1999. LAYER - A computer program for the graphic display of intensity data as simulated precession photographs. *Journal of Applied Crystallography*, 32(2): 351–352. http://scripts.iucr.org/cgi-bin/paper?gl0581 1 December 2021.

Barbour, L.J. 2001. X-seed - A software tool for supramolecular crystallography. *Journal of Supramolecular Chemistry*, 1(4–6): 189–191.

Bruno, I.J., Cole, J.C., Edgington, P.R., Kessler, M., Macrae, C.F., McCabe, P., Pearson, J. & Taylor, R. 2002. New software for searching the Cambridge Structural Database and visualising crystal structures. *Acta Crystallographica Section B: Structural Science*, 58(3 PART 1): 389–397. http://scripts.iucr.org/cgi-bin/paper?an0609 1 December 2021.

Calculator Plugins were used for structure-property prediction and calculation, M., 2016, ChemAxon(http://www.chemaxon.com). #The pKa prediction is done on the basis of the partial charge distribution calculated for the atoms in the molecule and this method provides an efficient and robust way to locate the most acidic and basic sites."

Cason, C., Froehlich, T., Lipka, C. & 3.7, V. 2013. POV-Ray - The Persistence of Vision Raytracer.

: version 3.7. http://www.povray.org/.

Groom, C.R., Bruno, I.J., Lightfoot, M.P. & Ward, S.C. 2016. The Cambridge structural database. *Acta Crystallographica Section B: Structural Science, Crystal Engineering and Materials*, 72(2): 171–179. http://dx.doi.org/10.1107/S2052520616003954171.

MacRae, C.F., Sovago, I., Cottrell, S.J., Galek, P.T.A., McCabe, P., Pidcock, E., Platings, M., Shields, G.P., Stevens, J.S., Towler, M. & Wood, P.A. 2020. Mercury 4.0: From visualisation to analysis, design and prediction. *Journal of Applied Crystallography*, 53(Pt 1): 226–235. /pmc/articles/PMC6998782/ 30 November 2021.

PHOTON III - Detector, Single Crystal X-ray Diffraction - Detectors - Single Crystal X-ray Diffraction | Bruker. Available at: https://www.bruker.com/products/x-raydiffraction- and-elemental-analysis/single-crystal-x-ray-diffraction/sc-xrdcomponents/ sc-xrd-components/overview/sc-xrd-components/detectors/photoniii. html?gclid=Cj0KCQjwh8jrBRDQARIsAH7BsXckgx4tB2KCy1AaA6w7qPcK72VXku. (*Accessed: 10 October September 2021*)

Poleti, D., Balić-Žunić, T., Hope, H. & Karanović, L. 2003. A BEGINNER ' S GUIDE TO THE BRUKER AXS PACK and other noble time wasters. *Bruker-AXS*: 106.

POV-Ray - The Persistence of Vision Raytracer. Available at: http://www.povray.org/. (Accessed: 10 October 2021)

Sheldrick, G.M. 2008. A short history of SHELX. *Acta Crystallographica Section A: Foundations of Crystallography*, 64(1): 112–122.

Sheldrick, G.M. 2015. Crystal structure refinement with SHELXL. *Acta Crystallographica Section C: Structural Chemistry*, 71(1): 3–8. http://scripts.iucr.org/cgi-bin/paper?fa3356 1 December 2021.

Sugandha,K., Kaity,S., Mukherjee,S., Isaa,J.& Animesh,G.2014. Solubility Enhancement of Ezetimibe by a Cocrystal Engineering Technique.*Crystal Growth Design*,14(9):4475-4486

Yvon, K., Jeitschko, W. & Parthé, E. 1977. LAZY PULVERIX , a computer program, for calculating X-ray and neutron diffraction powder patterns. *Journal of Applied Crystallography*, 10(1): 73–74. //scripts.iucr.org/cgi-bin/paper?a15322 1 December 2021.

Chapter 3

Discussion of crystal structures

In this chapter, the crystal structures of furosemide (FUR) with pyridine (PYR) and its derivatives including 3-methyl pyridine or 3-picoline (3PIC), 4-methyl pyridine or 4-picoline (4PIC), 2,3-dimethyl pyridine or 2,3-lutidine (23LUT), and 2,4-dimethyl pyridine or 2,4-lutidine (24LUT) are presented. The cocrystallisations of these multicomponent crystals (MCCs) were carried out by the slow evaporation crystallisation (SEC) method, and the details are given in Chapter 2.

3.1 The crystal structure of FUR·3PIC

Furosemide was crystallised with 3-picoline and resulted in crystals of FUR·3PIC that contain 1:1 ratio of the drug and the solvent molecule, thus the crystal can be classified as a solvate (Grothe et al., 2016). The crystal structure was solved in the centrosymmetric triclinic space group of *P*-1 (No. 2) with one molecule of FUR and one molecule of 3PIC in the asymmetric unit (ASU). The crystal data and hydrogen bonds are listed in Tables 3.1 and 3.2. An intramolecular hydrogen bond is formed between the secondary amine and the carbonyl group (N2-H2···O3). The prominent interaction between the drug and the solvent molecule is the carboxylic acid-aromatic amine hydrogen bond (O4-H4···N3), but no interaction is noted between the ortho-hydrogen (H17) and the carbonyl oxygen (O3) atoms (Fig. 3.1). The protonated nature of the carboxylic acid group was supported by the heavy atom distances that resemble a double and a single C-O bond (C7-O3: 1.2363(15) Å) and C7-O4: 1.3038(15) Å, respectively).

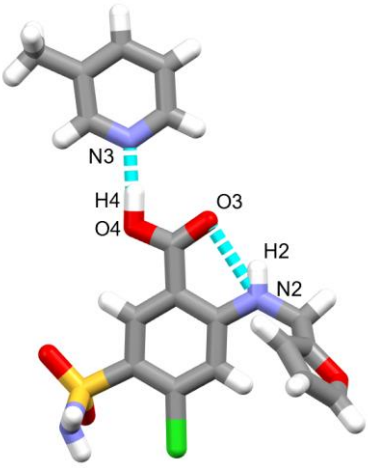

Figure 3. 1 The ASU of FUR·3PIC with the relevant hydrogen bonds.

Table 3. 1 Crystallographic data of FUR·3PIC

Compounds	FUR·3PIC
Molecular formula	$C_{18}H_{18}N_3O_5SCl$
Formula weight (g.mol^{-1})	423.86
Crystal system	triclinic
Space group (No.)	*P*-1 (No. 2)
a (Å)	7.2607(3)
b (Å)	11.1014(5)
c (Å)	11.1014(5)
α (°)	107.2970(10)
β (°)	91.1100(10)
γ (°)	101.3440(10)
V (A^3)	940.75(7)
Z	2
ρ_{calc}(g.cm^{-3})	1.496
μ(MoKα) (mm^{-1})	0.351
F(000)	440.0
Crystal size(mm)	0.189 × 0.152 × 0.037
Temperature (K)	173(2)
Radiation (Å)	MoKα, 0.71073
2Theta min-max (°)	3.422 to 59.194
Dataset (±h; ±k; ±l)	-10 ≤ h ≤ 10, -15 ≤ k ≤ 15, -17 ≤ l ≤ 17
Reflections collected	53828
Independent reflections	5282 [R_{int} = 0.0327, R_{sigma} = 0.0161]
Data/restraints/parameters	5282/0/258
Goodness-of-fit on F^2	1.046
Final R indices [I>2σ(I)]	R_1 = 0.0321, wR_2 = 0.0835
Final R indexes [all data]	R_1 = 0.0354, wR_2 = 0.0859
Largest diff. peak/hole / e Å^{-3}	0.50/-0.46

Table 3. 2 Hydrogen bonding found in FUR·3PIC

D-H···A	d(D-H) (Å)	d(H···A) (Å)	d(D···A) (Å)	D-H···A (°)	Symmetry operators
O4-H4···N3	0.979	1.585	2.558	172.28	
N2-H2···O3	0.820	2.049	2.696	135.58	
N1-H1A···O3	0.857	2.083	2.913	162.87	[-x+1, -y+1, -z+1]
N1-H1B···O2	0.820	2.194	2.992	164.43	[-x, -y, -z+1]

The main supramolecular unit of the crystal is a dimer formed between two FUR moieties. This was concluded by calculating the intermolecular potentials using the UNI force field (Gavezzotti & Filippini, 1994) with normalised hydrogen atom positions (Fig. 3.2). The highest interaction energy (-98.3 KJ mol^{-1}) was noted between two FUR units—from now on called the dimer—that are hydrogen-bonded via N1-H1A···O3 bonds formed between the sulfonamide and the carboxylic acid groups. The hydrogen bond pattern of the dimer can be described with the

$R_2^2(16)$ graph set. The distance between the two planes of the benzene rings is 3.39 Å (Fig. 3.3). The second highest interaction value (-87.0 KJ mol^{-1}) suggests that these dimers are interacting with neighbouring dimers via aromatic interactions (3.37 Å) and forming molecular columns in the [100] direction. Interestingly, the distance between the rings that interact stronger, i.e. in the dimer, is longer. Hence the interaction energy calculation considers all interactions between the selected molecular pairs, the longer distance between the rings is only an indicator that the aromatic interactions contribute less to the dimer formation. The other prominent interaction in the FUR·3PIC crystal is the centrosymmetric sulfonamide dimer formed via N1-H1B···O2 hydrogen bonds. This interaction can be described by the $R_2^2(8)$ graph set.

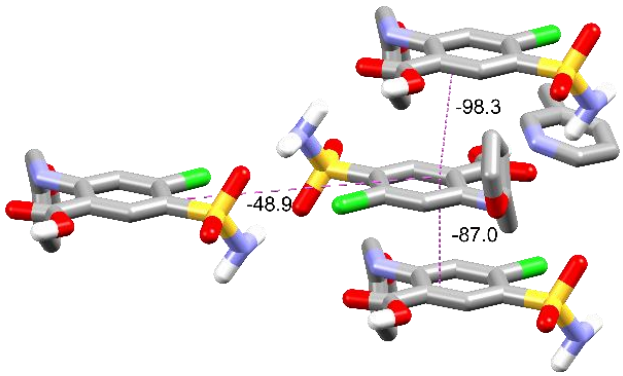

Figure 3. 2 The interaction energies in KJ mol^{-1} between neighbouring FUR molecules in FUR·3PIC.

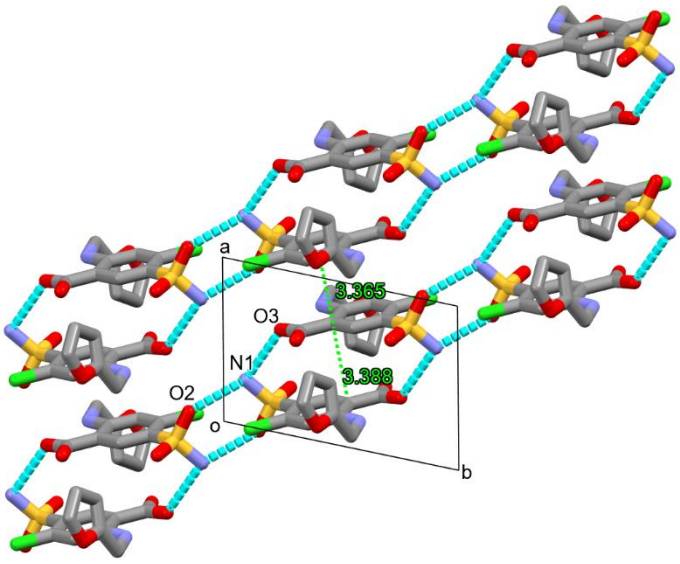

Figure 3. 3 Hydrogen bonds and ring distances in FUR·3PIC. Solvent molecules were omitted for clarity.

The solvent molecules are positioned in channels running parallel to the *a* axis (Fig. 3.4). The tubulate nature (Nassimbeni, 2003) of the structure was proved by calculating the solvent accessible surface with a probe radius of 1.2 Å and an approximate 0.7 Å grid spacing (Fig. 3.5).

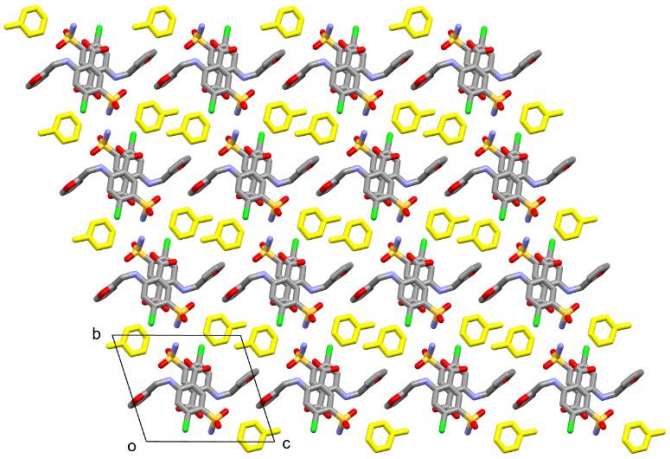

Figure 3. 4 The packing diagram of FUR·3PIC viewed down the a axis. (3PIC molecules are yellow and the hydrogen atoms are omitted for clarity.)

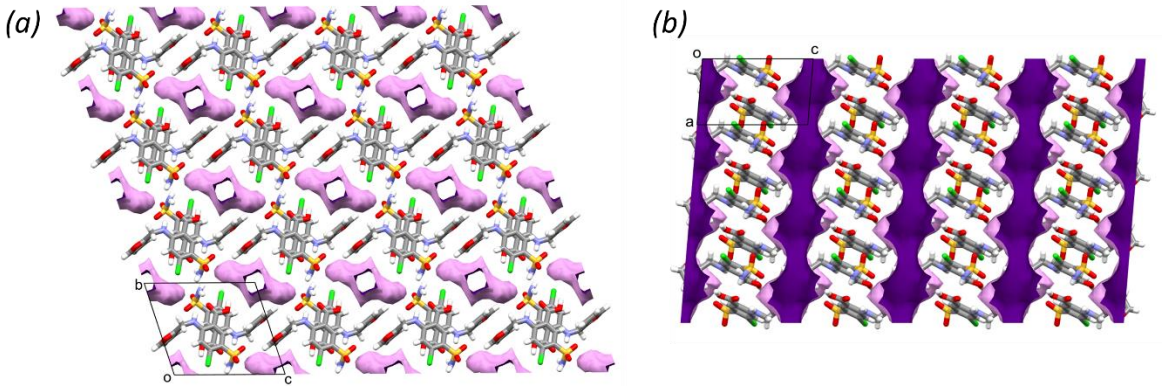

Figure 3. 5 Solvent accessible surface in FUR·3PIC view down the a axis (a) and down the b axis (b) in FUR·3PIC. Solvent molecules were omitted for clarity.

3.2 The crystal structure of FUR·4PIC

Furosemide was crystallised with 4-picoline and resulted in crystals containing 1:1 ratio of the drug and the solvent. The crystal structure was solved in the centrosymmetric triclinic space group of *P*-1 (No. 2) with one molecule of FUR and one molecule of 4PIC in the ASU. The crystal data and hydrogen bonds are listed in Tables 3.3 and 3.4. Like the FUR·3PIC structure, an

intramolecular hydrogen bond is formed between the secondary amine and the carbonyl group (N2-H2···O3). The carboxylic acid protonated the solvent molecule, thus the crystal can be classified as a true salt (Grothe *et al*., 2016). The position of the hydrogen atom was thoroughly investigated. The difference electron density map (Fig. 3.6a) revealed an elongated high electron density area between N3 and O4 atoms, and this suggested that the crystal is a representation of the so-called *salt-cocrystal continuum* protonation stage, i.e. the H4 hydrogen atom can be found bonded to O4 (cocrystal) and also can be bonded to the N3 (salt). First, a disordered H4 atom was modelled, but the refinement of the site occupancies was unsuccessful. The best result was obtained when the 4PIC moiety was protonated. This model is supported by the heavy atom distances of the carboxylate moiety (C7-O3: 1.2489(14) Å and C7-O4: 1.2882(14) Å, respectively). The prominent interaction between the drug and the solvent molecule is the charge assisted hydrogen bond formed between the carboxylate and the pyridinium moieties (N3-H4···O4) (Fig. 3.6a).

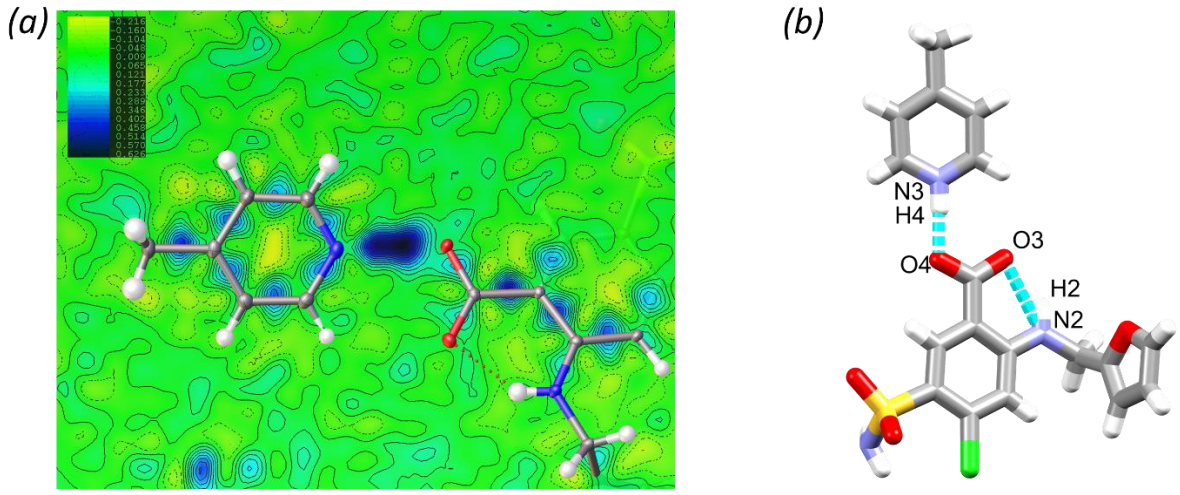

Figure 3. 6 The difference electron density map (a) and (b) the ASU of FUR·4PIC with the relevant hydrogen bonds.

Table 3. 3 Crystallographic data of FUR·4PIC

Compounds	FUR·4PIC
Molecular formula	$C_{18}H_{18}N_3O_5SCl$
Formula weight (g.mol^{-1})	423.86
Crystal system	triclinic
Space group (No.)	*P*-1 (No. 2)
a (Å)	8.4206(5)
b (Å)	10.9902(7)
c (Å)	12.1116(8)
α (°)	63.6330(10)
β (°)	70.7870(10)
γ (°)	78.2130(10)
V (A^3)	946.08(10)
Z	2
ρ_{calc} (g.cm^{-3})	1.488
μ (MoKα) (mm^{-1})	0.349
F(000)	440.0
Crystal size(mm)	0.182 × 0.108 × 0.069
Temperature (K)	173(2)
Radiation (Å)	MoKα, 0.71073
2Theta min-max (°)	3.9 to 59.246
Dataset (±h; ±k; ±l)	-11 ≤ h ≤ 11, -15 ≤ k ≤ 15, -16 ≤ l ≤ 16
Reflections collected	57161
Independent reflections	5308 [R_{int} = 0.0300, R_{sigma} = 0.0145]
Data/restraints/parameters	5308/0/257
Goodness-of-fit on F^2	1.038
Final R indices [I>2σ(I)]	R_1 = 0.0302, wR_2 = 0.0793
Final R indexes [all data]	R_1 = 0.0327, wR_2 = 0.0808
Largest diff. peak/hole / e Å^{-3}	0.50/-0.49

Table 3. 4 Hydrogen bonding found in FUR·4PIC

D-H···A	d(D-H) (Å)	d(H···A) (Å)	d(D···A) (Å)	D-H···A (°)	Symmetry operators
N3-H4···O4	0.880	1.645	2.522	174.29	
N2-H2···O3	0.848	1.975	2.673	139.00	
N1-H1A···O2	0.840	2.276	3.050	153.45	[-x+1, -y+2, -z]
N1-H1B···O3	0.862	2.041	2.867	160.09	[-x+1, -y+1, -z+1]

The intermolecular potentials revealed that the main supramolecular unit is the FUR dimer (Fig. 3.7), which is held together by N1-H1B···O3 hydrogen bonds formed between the sulfonamide and the carboxylate oxygen atoms. The hydrogen bond pattern of the dimer—similar to the 3PIC solvate—can be described with the $R_2^2(16)$ graph set. The molecular conformation of the FUR moiety differs from the one in the FUR·3PIC structure, and consequently, the FUR dimers do not

form columns because of the steric hindrance caused by the furan ring. The distance between the two planes of the benzene rings is 3.22 Å (Fig. 3.8a). Centrosymmetric $R_2^2(8)$ sulfonamide dimers are formed via N1-H1A···O2 hydrogen bonds between the FUR dimers. The graphical representation of the solvent-accessible surface, mapped by 1.2 Å probe radius and 0.7 Å grid spacing, showed that the solvent molecules are positioned in zigzag channels running parallel to the *a* axis (Fig. 3.8b).

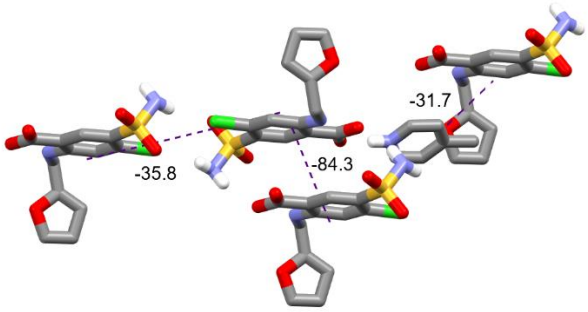

Figure 3. 7 The interaction energies in KJ mol^{-1} between neighbouring FUR molecules in FUR·4PIC.

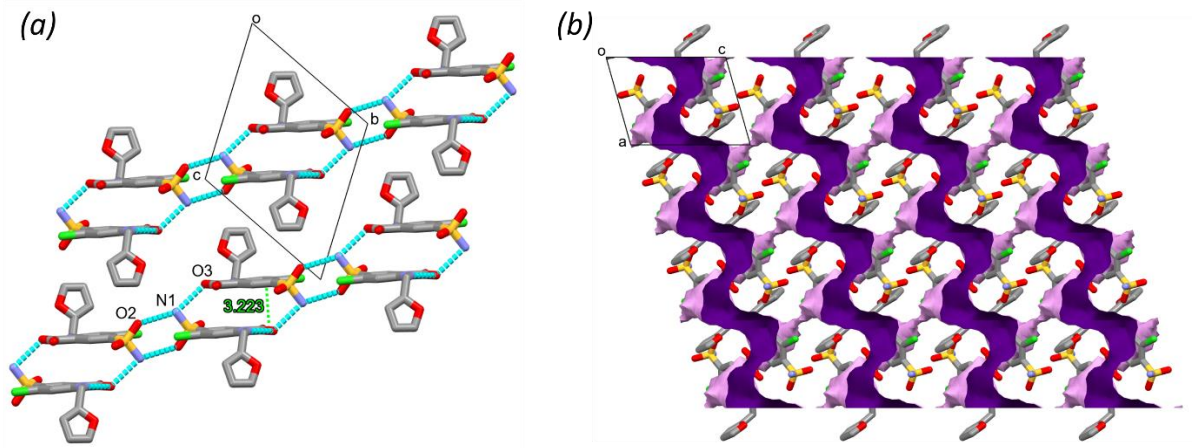

Figure 3. 8 Hydrogen bonds and ring distances (a) and solvent accessible surface in FUR·4PIC view down the b axis (b) in FUR·4PIC. Solvent molecules were omitted for clarity.

3.3 The crystal structure of FUR·23LUT

The crystal structure of FUR·23LUT was solved in the centrosymmetric monoclinic space group of $P2_1/n$ (No. 14) with one molecule of furosemide and one molecule of 2,3-lutidine (23LUT) in the ASU. The crystal data and hydrogen bonds are listed in Tables 3.5 and 3.6. The formation of

the intramolecular hydrogen bond between the secondary amine and the carbonyl group (N2-H2···O3) is observed. The deprotonated nature of the carboxylic acid group was suspected by evaluating the heavy atom distances (C7-O3: 1.2553(13) Å) and C7-O4: 1.2755(13) Å, respectively) and the H4 hydrogen atom was also found in the difference electron density map. The crystal was classified as a true salt (Grothe et al., 2016). The FUR and the 23LUT form charge assisted hydrogen bonds between the carboxylate and the pyridinium moieties (N3-H4···O4) (Fig. 3.9a). Contrary to the previous structures, the main packing feature of the crystal is the hydrogen-bonded molecular tapes formed by the FUR moieties via N1-H1B···O4 and N1-H1A···O3, which can be described with the $R_3^3(14)$ graph set (Fig. 3.9b). The mapping of the solvent-accessible surface of the 'emptied' structure (1.2 Å probe radius, 0.7 Å grid spacing)—i.e. when the solvent molecules are omitted—revealed that the voids are minimally interconnected.

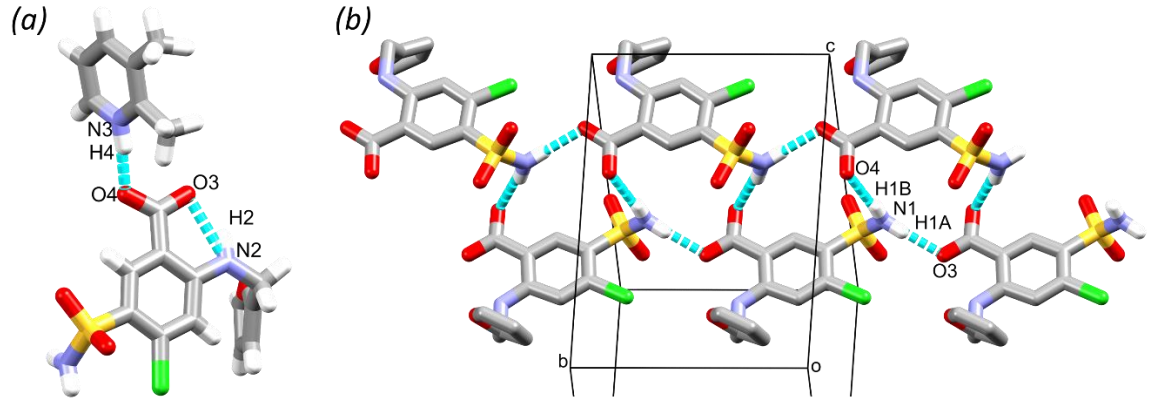

Figure 3. 9 The ASU (a) and the relevant hydrogen bonds (b) in FUR·23LUT. Solvent molecules were omitted for clarity on part b.

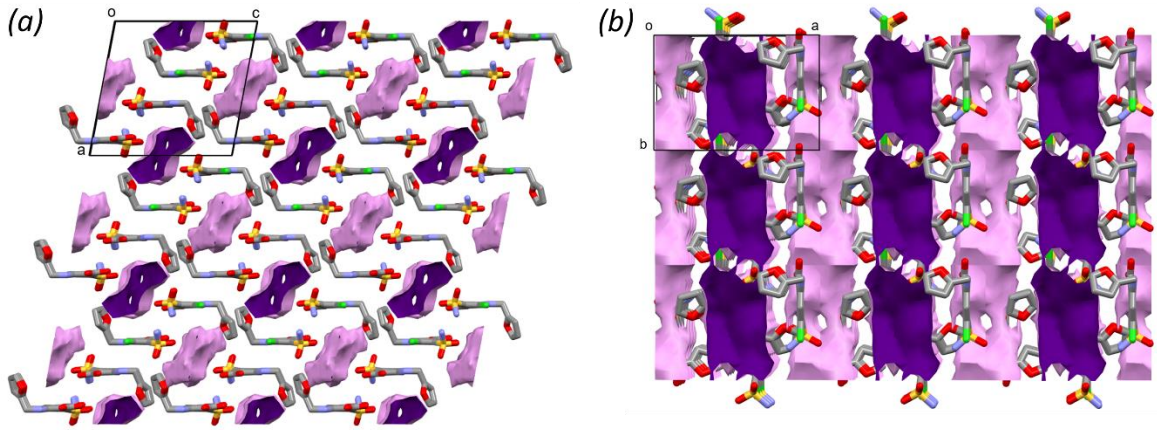

Figure 3. 10 Solvent accessible surface in FUR·23LUT view down the b axis (a) and down the a axis (b). Solvent molecules were omitted for clarity.

Table 3. 5 Crystallographic data of FUR·23LUT

Compounds	FUR·23LUT
Molecular formula	$C_{19}H_{20}N_3O_5SCl$
Formula weight (g.mol^{-1})	437.89
Crystal system	monoclinic
Space group (No.)	$P2_1/n$ (No. 14)
a (Å)	14.1621(7)
b (Å)	9.6366(5)
c (Å)	14.7725(7)
α (°)	90
β (°)	100.7990(10)
γ (°)	90
V (A^3)	1980.37(17)
Z	4
ρ_{calc} (g.cm^{-3})	1.469
μ (MoKα) (mm^{-1})	0.336
F(000)	912.0
Crystal size(mm)	0.268 × 0.21 × 0.172
Temperature (K)	173(2)
Radiation (Å)	MoKα, 0.71073
2Theta min-max (°)	3.656 to 59.178
Dataset (±h; ±k; ±l)	-19 ≤ h ≤ 19, -13 ≤ k ≤ 13, -20 ≤ l ≤ 20
Reflections collected	50795
Independent reflections	5561 [R_{int} = 0.0250, R_{sigma} = 0.0124]
Data/restraints/parameters	5561/0/268
Goodness-of-fit on F^2	1.053
Final R indices [I>2σ(I)]	R_1 = 0.0288, wR_2 = 0.0778
Final R indexes [all data]	R_1 = 0.0310, wR_2 = 0.0793
Largest diff. peak/hole / e Å^{-3}	0.41/-0.41

Table 3. 6 Hydrogen bonding found in FUR·23LUT

D-H···A	d(D-H) (Å)	d(H···A) (Å)	d(D···A) (Å)	D-H···A (°)	Symmetry operators
N3-H4···O4	0.917	1.713	2.623	170.47	
N2-H2···O3	0.851	1.943	2.656	140.68	
N1-H1A···O3	0.863	1.957	2.813	170.93	[x, y-1, z]
N1-H1B···O4	0.855	2.073	2.917	168.79	[-x+1/2, y-1/2, -z+3/2]

3.4 The crystal structure of FUR·24LUTw

The crystal structure of FUR·24LUTw was solved in the orthorhombic space group of $P2_12_12_1$ (No. 19) with one molecule of furosemide, one molecule of 2,4-lutidine (24LUT) and one molecule of water in the ASU. It is rather unexpected that an achiral compound, such as FUR, crystallises in a Sohncke (non-centrosymmetric chiral) space group. In addition, FUR is a conformational flexibility molecule, and it can be assumed that it would take up a conformation that would allow its crystallisation in a centrosymmetric space group (Pidcock, 2005). (The conformational flexibility of FUR will be investigated later). The crystal data and the details of the hydrogen bonds are listed in Tables 3.7 and 3.8. A careful examination of the thermal ellipsoids of the furan ring suggest that the ring may be disordered. The attempt to refine the disordered model resulted in an unstable refinement, thus the final model was an ordered solution with low R values and a residual electron density peak of 1.10 e $Å^{-3}$.) Like all the previous structures, there is an intramolecular hydrogen bond between the secondary amine and the carbonyl group (N2-H2···O4). The carboxylic acid group is deprotonated (C7-O3: 1.249(4)Å) and C7-O4: 1.274(3) Å), and the H4 hydrogen atom was located from the difference electron density map. The crystal is classified as a salt solvate (Grothe et al., 2016). The carboxylate group and the pyridine ring are close to co-planar (3.96°) and form two hydrogen bonds (N3-H4···O4 and C17-H17···O3) that can be described by the $R_2^2(7)$ graph set (Fig. 3.11a). Contrary to the previous structures, this crystal contains water. The ordered water molecules form hydrogen bonds with each other (O6-H6B···O6), and act both as acceptors and donors of hydrogen bonds (N1-H1A···O6 and O6-H6A···O3, respectively) with FUR moieties (Fig. 3.11b). The mapping of the solvent-accessible surface with a 1.2 Å probe radius and a 0.7 Å grid spacing shows the interconnected cavities occupied by the 24LUT and water molecules (Fig. 3.12).

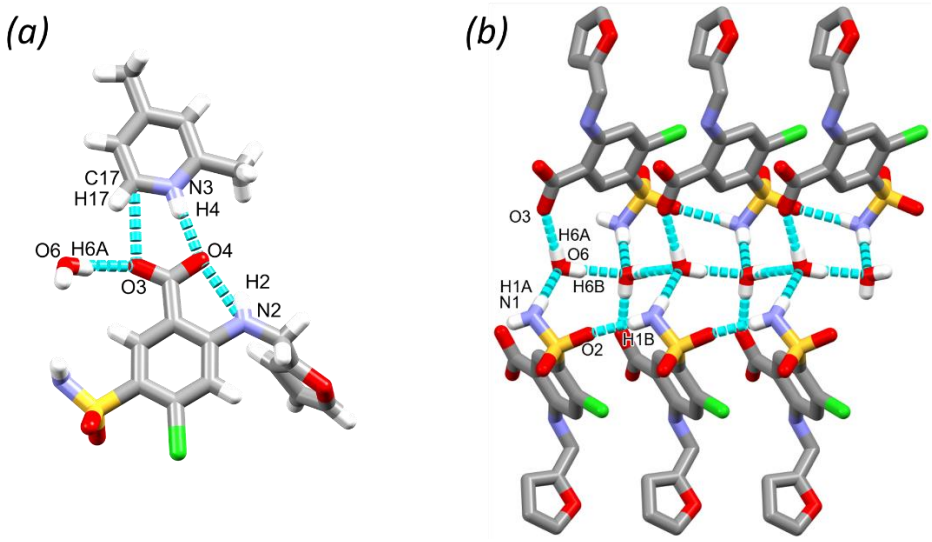

Figure 3. 11 The ASU (a) and the relevant hydrogen bonds (b) in FUR·24LUT. 24LUT molecules were omitted for clarity on part b.

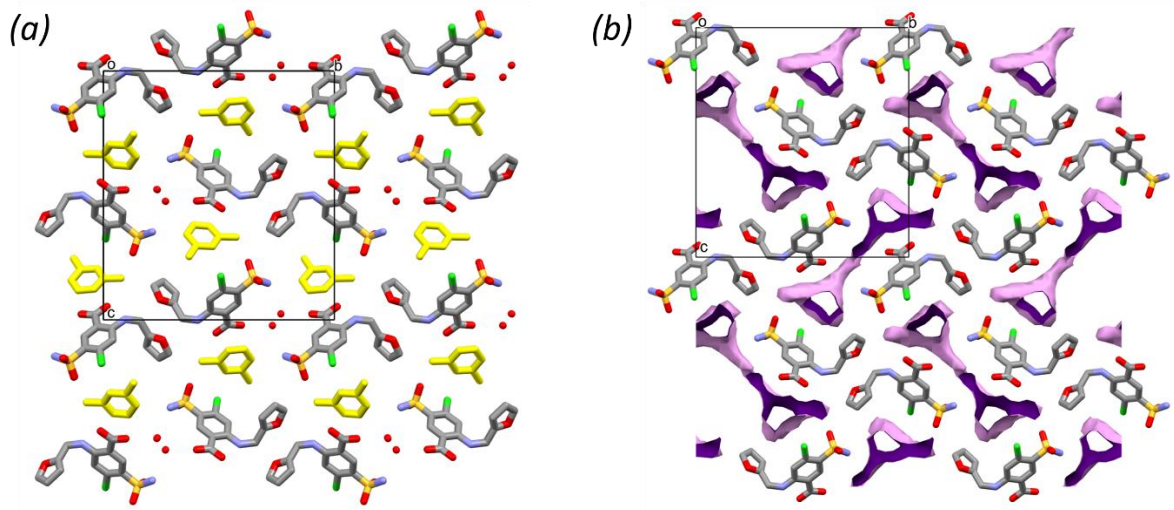

Figure 3. 12 Crystal packing (a) and solvent accessible surface (b) in FUR·24LUTw view down the a axis. Solvent molecules were omitted for clarity.

Table 3. 7 Crystallographic data of FUR·24LUTw

Compounds	FUR·24LUTw
Molecular formula	$C_{19}H_{22}N_3O_6SCl$
Formula weight (g.mol^{-1})	455.90
Crystal system	orthorhombic
Space group (No.)	$P2_12_12_1$ (No. 19)
a (Å)	5.0757(3)
b (Å)	19.3352(11)
c (Å)	20.7883(12)
α (°)	90
β (°)	90
γ (°)	90
V (A^3)	2040.2(2)
Z	4
ρ_{calc} (g.cm^{-3})	1.484
μ (MoKα) (mm^{-1})	0.333
F(000)	952.0
Crystal size(mm)	0.384 × 0.086 × 0.038
Temperature (K)	173(2)
Radiation (Å)	MoKα, 0.71073
2Theta min-max (°)	2.876 to 59.172
Dataset (±h; ±k; ±l)	-7 ≤ h ≤ 6, -26 ≤ k ≤ 26, -28 ≤ l ≤ 28
Reflections collected	35772
Independent reflections	5698 [R_{int} = 0.0454, R_{sigma} = 0.0303]
Data/restraints/parameters	5698/0/279
Goodness-of-fit on F^2	1.040
Final R indices [I>2σ(I)]	R_1 = 0.0399, wR_2 = 0.0968
Final R indexes [all data]	R_1 = 0.0428, wR_2 = 0.0987
Largest diff. peak/hole / e Å^{-3}	1.10/-0.45
Flack parameter	0.022(19)

Table 3. 8 Hydrogen bonding found in FUR·24LUTw

D-H···A	d(D-H) (Å)	d(H···A) (Å)	d(D···A) (Å)	D-H···A (°)	Symmetry operators
N3-H4···O4	0.831	1.882	2.711	175.20	
N2-H2···O4	0.804	1.992	2.674	142.24	
C17-H17···O3	0.950	2.316	2.958	124.35	
O6-H6A···O3	0.753	1.898	2.643	170.64	
O6-H6B···O6	0.808	2.024	2.812	164.62	[x+1/2, -y+1/2, -z+1]
N1-H1A···O6	0.874	1.999	2.873	177.14	[x+1/2, -y+1/2, -z+1}
N1-H1B···O2	0.813	2.037	2.840	169.43	[x-1, y, z]

3.5 The crystal structure of FUR·PYRw

The crystallisation of furosemide from pyridine resulted in crystals that can be classified as salt hydrate (Grothe *et al*., 2016). The structure was solved in the triclinic space group *P*-1 (No. 2) with one molecule of furosemide, one molecule of pyridine (PYR) and one molecule of water in the ASU. The crystal data and the details of the hydrogen bonds are listed in Tables 3.9 and 3.10. The interactions between the moieties are very similar to those described in FUR·24LUTw. The intramolecular hydrogen bond was formed between the secondary amine and the carbonyl group (N2-H2···O3), and the hydrogen bonds were formed between the PYR, and the FUR moieties can be described by the $R_2^2(7)$ graph set (Fig. 3.13a), although there is a subtle difference in the connectivity. Also, the water molecule is described with a model where H6A hydrogen atom has full occupancy, but H6B and H6C atoms are modelled with 50 % site occupancy factors. Although the conformation of the FUR moiety is different from those in the FUR·24LUTw crystal, the hydrogen bonding formed between the FUR and the water molecules is the same (Fig. 3.13b). The mapping of the solvent-accessible surface (1.2 Å probe radius, 0.7 Å grid spacing) shows that the shape of the voids occupied by the PYR, and water molecules differ significantly in the PYR and the 24LUT structures as a consequence of the different conformations of the FUR moieties (Fig. 3.14b).

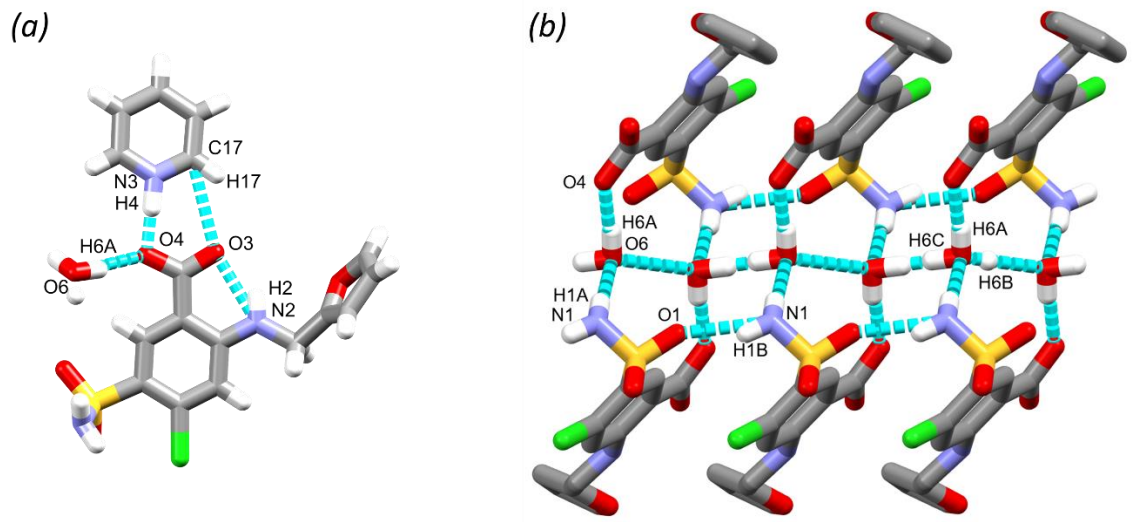

Figure 3. 13 The ASU (a) and the relevant hydrogen bonds (b) in FUR·PYRw. Solvent molecules were omitted for clarity on part b.

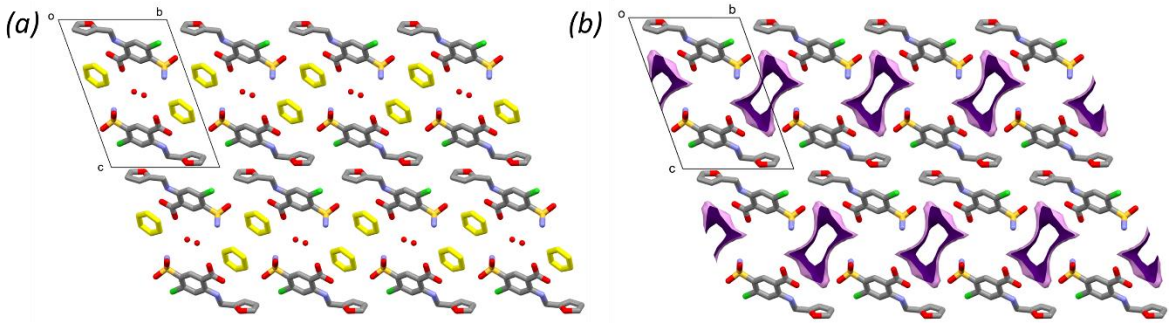

Figure 3. 14 Crystal packing (a) and solvent accessible surface (b) in FUR·PYRw view down the a axis. Solvent molecules were omitted for clarity.

Table 3. 9 Crystallographic data of FUR·PYRw

Compounds	FUR·PYRw
Molecular formula	$C_{17}H_{18}ClN_3O_6S$
Formula weight (g.mol^{-1})	427.85
Crystal system	triclinic
Space group (No.)	*P*-1 (No. 2)
a (Å)	5.2827(11)
b (Å)	11.540(2)
c (Å)	16.446(3)
α (°)	69.81(3)
β (°)	85.87(3)
γ (°)	79.15(3)
V (A^3)	924.1(4)
Z	2
ρ_{calc} (g.cm^{-3})	1.538
μ (MoKα) (mm^{-1})	0.362
F(000)	444.0
Crystal size(mm)	0.26 × 0.16 × 0.06
Temperature (K)	173(2)
Radiation (Å)	MoKα, 0.71073
2Theta min-max (°)	2.876 to 59.172
Dataset (±h; ±k; ±l)	-7 ≤ h ≤ 7, -16 ≤ k ≤ 16, -23 ≤ l ≤ 23
Reflections collected	84416
Independent reflections	5800 [R_{int} = 0.0540, R_{sigma} = 0.0234]
Data/restraints/parameters	5800/0/267
Goodness-of-fit on F^2	5800/0/267
Final R indices [I>2σ(I)]	R_1 = 0.0337, wR_2 = 0.0793
Final R indexes [all data]	R_1 = 0.0434, wR_2 = 0.0839
Largest diff. peak/hole / e Å^{-3}	0.44/-0.48

Table 3. 10 Hydrogen bonding found in FUR·PYRw

D-H···A	d(D-H) (Å)	d(H···A) (Å)	d(D···A) (Å)	D-H···A (°)	Symmetry operators
N3-H4···O4	1.035	1.536	2.571	176.90	
N2-H2···O3	0.827	1.962	2.642	138.85	
C17-H17···O3	0.950	2.514	3.144	123.82	
O6-H6A···O4	0.875	1.820	2.689	172.01	
O6-H6B···O6	0.865	2.047	2.908	173.56	[-x, -y+1, -z+1]
O6-H6C···O6	0.944	1.872	2.815	177.28	[-x+1, -y+1, -z+1]
N1-H1A···O6	0.901	2.034	2.933	175.00	[-x, -y+1, -z+1]
N1-H1B···O1	0.862	2.082	2.896	157.29	[x-1, y, z]

3.6 Protonation state of FUR and the coformers in the multicomponent crystals

In the previous section, the differing protonation state of the FUR moiety was noted. Predicting the formation of a salt or a cocrystal (or solvate) is possible for specific compound pairs by evaluating the difference in their pKa values (Bhogala *et al*., 2005). The pKa values for the cocrystallised compounds, FUR and the bases, were calculated with Marvin (https://docs.chemaxon.com/display/docs/calculations-plugins-in-marvinsketch.md), and the results are shown in Table 3.11. The ΔpKa values were calculated (ΔpKa = pKa (base) – pKa (acid)), and the quantitative pKa rule by Cruz Cabeza (Cruz-Cabeza, 2012) was applied to evaluate them. The quantitative pKa rule states that cocrystals are expected to form if the ΔpKa is below -1 (zone 1), salt formation is expected if the ΔpKa is higher than 4 (zone 3) and, between these two boundaries lies the so-called 'salt-cocrystal continuum' (zone 2) where, around ΔpKa = 1, the formation of a salt or a cocrystal practically equal. It is important to note that all coformers are liquids and were used as the 'solvent' during the cocrystallisation experiments. This carries significance, hence the pKa value of a compound—in our case the FUR moiety—depends significantly on the solvent used to dissolve it (Cox, 2013).

The obtained ΔpKa values varied from 2.42 to 3.88, Table 3.11, and thus they fit into zone 2 (-1 < ΔpKa < 4). In this zone, the relative occurrence of ionised complexes increases linearly with increasing ΔpKa values. Based on a recent MCC classification system (Grothe et al., 2016), the five crystals can be classified as a solvate (FUR·3PIC), true salts (FUR·4PIC and FUR·23LUT) or salt hydrates (FUR·24LUTw and FUR·PYRw). The quantitative pKa rule predicted the formation of a salt rightfully for the compounds with the exception of the FUR·3PIC structure. It is interesting to note that based on the ΔpKa value for the PYR structure being lower than for the 3PIC system,

thus it would be expected that the PYR would form a solvate. The reason for this inconsistency can be the already mentioned uncertainty of the calculated pKa values for the FUR moiety in the different solvents. Additionally, the inclusion of water complicates this further.

Table 3. 11 ΔpKa values for FUR and selected coformers (ΔpKa = pKa (base) – pKa (acid))

Compounds	pKa	ΔpK_{a1}*	Prediction	Outcome*
FUR	-COOH: 2.70 -NH: -0.97 SO_2-NH_2: 9.57	n.a.	n.a.	n.a.
3PIC	5.63	2.93	cocrystal < salt	Cocrystal (solvate)
4PIC	5.85	3.15	cocrystal < salt	Salt
23LUT	6.28	3.58	cocrystal < salt	Salt
24LUT	6.58	3.88	cocrystal < salt	Salt
PYR	5.12	2.42	cocrystal < salt	Salt

*Outcome was classified based on ref 4

3.7 Comparative conformation analysis of the FUR moieties

The detailed structural analysis of the MCCs revealed the conformational variety of the FUR moiety, thus a comparative conformational analysis was carried out.

The following four torsion angles can describe the conformational flexibility of FUR: τ1 indicates the rotation of the sulfonamide moiety, τ2 describes the rotation of the methyl-furan moiety, τ3 represents the tilt of the furan ring, and τ4 indicates the tilt of the -COOH/COO^- moiety relative to the phenyl ring (Fig. 3.15). These torsion angles for the five MCCs and the three known polymorphs of FUR are listed in Table 3.12. The molecular conformations of the FUR moieties of the MCCs in the polymorphs are presented in Fig. 3.16 and 3.17, respectively.

The values of τ4 torsion angle show little variation, resulting from the formation of the intramolecular hydrogen bond with the secondary amine. It is important to note that this intramolecular hydrogen bond was formed in all the crystal structures of furosemide (found in the CSD or the current work). The absolute values of the τ3 torsion angle cluster around ± 60° and ± 160°. This group is also disordered in some structures. It may be concluded that the two torsion angles that are primarily responsible for the conformational flexibility of the FUR moiety

are τ1 and τ2. A conformational search was conducted by scanning these two torsion angles of the FUR moiety and the results are shown in Fig.3.18. A two-dimensional relaxed potential energy scan of the two torsion angles was done using the B3LYP-D3(BJ) hybrid functional (Stephens *et al*., 1994; Becke, 1993; *Lee et al*., 1988) and the def2-SVP basis set (Weigend & Ahlrichs, 2005). The DFT-D3(BJ) empirical dispersion correction of Grimme with the Becke-Johnson (BJ) dampening function was used to account for intramolecular dispersion interactions (Grimme *et al*., 2011; Grimme *et al*., 2010). The scan was done in steps of 20° for both angles. The Gaussian 16 software was used (Frisch *et al*,2016).

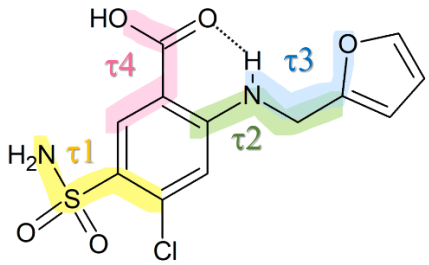

Figure 3. 15 Torsion angles describing the conformational flexibility of furosemide

Table 3. 12 Torsion angles of furosemide moieties in the MCCs and the known polymorphs. (The polymorphs are identified with their CSD Ref codes.)

Structure	Space Group	τ1 (°)	τ2 (°)	τ3 (°)	τ4 ()
FUR·3PIC	*P*-1	60.21	-73.71	162.38	-4.20
FUR·4PIC	*P*-1	-55.19	-77.00	-66.60	-0.07
FUR·23LUT	$P2_1/n$	-59.82	75.23	67.46	-4.86
FUR·24LUTw	$P2_12_12_1$	-179.15	71.88	-169.26	4.46
FUR·PYRw	*P*-1	76.18	-164.90	-67.04	7.03
Form I (FUROSEM03) molA	*P*-1	-166.00	83.98	-68.20	10.62
molB		163.22	-61.40	-57.60	-4.53
Form II (FUROSEM14)	$P2_1/n$	-79.92	-166.37	-78.22	-4.32
Form III (FUROSEM16)	*P*-1	55.68	91.31	-59.97	-1.80

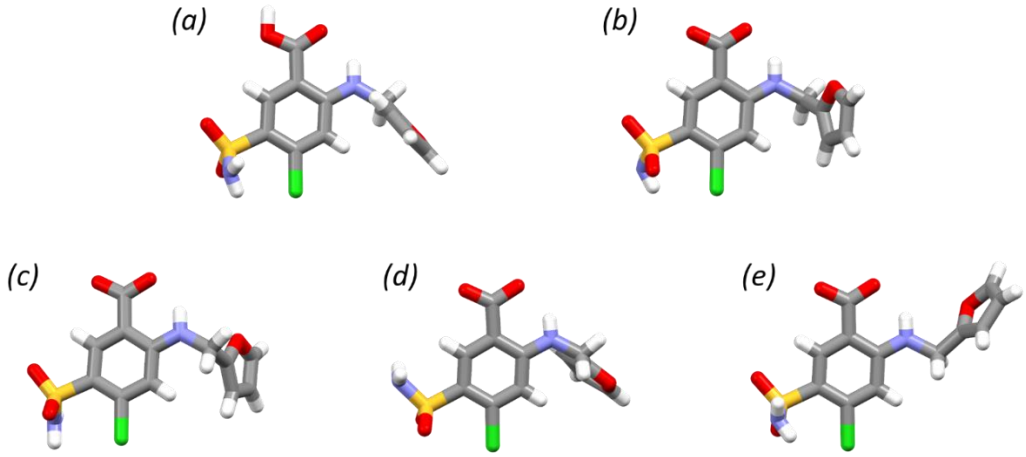

Figure 3. 16 Molecular conformations of the FUR moieties FUR·3PIC (a), FUR·4PIC (b), FUR·23LUT(c), FUR·24LUTw(d), and FUR·PYRw (e).

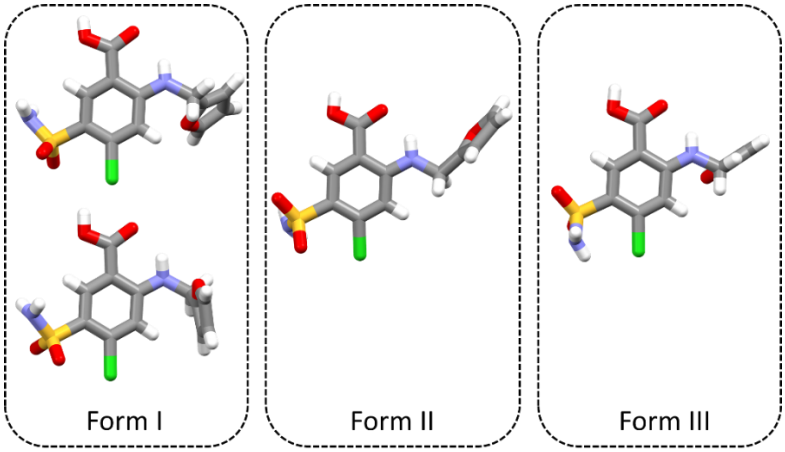

Figure 3. 17 Molecular conformations of the FUR moieties in polymorphs of furosemide.

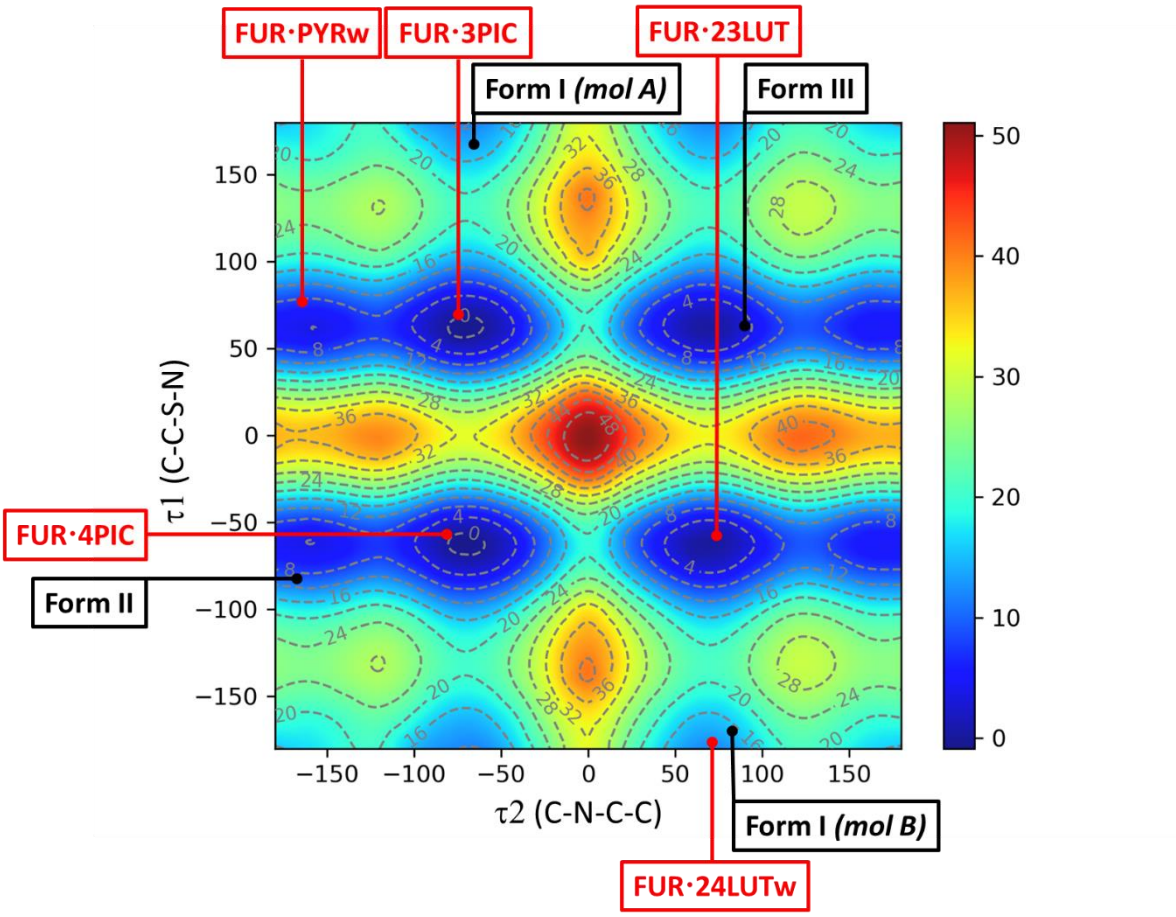

Figure 3. 18 Result of the conformational search for FUR scanning τ1 and τ2 torsion angles (in KJ mol^{-1})

Fig. 3.18 shows the potential energy surface with colour coding (red-high, blue-low), and also, the FUR conformers from the MCCs and the polymorphs are pointed out on the diagram. It is important to note that all the discussed crystal structures—with the exception of the FUR·23LUT structure—were solved in centrosymmetric space groups (*P*-1 or $P2_1/n$), thus the crystals contain both the conformer that is in the ASU (pointed out on the figure) and its mirror image molecule (not shown for clarity). Thus, the crystals are represented by two conformers with equal but opposite τ1 and τ2 torsion angles. FUR·23LUT was solved in the chiral space group $P2_12_12_1$, and because FUR is an achiral molecule, it is rightfully assumed that it crystallised as a conglomerate (Pidcock,2005). The analysed crystal was a random selection, and thus the bulk contains crystals with conformers with the opposite handedness, i.e. the mirror image of the observed FUR conformer. It is important to mention that in the case of Form I, the ASU contains two molecules

of FUR. The relation between the two conformers shows quasi-mirror symmetry caused by the different positions of the furane moieties (Fig. 3.19).

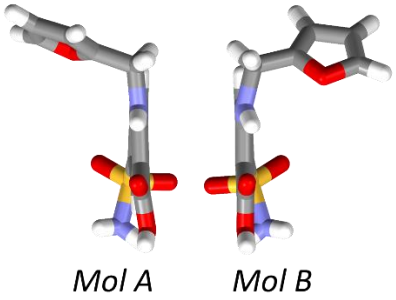

Figure 3. 19 The two molecules of the ASU of Form I are arranged to highlight their quasi symmetry caused by the different positions of the furane moieties.

The symmetrical nature of the plot is evident, but it is important to emphasise that only the scanning of τ1 and τ2 was done. While excluding the scanning of τ4 for the energetically favoured formation of the intramolecular hydrogen bond is reasonable, the presented energy diagram (Fig. 3.18) does not consider τ3, which torsion angle may have a significant effect on the overall picture of the energies of the conformers. The molecules of Form I is an excellent example of this problem.

The simplified analysis of the conformers of the polymorphs reveals that Form III has the lowest energy conformer and Form I conformers have the highest energy. An interesting observation is that the highest energy conformers of FUR can be found in the hydrated salts of the MCCs, i.e. FUR·24LUTw and FUR·PYRw.

3.8 Comparative analysis of the synthons formed by the FUR moieties

The carboxylic acid/carboxylate functional group is one of the most promiscuous hydrogen bond former in organic supramolecular chemistry because of its dual hydrogen bond donor and acceptor nature and its high occurrence in organic molecules. To better understand the solid-state structures of FUR and its MCCs, a Cambridge Structural Database analysis was carried out (CSD version 5.42 November 2020, Update 3 Sep 2021) with the aid of ConQuest (version 2021.2.0, Build 327809). General search filters were applied: 3D coordinates determined, no

errors, non-polymeric structures, and only single crystal organic structures were included. The search resulted in 79 crystal structures, including the most representative of the furosemide polymorphs (FURSEM03, FURSEM14 and FURSEM16 for Forms I, II and III, respectively). Ten structures have two symmetry independent FUR moieties in their structures, and these were listed as individual hits in Table 3.13, which also contains the current crystal structures. Overall, the number of FUR moieties analysed is 89.

The hydrogen bonds formed via the carboxylic acid/carboxylate group of the 89 FUR moieties can be classified as one of the 14 different synthons shown in Fig. 3.20. The variety of the synthons is a good representation that the carboxylic acid/carboxylate group forms hydrogen bonds with a large variety of functional groups. The occurrence of the synthons is presented in Fig. 3.21. The carboxylic acid/carboxylate···aromatic amine synthon (no. 2) has the highest occurrence (26%), followed by synthon 3 (20%) in what the carboxylic acid/carboxylate hydrogen bonds to an aromatic amine and a primary amine. The third most observed motif is the carboxylic acid/carboxylate···amide, synthon 6 (12%), and the fourth is synthon 10 (8%). The fifth most observed synthon is the carboxylic acid dimer (no. 1, 8%). In the case of synthons 2, 3 and 10, the coformer has at least one basic component. In case of synthons 6 and 1, a high level of electrostatic complementarity is noted between the interacting groups. These five most occurring synthons represent 74% of the observed interactions.

Table 3. 13 Synthons in the crystals of furosemide

	[REFCODE]	synthon		[REFCODE]	synthon		[REFCODE]	synthon
1	BOKHAM	2	*31*	HUQWAT (mol B)	2	*61*	VARGAZ (mol A)	3
2	BOKHAM01	2	*32*	HUQWEX (mol A)	3	*62*	VARGAZ (mol B)	3
3	BOKHAM02	3	*33*	HUQWEX (mol B)	3	*63*	VARGED (mol A)	3
4	BOKHEQ	2	*34*	IWERIM	6	*64*	VARGED (mol B)	3
5	BOKHIU	2	*35*	IWERUY	14	*65*	VARGIH	2
6	BOKHOA	2	*36*	JUYTUU	5	*66*	VARGON	2
7	BOKHUG	2	*37*	LODFUH	10	*67*	VARGUT	2
8	BOKJAO	2	*38*	LODGAO (mol A)	9	*68*	VARHAA	3
9	BUQQEM	4	*39*	LODGAO (mol B)	9	*69*	VARHEE	3
10	BUQTAL	13	*40*	LODGAO01	10	*70*	VARHII (mol A)	3
11	BUQTEP	3	*41*	LODGAO02 (mol A)	7	*71*	VARHII (mol B)	3
12	ESAVIF	6	*42*	LODGAO02 (mol B)	7	*72*	VARHOO	10
13	ESAVOL	5	*43*	LODGES	10	*73*	VUTCEV	13
14	ESAVUR	6	*44*	LOFLAV	1	*74*	XAVTEV	2
15	ESAWAY	13	*45*	LOFLEZ (mol A)	6	*75*	XAVTIZ	8
16	ESAWEC	6	*46*	LOFLEZ (mol B)	2	*76*	XIFRAH	8
17	ESAWIG	6	*47*	LOFLID	2	*77*	XUDYED	1
18	ESAWOM	6	*48*	LUTBIO	3	*78*	YASGOQ	2
19	ESAWUS	1	*49*	LUTBOU	8	*79*	YASGOQ01	3
20	ESAXAZ	5	*50*	MODWIO	11	*80*	YASGOQ02	2
21	EZIPIO	7	*51*	NOLBAU	6	*81*	YASGOQ03	6
22	FEFYAS	2	*52*	NOLBEY	10	*82*	YASGOQ04	2
23	FEFYEW	2	*53*	NOLBIC	6	*83*	YASHIL	6
24	FEFYIA	2	*54*	TARPIO	10	*84*	YODTOC	11
25	FURSEM03 (mol A)	1	*55*	TARPIO01 (mol A)	12	*85*	FUR·3PIC	3
26	FURSEM03 (mol B)	1	*56*	TARPIO01 (mol B)	12	*86*	FUR·4PIC	3
27	FURSEM14	1	*57*	TARPIO02	7	*87*	FUR·23LUT	3
28	FURSEM16	1	*58*	TARPOU	10	*88*	FUR·24LUTw	2
29	HIQXEN	8	*59*	TUQBOY	11	*89*	FUR·PYRw	2
30	HUQWAT (mol A)	2	*60*	VARFUS	3			

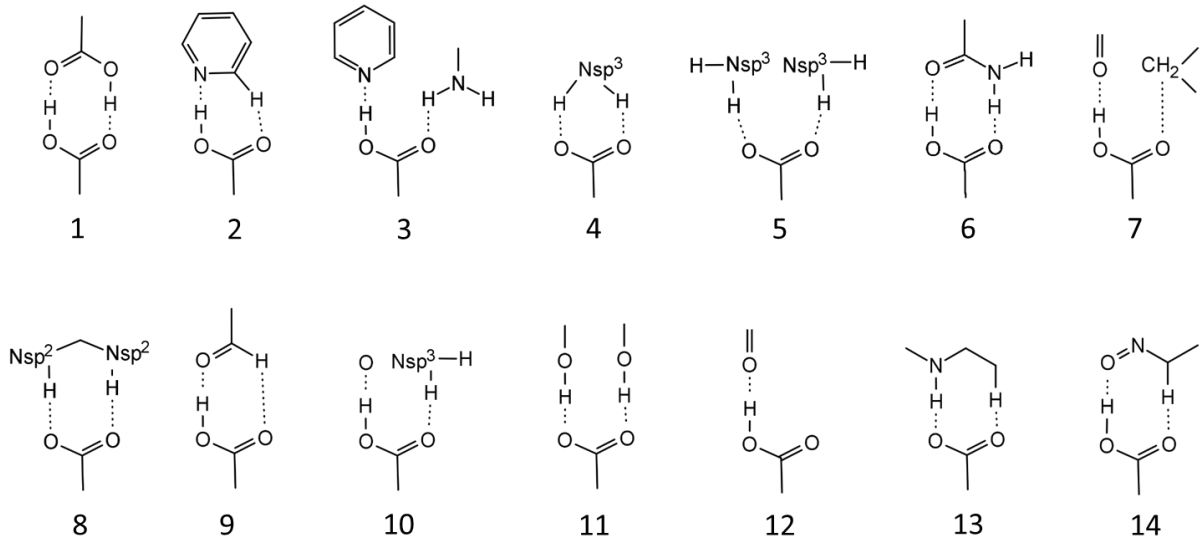

Figure 3. 20 Synthons identified in the currently known crystal structures of furosemide formed by the carboxylic acid moiety

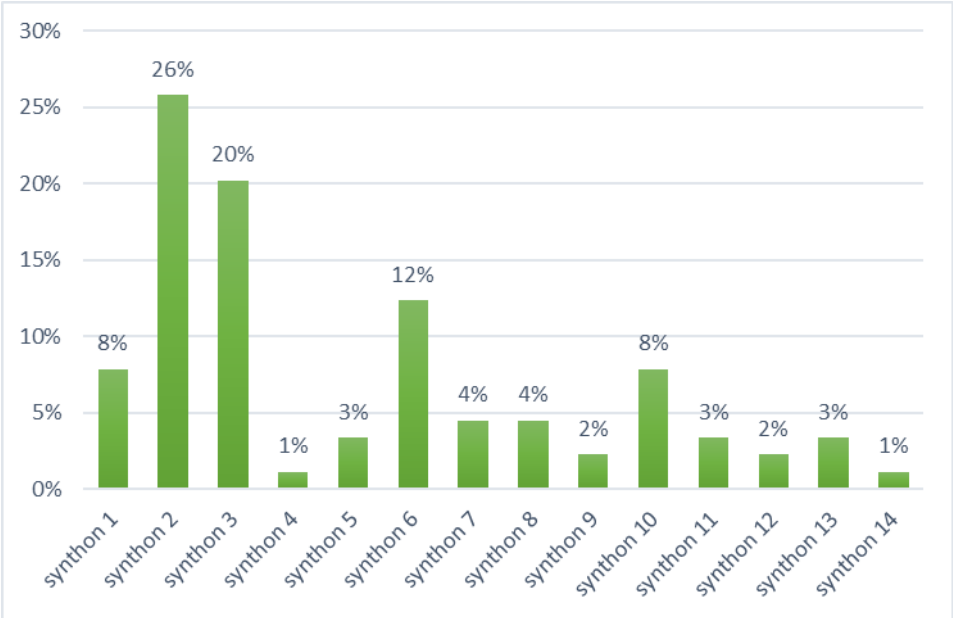

Figure 3. 21 Occurrence of synthons in the furosemide crystals

References

Becke, A.D. 1993. Density-functional thermochemistry. III. The role of exact exchange. *The Journal of Chemical Physics*, 98(7): 5648–5652. https://aip.scitation.org/doi/abs/10.1063/1.464913 6 December 2021.

Bhogala, B.R., Basavoju, S. & Nangia, A. 2005. Tape and layer structures in cocrystals of some di- and tricarboxylic acids with 4,4'-bipyridines and isonicotinamide. From binary to ternary cocrystals. *CrystEngComm*, 7(90): 551–562. https://pubs.rsc.org/en/content/articlehtml/2005/ce/b509162d 16 November 2021.

Cox, B.G. 2013. Acids and Bases. Solvent Effects on Acid-Base Strength. By Brian G. Cox. *Angewandte Chemie International Edition*, 52(30): 7638–7638.

Cruz-Cabeza, A.J. 2012. Acid-base crystalline complexes and the pKa rule. *CrystEngComm*, 14(20): 6362–6365. https://pubs.rsc.org/en/content/articlehtml/2012/ce/c2ce26055g 15 November 2021.

Gavezzotti, A. & Filippini, G. 1994. Geometry of the intermolecular X-H···Y (X, Y = N, O) hydrogen bond and the calibration of empirical hydrogen-bond potentials. *Journal of Physical Chemistry*, 98(18): 4831–4837. https://pubs.acs.org/doi/abs/10.1021/j100069a010 16 November 2021.

Grimme, S., Antony, J., Ehrlich, S. & Krieg, H. 2010. A consistent and accurate ab initio parametrization of density functional dispersion correction (DFT-D) for the 94 elements H-Pu. *Journal of Chemical Physics*, 132(15): 154104. https://aip.scitation.org/doi/abs/10.1063/1.3382344 6 December 2021.

Grimme, S., Ehrlich, S. & Goerigk, L. 2011. Effect of the damping function in dispersion corrected density functional theory. *Journal of Computational Chemistry*, 32(7): 1456–1465. https://onlinelibrary.wiley.com/doi/full/10.1002/jcc.21759 6 December 2021.

Grothe, E., Meekes, H., Vlieg, E., Ter Horst, J.H. & De Gelder, R. 2016. Solvates, Salts, and Cocrystals: A Proposal for a Feasible Classification System. *Crystal Growth and Design*, 16(6): 3237–3243. https://pubs.acs.org/doi/full/10.1021/acs.cgd.6b00200 16 November 2021.

Lee, C., Yang, W. & Parr, R.G. 1988. Development of the Colle-Salvetti correlation-energy

formula into a functional of the electron density. *Physical Review B*, 37(2): 785. https://journals.aps.org/prb/abstract/10.1103/PhysRevB.37.785 6 December 2021.

Marvin was used for drawing, displaying and characterizing chemical structures, substructures and reactions. Calculator Plugins were used for structure property prediction and calculation. Marvin 16.4.25.0, 2016,

M. J. Frisch, G. W. Trucks, H. B. Schlegel, G. E. Scuseria, M. A. Robb, J. R. Cheeseman, G. Scalmani, V. Barone, G. A. Petersson, H. Nakatsuji, X. Li, M. Caricato, A. V. Marenich, J. Bloino, B. G. Janesko, R. Gomperts, B. Mennucci, H. P. Hratchian, J. V. Ortiz, A. F. Izmaylov, J. L. Sonnenberg, Williams, F. Ding, F. Lipparini, F. Egidi, J. Goings, B. Peng, A. Petrone, T. Henderson, D. Ranasinghe, V. G. Zakrzewski, J. Gao, N. Rega, G. Zheng, W. Liang, M. Hada, M. Ehara, K. Toyota, R. Fukuda, J. Hasegawa, M. Ishida, T. Nakajima, Y. Honda, O. Kitao, H. Nakai, T. Vreven, K. Throssell, J. A. Montgomery Jr., J. E. Peralta, F. Ogliaro, M. J. Bearpark, J. J. Heyd, E. N. Brothers, K. N. Kudin, V. N. Staroverov, T. A. Keith, R. Kobayashi, J. Normand, K. Raghavachari, A. P. Rendell, J. C. Burant, S. S. Iyengar, J. Tomasi, M. Cossi, J. M. Millam, M. Klene, C. Adamo, R. Cammi, J. W. Ochterski, R. L. Martin, K. Morokuma, O. Farkas, J. B. Foresman and D. J. Fox, *Gaussian 16 Rev. C.01*, Wallingford, CT, 2016.

Nassimbeni, L.R. 2003. Physicochemical aspects of host - Guest compounds. *Accounts of Chemical Research*, 36(8): 631–637. https://pubs.acs.org/doi/full/10.1021/ar0201153 16 November 2021.

Pidcock, E. 2005. Achiral molecules in non-centrosymmetric space groups. *Chemical Communications*, (27): 3457–3459. https://pubs.rsc.org/en/content/articlehtml/2005/cc/b505236j 16 November 2021.

Stephens, P.J., Devlin, F.J., Chabalowski, C.F. & Frisch, M.J. 1994. Ab Initio calculation of vibrational absorption and circular dichroism spectra using density functional force fields. *Journal of Physical Chemistry®*, 98(45): 11623–11627. https://pubs.acs.org/sharingguidelines 6 December 2021.

Weigend, F. & Ahlrichs, R. 2005. Balanced basis sets of split valence, triple zeta valence and quadruple zeta valence quality for H to Rn: Design and assessment of accuracy. *Physical Chemistry Chemical Physics*, 7(18): 3297–3305. https://pubs.rsc.org/en/content/articlehtml/2005/cp/b508541a 6 December 2021.

Chapter 4

Supramolecular manipulation of multicomponent crystals

In this chapter, the XRD analysis of the bulk material will be discussed, as well as the outcome of the MCCs which were used to prepare furosemide polymorphs via drying.

4.1 Identification of the starting material

Identifying the bulk furosemide used for the formation of the MCCs required knowing the XRD pattern of the different known polymorphs of the drug. There are ten crystal structures listed in the CSD, but these are recollections of three polymorphs only. After evaluating their cell descriptors and some quality indicators, FURSEM03 was selected as the best representation of form I, FURSEM14 for form II, and FURSEM16 to represent form III. The comparison of the XRD patterns (Fig. 4.1) concluded that the bulk material used for the MCCs is form I. (The minor differences between the peak positions can be attributed to the temperatures used when the samples were analysed.)

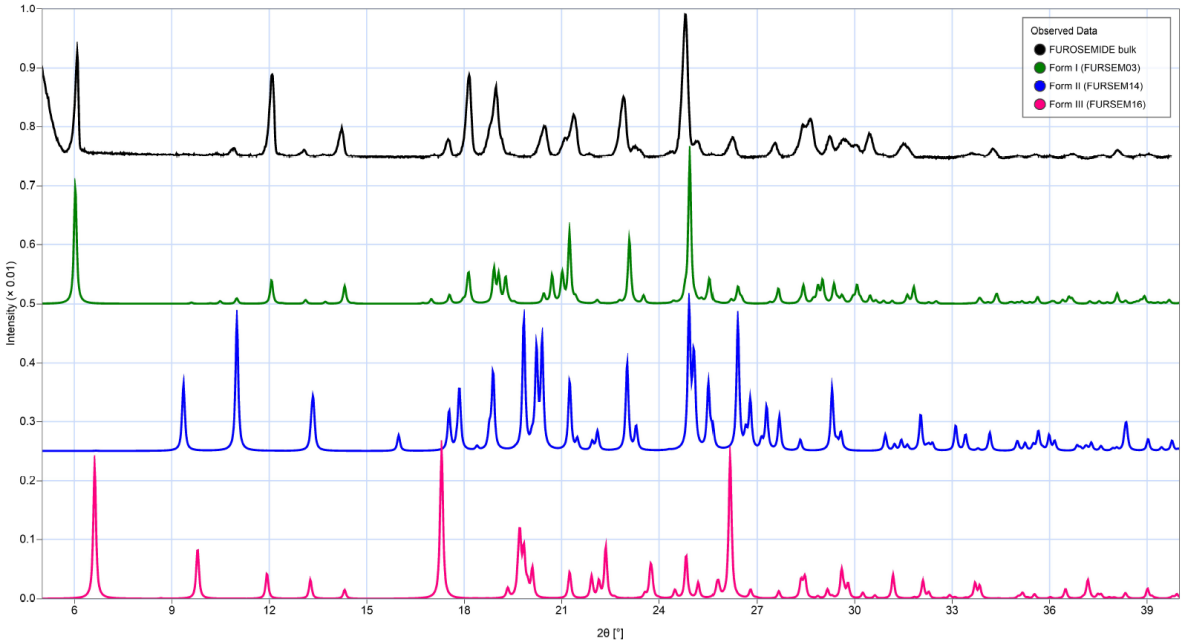

Figure 4. 1 The powder pattern of the furosemide used as starting material (black), and the generated patterns of forms I (green), II (blue) and III (magenta).

4.2 Analysis of the bulk forms of the multicomponent crystals and the results of the desolvation experiments

The analysis of the XRD patterns was carried out for two reasons. Firstly, to check if the structure of the randomly selected single crystal is a good representation of the bulk. Secondly, the MCCs were gently desolvated to produce polymorphs under controlled conditions, and XRD was used to follow the process. The logic behind using solvates to form selected polymorphs is well-reasoned. The lattice energies of pairs of polymorphs are very close (Price, 2013) (in the order of 1 KJ.mol^{-1}), and thus, the environmental conditions forming only the desired one can be very similar. Occasionally, multiple polymorphs crystallise from the same batch, and these so-called concomitant polymorphs (Lemmerer et al., 2009) cannot be separated at an industrial scale. Sometimes, the once identified polymorph cannot be reproduced for an unknown reason. These are the so-called disappearing polymorphs (Bučar et al., 2015; Dunitz & Bernstein, 1995). These problems need solutions that can reliably result in the formation of the desired polymorph.

FUR is a polymorphic drug, with three known polymorphs best represented by FURSEM03, FURSEM14 and FURSEM16 structures in the CSD: form I, form II, and form III, respectively (Babu et al., 2010a). A series of recrystallisation experiments, where both the solvents and the method of crystallisation are varied, were conducted by Matsuda and Tatsumi (Matsuda & Tatsumi, 1990). It was observed that in many cases, a mixture of the polymorphs was obtained. It was also noted that heating the metastable form will result in its transformation into the stable form.[1] Therefore, this work is an excellent example of the difficulties of the directed formation of the selected pure form of a polymorph.

Minkov (Minkov *et al.*, 2014) speculated that forming solvates of FUR and subsequently desolvating the solvates may lead to the formation of pure polymorphs of FUR. Four solvates of furosemide were formed with tetrahydrofuran (THF), 1,4-dioxane (DIOX), N,N-dimethylformamide (DMF), and dimethyl sulfoxide (DMSO). The outcome of the desolvation experiments was the following: form III of FUR was obtained from the desolvation of the fine powder of the THF solvate, and the desolvation of the crystals of THF, DIOX and DMF solvates.

[1] In this early work, the forms were labelled differently.

However, form I of FUR was obtained when powders of DIOX, DMF, and DMSO were desolvated. This outcome suggests that the desolvation of the THF solvate yields form III, and the desolvation of the DMSO results in form I, exclusively.

Based on these papers (Babu *et al.*, 2010b, Matsuda and Tatsumi, 1990; Minkov *et al.*, 2014), we decided to (1) form solvates via forming the well-known carboxylic acid-aromatic amine synthon (Odounga and Báthori, 2020) (2) use solvents with relatively low boiling points to ensure the easy desolvation process of the crystals and (3) carry out the desolvation experiments without heating the crystals to prevent a possible polymorph transition.

The last two points are exceptionally important because we also aimed to find a link between the conformation of the FUR moiety in the solvate and the desolvated product, i.e. polymorph.

In the case of the FUR·3PIC system (Fig. 4.2), the single crystal structure (red pattern) is a good representation of the FUR·3pic bulk crystals (black pattern). After gentle grinding, the crystals were left to dry under ambient conditions. The XRD patterns were recorded after two months (dried 1-orange pattern) and six months (dried 2-brown pattern), but only the intensity of the peaks changed, but their position stayed the same. It was concluded that FUR·3PIC is a relatively stable crystal.

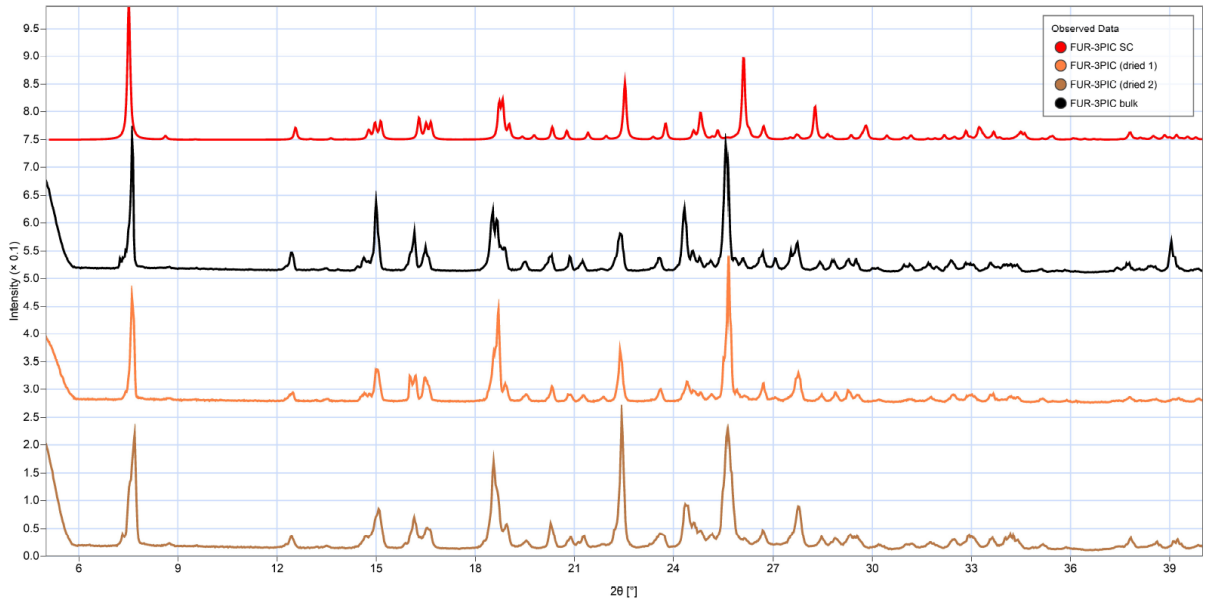

Figure 4. 2 XRD patterns of FUR·3PIC (single crystal-red, bulk-black, and dried 1-orange, dried 2-brown)

Based on the comparison of the XRD results of the single-crystal structure and the bulk material of FUR·4PIC (Fig. 4.3, red and black, respectively), it is evident that they differ significantly. Several months passed by before the bulk was analysed[2], and the crystals started to dry out. The process is more clearly shown with the yellow pattern (collected after another two months). A plausible conclusion is that the dried material can be described as a mixture of forms I and III. (The main reason for the careful phrasing is that the generated patterns are based on low-temperature data collections while the bulk analyses were carried out at room temperature. Thus, the peak positions may differ slightly, and this should be considered when results are concluded.)

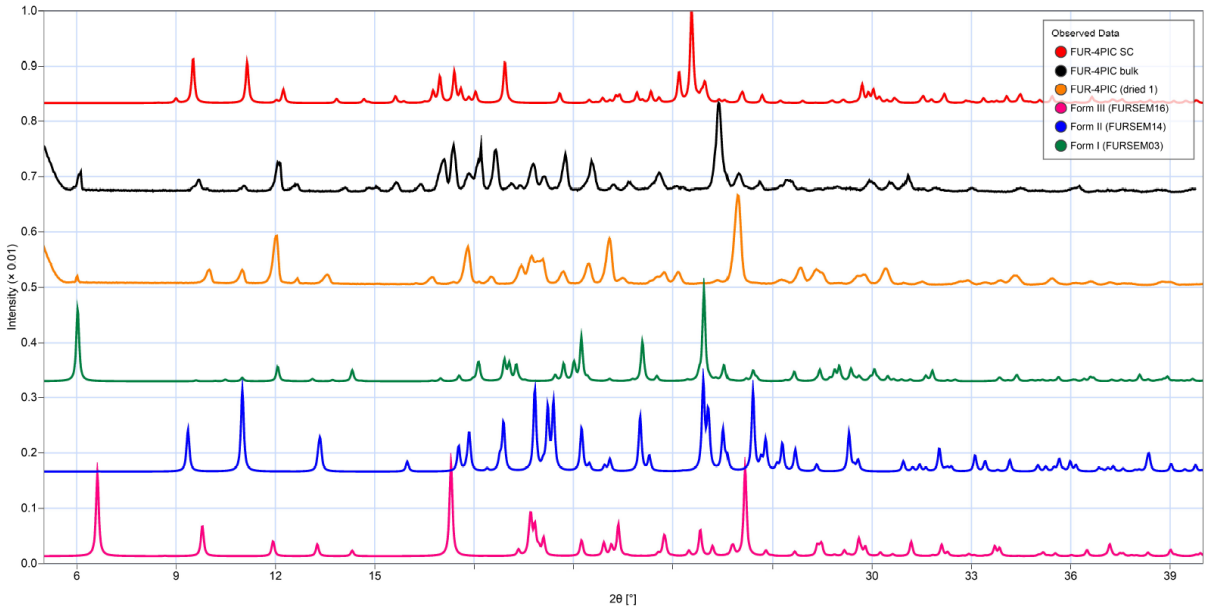

Figure 4. 3 XRD patterns of FUR·4PIC (single crystal-red, bulk-black, dried 1-yellow, form I-green, form II-blue, and form III-magenta)

In the case of FUR·23LUT crystals (Fig. 4.4), the pattern of the FUR·23LUT bulk (black) was recorded after a longer break in the experimental work, and the crystals desolvated by the time of the analysis. A further two months later, the XRD pattern was re-recorded (yellow), and further changes in the relative intensities of some peaks but not in their positions were noted. The identification of this new pattern is a challenging task. The comparison of the XRDs revealed new peaks at 7.66°, 15.14° and 16.37° and this suggests the formation of a new solid form of FUR. Currently, it is not proven that there is a link between the molecular structure of a compound and its ability to form polymorphs (Cruz-Cabeza *et al*., 2015), but based on the fact that FUR has

[2] It was extremely challenging, unpredictable, and occasionally impossible to get access to laboratories during the COVID-19 pandemic and this explains the unfortunately delayed bulk property analyses.

three known polymorphs, it would not be surprising if this new form would be a new polymorph. To establish a solid proof, further experimental works need to be done in the future.

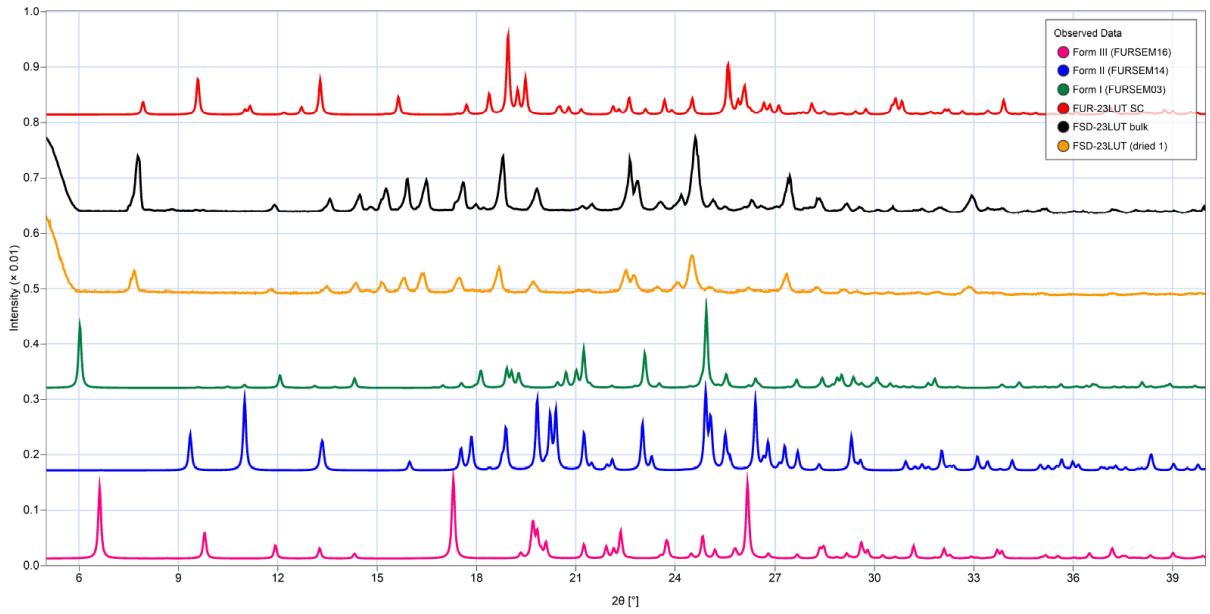

Figure 4. 4 XRD patterns of FUR·23LUT (single crystal-red, bulk-black, dried 1-yellow, form I-green, form II-blueI, and form III-magenta)

The case of FUR·24LUTw (Fig. 4.5) is very similar to the 23LUT solvate. The bulk crystals started to desolvate by the time the XRD was collected, and this extensive drying process resulted in a new form (orange) which has a different XRD pattern when compared to all the solid forms. Because of the gentle desolvation process, this solid form can be a new polymorph, or a partial solvate of FUR·24LUTw. Nonetheless, in this case, the appearance of several new peaks (10.37°, a dyad of 12.34° and 12.77°, the cluster of four peaks at 15.13°, 15.42°, 15.78° and 16.27°, and the two prominent peaks at 24.26° and 27.59°) is suggesting the formation of a new solid phase.

When the generated pattern of the crystal of FUR·PYRw (Fig. 4.6, red) was compared to the bulk (black), it revealed that the crystal structure is representative of the bulk. The XRD collected two months later (orange) shows little difference to the bulk (some peaks' intensities are lower), except for the appearance of an intensive peak at 7.76°. This peak cannot be related to any of the known forms and very likely indicates the appearance of a new solid form that can be either a new polymorph of FUR·PYRw, a new partial solvate of FUR, or a new polymorph of FUR. To confirm this hypothesis, further experimental works will be carried out.

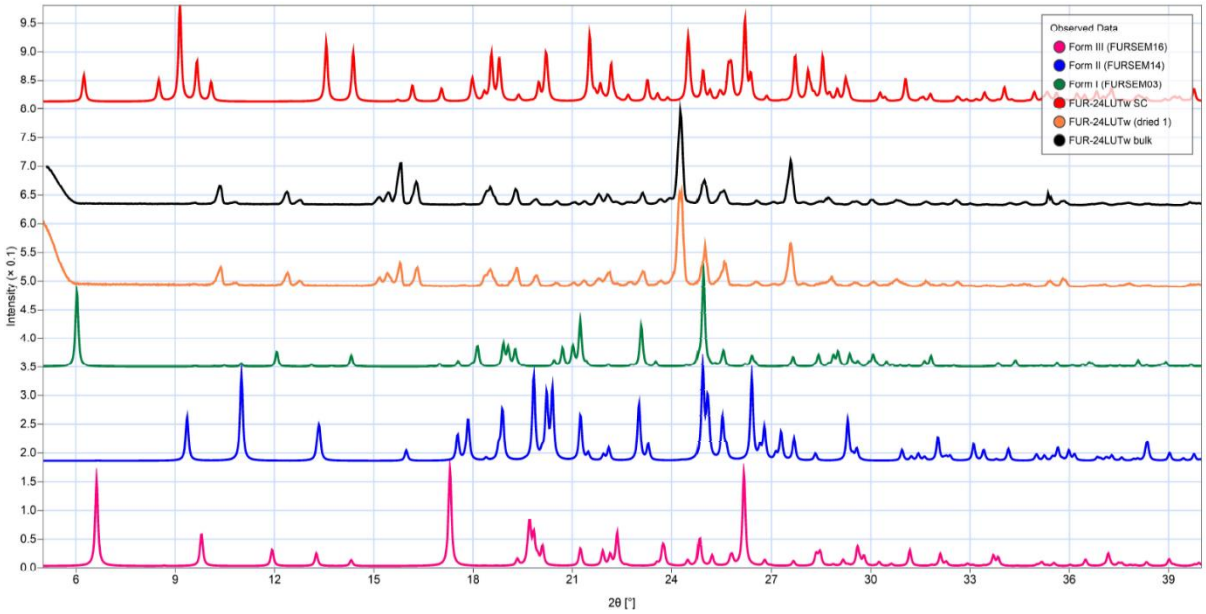

Figure 4. 5 XRD patterns of FUR·24LUTw (single crystal-red, bulk-black, dried 1-orange, form I-green, form II-blue, and form III-magenta)

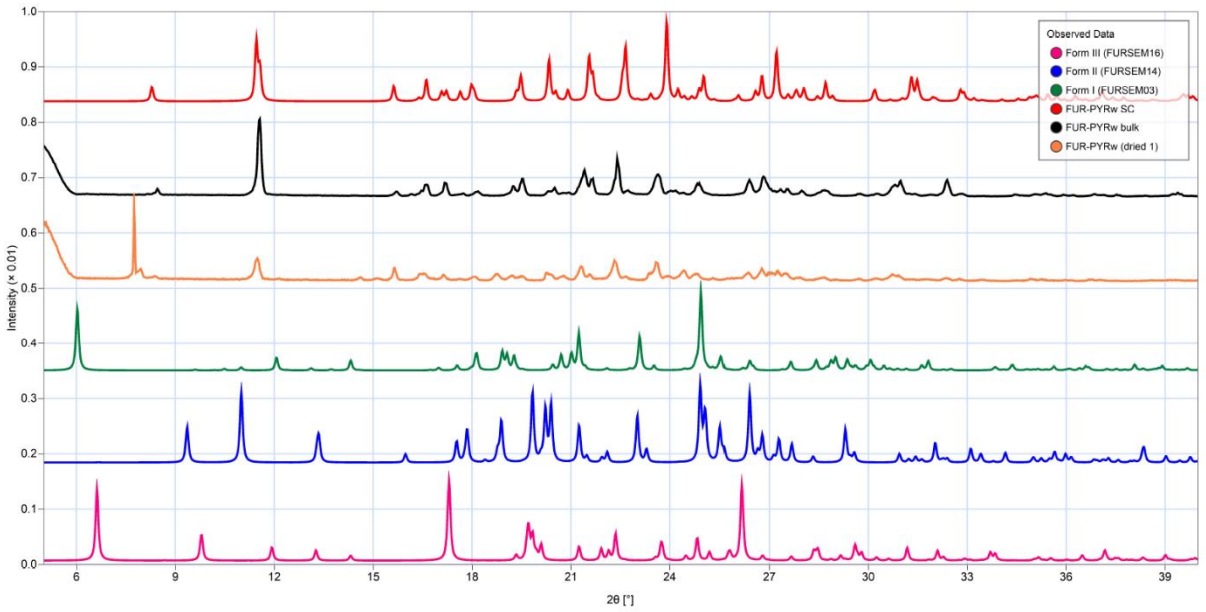

Figure 4. 6 XRD patterns of FUR·PYRw (single crystal-red, bulk-black, dried 1-orange, form I-green, form II-blue, and form III-magenta)

In conclusion, the desolvation of the selected solvates did not result in the exclusive formation of any of the known polymorphs of FUR, but the results are exciting, nonetheless (Scheme 4.1). FUR·3PIC crystals stay intact for at least six months under ambient conditions despite that this is the only structure in which the FUR and the 3PIC are neutral. The desolvation of crystals of FUR·4PIC results in the physical mixture of forms I and III. The desolvation of crystals of

FUR·23LUT, FUR·24LUTw, and FUR·PYRw resulted in three new solid forms, and the complete identification of these forms is the aim of another project.

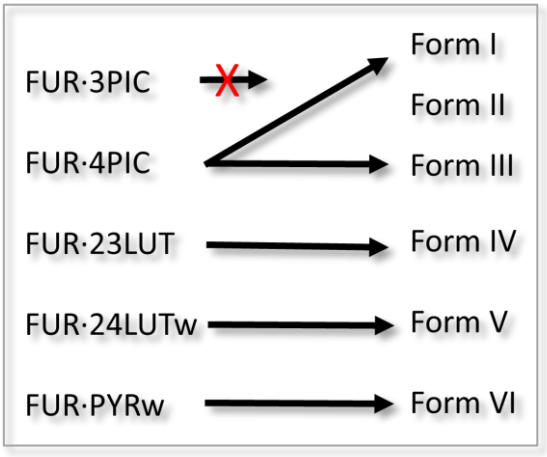

Scheme 4. 1 Summary of the results of the desolvation experiments

References

Babu, N. J. *et al.* (2010a) 'Conformational and synthon polymorphism in furosemide (Lasix)', *Crystal Growth and Design*, 10(4), pp. 1979–1989. doi: 10.1021/cg100098z.

Babu, N. J. *et al.* (2010b) 'Conformational and synthon polymorphism in furosemide (Lasix)', *Crystal Growth and Design*, 10(4), pp. 1979–1989. doi: 10.1021/cg100098z.

Bučar, D. K., Lancaster, R. W. and Bernstein, J. (2015) 'Disappearing Polymorphs Revisited', *Angewandte Chemie - International Edition*, 54(24), pp. 6972–6993. doi: 10.1002/anie.201410356.

Cruz-Cabeza, A. J., Reutzel-Edens, S. M. and Bernstein, J. (2015) 'Facts and fictions about polymorphism', *Chemical Society Reviews*, pp. 8619–8635. doi: 10.1039/c5cs00227c.

Dunitz, J. D. and Bernstein, J. (1995) 'Disappearing Polymorphs', *Accounts of Chemical Research*, 28(4), pp. 193–200. doi: 10.1021/ar00052a005.

Lemmerer, A. *et al.* (2009) 'Concomitant polymorphs of the antihyperlipoproteinemic bezafibrate', *Crystal Growth and Design*, 9(6), pp. 2646–2655. doi: 10.1021/cg8011298.

Matsuda, Y. and Tatsumi, E. (1990) 'Physicochemical characterization of furosemide modifications', *International Journal of Pharmaceutics*, 60(1), pp. 11–26. doi: 10.1016/0378-5173(90)90185-7.

Minkov, V. S. *et al.* (2014) 'Furosemide solvates: Can they serve as precursors to different polymorphs of furosemide?', *Crystal Growth and Design*, 14(2), pp. 513–522. doi: 10.1021/cg401257w.

Odounga Odounga, J. E. and Báthori, N. B. (2020) 'Systematic comparison of racemic and enantiopure multicomponent crystals of phenylsuccinic acid - The role of chirality', *CrystEngComm*, 22(12), pp. 2208–2218. doi: 10.1039/d0ce00072h.

Price, S. L. (2013) 'Why don't we find more polymorphs?', *Acta Crystallographica Section B: Structural Science, Crystal Engineering and Materials*, 69(4), pp. 313–328. doi: 10.1107/S2052519213018861.

Chapter 5

Bulk analysis of multicomponent crystals

In this chapter, the analysis of the bulk material of the five FUR MCCs will be discussed with the focus on the thermoanalytical results (TGA and DSC) and FTIR analysis. Original data are shown on individual figures and included in the Appendix.

5.1 Thermal analysis of the furosemide multicomponent crystals

Thermogravimetric analysis (TGA) and differential scanning calorimetry (DSC) were used to monitor the thermal behaviour of the five FUR MCCs. The TGA was used for determining the presence and the amount i.e. the API: solvent ratio of the MCC, and the DSC was employed to determine the melting temperatures and enthalpies of the MCCs. The results for the bulk material analysis are summarised in Table 5.1 and the individual TGA and DSC curves for the MCCs are presented in the Appendix (Figure A1-A10).

Table 5.1 Thermal analysis of FUR MCCs

	TGA					DSC		
	% Composition					Melting/Decomposition Process		
	Measured %	Theoretical %	Δ %	API:Sol ratio		Onset °C	Peak °C	ΔH J/mol
				TGA	SCXRD			
FUR·3PIC	22	22	0	1:1	1:1	1. 140.50 2. 214.73	1. 146.94 2. 216.37	1.14720 2.-9169
FUR·4PIC	18	22	4	1:0.8	1:1	1. 58.25 2. 135.31	1. 65.10 2. 143.11	1. 1744 2. 9383
FUR·23LUT	NA	24	NA	NA	1:1	1. 113.17 2. 154.35	1. 127.67 2. 161.00	1. 6185 2. 14780
FUR·24LUTw	NA	27.5	NA	NA	1:1:1	1. 139.53 2. 211.20	1. 146.77 2. 218.94	1. 13939 2. -28199
FUR·PYRw	22	22	0	1:1:1	1:1:1	1. 76.87 2. 123.69 3. 222.21	1. 88.50 2. 141.33 3. 222.83	1. 4410 2. 10009 3. -21443

The melting temperature of furosemide depends on the polymorphic form. Based on the PXRD analysis, in this work, form I was used as the starting material for the experiments. The DSC analysis of FUR (Fig. 5.1) shows an endotherm around 136-139°C, the 'melting of the crystals' expected to happen around 218°C and followed by the degradation (218-227°C) (Doherty & York, 1988). It is interesting to note that the so-called melting process is followed by a ca. 2.73 % mass loss on the TGA analysis (see Appendix for TGA figures). Beyers *et al*. conclude that the reason for this is the decomposition of FUR to saluamine, a byproduct (Beyers *et al*., 2000), while in a

more recent work, da Cássia da Silva (De Cássia Da Silva *et al*., 2013) proved that this step reflects the dimerisation of two molecules of FUR via condensation reaction, and the second larger endotherm represent the decomposition of the dimers into robust and other smaller compounds.

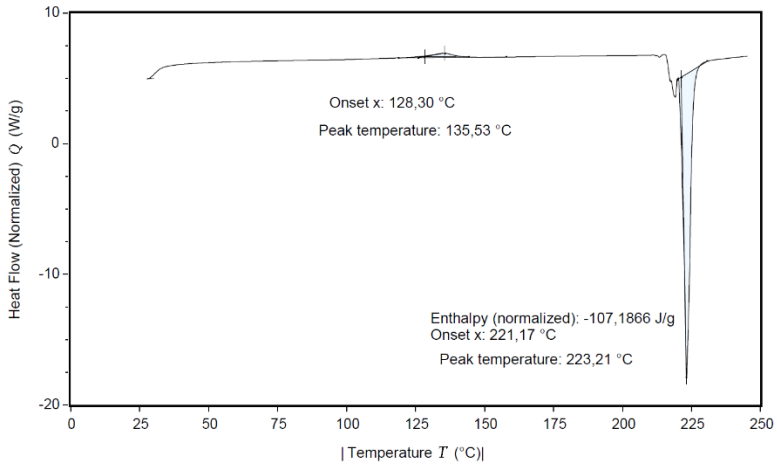

Figure 5.1 DSC analysis of the starting material furosemide

FUR·3PIC crystals are roboust under ambient conditions and thermally stable below ca. 100°C. (This was noted in Chapter 4, too.) The 22 % one-step mass loss between 100-200°C represents the complete desolvation of the 1:1 crystals, and the small, ca. 3% mass loss related to the decomposition of FUR to saluamine, is also noted around 218°C. FUR·4PIC crystals started to desolvate by the time the TGA analysis was carried out and this explains the 4 % difference between the measured and the theoretical mass loss related to the desolvation step. The desolvation and the thermal decomposition of the FUR·23LUT and the FUR·24LUTw crystals are complex and the steps related to the desolvation cannot be clearly identified.

Crystals of FUR·23LUT go through a congruent melting process, when the composition of the melt (liquid) is the same as the composition of the solid, and thus there is no distinguishable step on the TGA curve that can be related undoubtedly to the release of the solvent molecule. (Parallel to this, the DSC curve shows two endotherms that are related to the desolvation process.) The desolvation of FUR·PYRw crystals is a two-step process and the 22 % measured mass loss represents well—in agreement with the theoretical value—the complete desolvation of the crystals below 150°C. The decomposition of FUR to saluamine is also clearly noticeable around 218°C. These observations are clearly reflected on the DSC curve, in what the first endotherm is

related to the dehydration (loss of water) step, the second endotherm represents the desolvation (loss of PYR) process, followed by the decomposition of FUR.

5.2 Infrared spectrometry of the furosemide multicomponent crystals

The formation of new crystal structures of furosemide or in combination with coformers were investigated by examining the functional moieties on these molecules using Fourier transform infrared (FTIR) specrometry. The changes in bond-frequencies related to three functional groups—sulfonamide, carboxylic acid and secondary amine—with the potential of forming hydrogen bonds with complementary coformers were investigated. The O-H streching of a carboxylic acid appears around 3300-2500 cm^{-1}, centred around 3000 cm^{-1}, and the O-H bending can be noted around 1440-1395 cm^{-1}. The N-H stretching of a secondary amine (-NH) is noted in the region of 3350-3310 cm^{-1}, while the range for the primary amine ($-NH_2$) is 3500-3300 cm^{-1} with the asymmetric stretching observed at a higher wavenumber. The in plane bending of the secondary amine group appears around 1650-1580 cm^{-1}, and the scissoring of the NH_2 can be depicted around 1560 cm^{-1}. The stretching of the C=O group in a monomer carboxylic acid typically appears at 1760 cm^{-1} but if the acid is in a dimer form, this will shift to 1720-1706 cm^{-1}, or even to lower values. The in plane bending of the C-O-H and the streching of the C-O bond appears at 1205 cm^{-1}. The asymmetric S=O streching is noted around 1370-1335 cm^{-1}, while the symmetric counterpart is noted at a much lower frequency (ca. 1140 cm^{-1}).

For a start, the FTIR spectrum of FUR was recorded and the depicted vibrational bands were identified according to Bolukbasi and Yilmaz (Bolukbasi & Yilmaz, 2012). The selected bond-frequency values of the MCCs were compared to the pure FUR spectrum (Tabel 4.2) and the most prominent bands were successfully identified. (The IR spectra for the MCCs are in the Appendix, Fig. A11-15.)

Table 5. 2 The IR peak regions of interest for FUR and MCCs.

Compounds	N–H (cm^{-1})	O–H (cm^{-1})	C=O (cm^{-1})	C–O (cm^{-1})	S=O (cm^{-1})
FUR	3395: -NH_2 stretch, 1564: -NH_2 scissoring 3350: >NH stretch 1593: >NH in plane bend	3281: O-H stretch 1408: O-H bend	1668	1241	1326: S=O asym. stretch 1140: S=O sym. stretch
FUR·3PIC	3311, 1572	3180	1665	1232	1326, 1140
FUR·4PIC	3408, 1553, 3211, 1606	3079	1496*	1232	1325, 1140
FUR·23LUT	3338, 1571, 1606	3215	1571*	1257	1327, 1140
FUR·24LUTw	3364, 1593	3211	1593*	1250	1334, 1140
FUR·PYRw	1564	3298	1616	1250	1339, 1140

*****carboxylate C-O, signal a deprotonated carboxylic acid group

In general, the formation of hydrogen bonds would shift the O-H and the N-H frequencies to lower wavenumbers. Similarly, the deprotonation of the carboxylic acid group, i.e. salt formation, would shift the wavenumber related to C=O bond to a lower value. The expected trend in the N-H / O-H vibrations is not easily noticeable from the wavenumbers of the MCCs. The reason for this can be the occasionally included extra water molecule, which has the potential to diminish this region of the spectra. Interestingly, the C=O band is shifted to lower values in FUR·4PIC, FUR·23LUT, FUR·24LUTw and FUR·PYRw, which represent the deprotonation of the carboxylic acid group and thus suggest the salt nature of these compounds. This observation validates the refinement of the single crystal structures of these compounds.

References

Beyers, H., Malan, S.F., Van Der Watt, J.G. & De Villiers, M.M. 2000. Structure-solubility relationship and thermal decomposition of furosemide. *Drug Development and Industrial Pharmacy*, 26(10): 1077–1083.

Bolukbasi, O. & Yilmaz, A. 2012. X-ray structure analysis and vibrational spectra of Furosemide. *Vibrational Spectroscopy*, 62: 42–49. http://dx.doi.org/10.1016/j.vibspec.2012.06.002.

De Cássia Da Silva, R., Semaan, F.S., Novák, C. & Cavalheiro, E.T.G. 2013. Thermal behavior of furosemide. *Journal of Thermal Analysis and Calorimetry*, 111(3): 1933–1937.

Doherty, C. & York, P. 1988. Frusemide crystal forms; solid state and physicochemical analyses. *International Journal of Pharmaceutics*, 47(1–3): 141–155.

Chapter 6

Summary and conclusion

The knowledge of the various solid forms in which a drug molecule can exist is critical for drug discovery, development and formulation. The supramolecular synthesis of new solid forms of a selected drug may lead to forms with improved physicochemical properties, thus multicomponent crystal formation is a frequently used technique for optimising the physicochemical properties of pharmaceutical compounds.

This work focuses on solid-state forms of furosemide (4-chloro-2-[(2-furanylmethyl)-amino]-5-sulfamoylbenzoic acid, FUR), a loop diuretic commonly used to treat oedema and heart congestion. FUR is classified as a BCS IV drug, presenting low solubility and permeability. Also, FUR is a polymorphic drug, with three known polymorphs best represented by FURSEM03, FURSEM14 and FURSEM16 structures in the Cambridge Structural Database: form I, form II, and form III, respectively. In this study, the starting material was identified as form I.

The purpose of this research was to determine whether furosemide can form stable multicomponent crystals with the coformers selected via the screening of the Cambridge Structural Database. It was found that the carboxylic acid/carboxylate···aromatic amine synthon has the highest occurrence (26%), followed by the synthon (20%) in what the carboxylic acid/carboxylate group hydrogen bonds to an aromatic amine and a primary amine. These results reasoned the selection of pyridine and its derivatives as possible coformers for FUR. Five multicomponent crystals of FUR were formed with pyridine and its derivatives (3-methyl pyridine or 3-picoline (3PIC), 4-methyl pyridine or 4-picoline (4PIC), 2,3-dimethyl pyridine or 2,3-lutidine (23LUT), and 2,4-dimethyl pyridine or 2,4-lutidine (24LUT)) via slow evaporation crystallisation method.

The crystals were analysed by single-crystal X-ray diffraction, powder X-ray diffraction, thermogravimetry, differential scanning calorimetry, and Fourier transform infrared spectrometry. The drug:coformer ratio was found to be 1:1 in all the single crystals and based on the protonation states of the components, the five crystals can be classified as a solvate (FUR·3PIC), true salts (FUR·4PIC and FUR·23LUT) or salt hydrates (FUR·24LUTw and FUR·PYRw). The thermogravimetry results verified the solvent content of the crystals, and the protonation state of the components was confirmed by the shifts of the relevant infrared bands. The structural analysis revealed the conformational flexibility of the FUR molecule.

Powder X-ray analysis of the bulk showed that the single crystal of FUR·3PIC and FUR·PYRw are good representations of the bulk material, while in the case of structures FUR·4PIC, FUR·23LUT and FUR·24LUTw the bulk is different, and this is very likely the result of the advanced desolvation of the material.

In the second section of the work, the five multicomponent crystals were desolvated at ambient temperature and pressure with the aim to produce polymorphs of FUR in their pure forms. The desolvation process was followed by powder X-ray analysis, and the XRD patterns were compared to the crystal structures of the known polymorphs. Interestingly, the desolvation of the selected solvates did not lead to any of the pure forms of the known polymorphs of FUR. The desolvation of FUR·4PIC resulted in the physical mixture of forms I and III, while desolvation of crystals of FUR·23LUT, FUR·24LUTw, and FUR·PYRw resulted in three new solid forms. The crystals of FUR·3PIC showed excellent stability over at least six months under ambient conditions. The complete identification of these new forms is a challenging task and will form the basis of a new project.

In conclusion, while it has been demonstrated that furosemide can form multicomponent crystals with the selected coformers, there is insufficient information to determine whether known or novel distinct polymorphs of FUR can be generated via these multicomponent crystals. Nonetheless, the directed formation of polymorphs of a given compound is still a challenge, and thus the experimental preparation of polymorphs remains a topic of interest in materials science, with each drug posing a new challenge.

APPENDICES

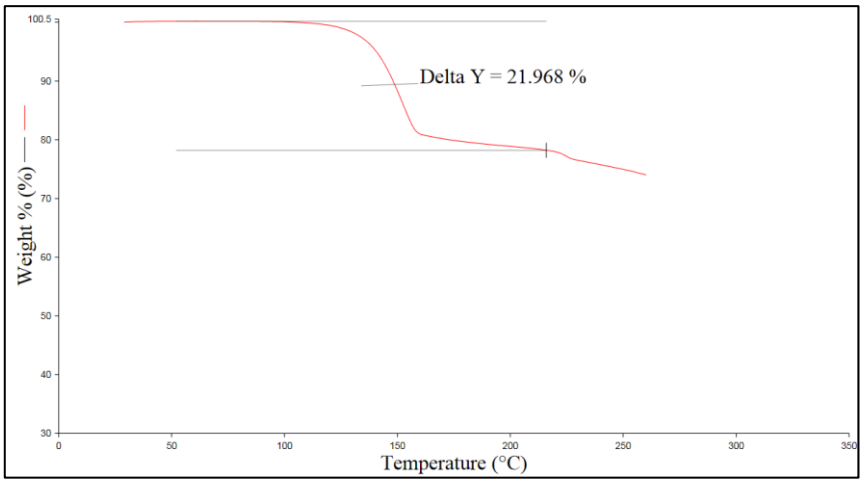

Figure A 1 TGA analysis of FUR·3PIC

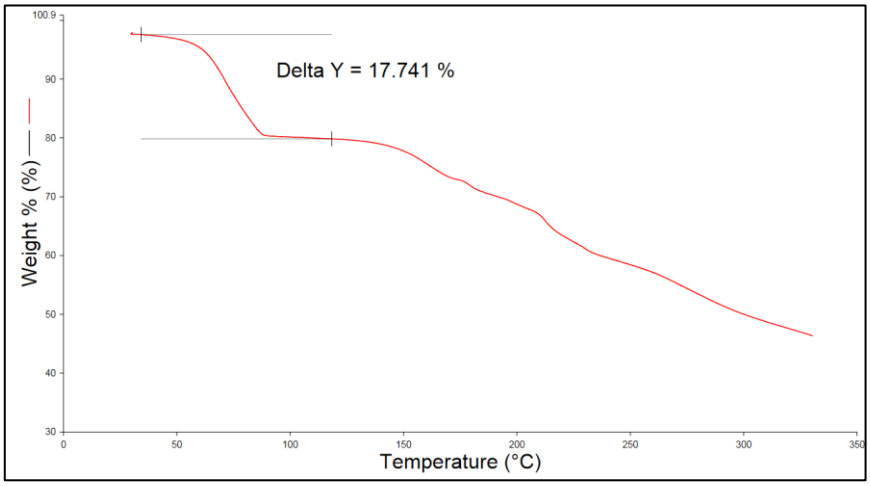

Figure A 2 TGA analysis of FUR·4PIC

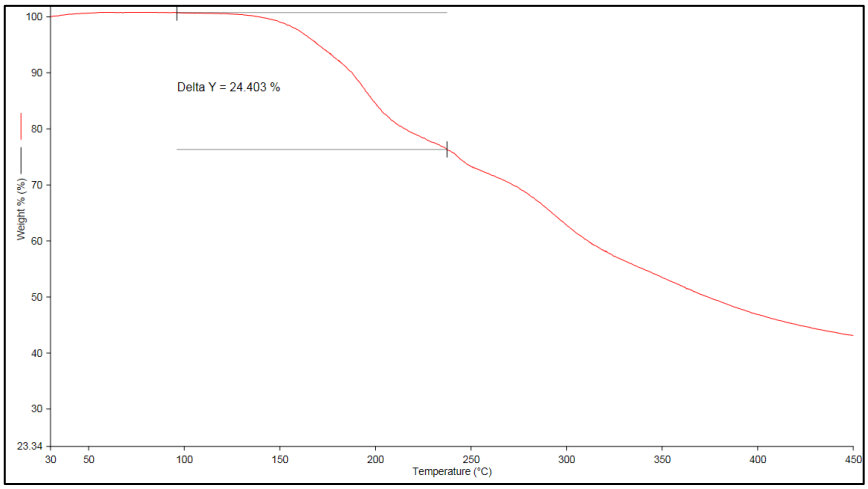

Figure A 3 TGA analysis of FUR·23LUT

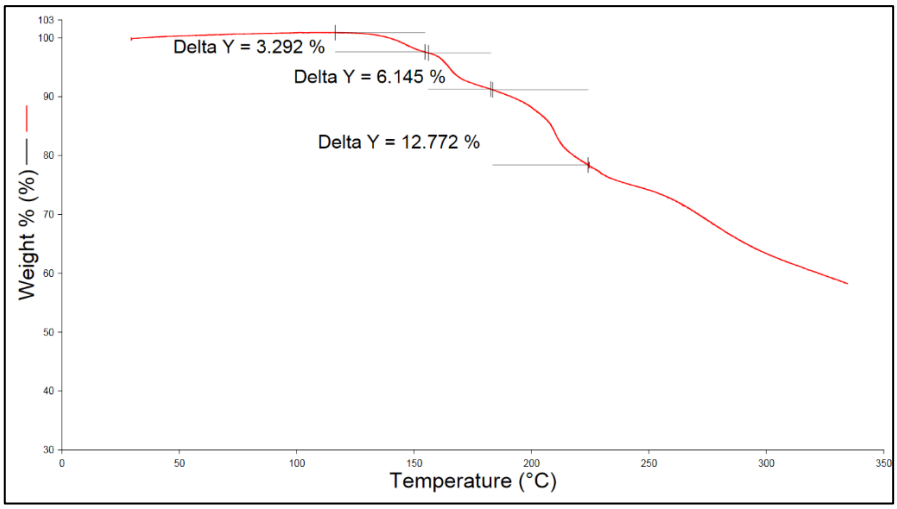

Figure A 4 TGA analysis of FUR·24LUTw

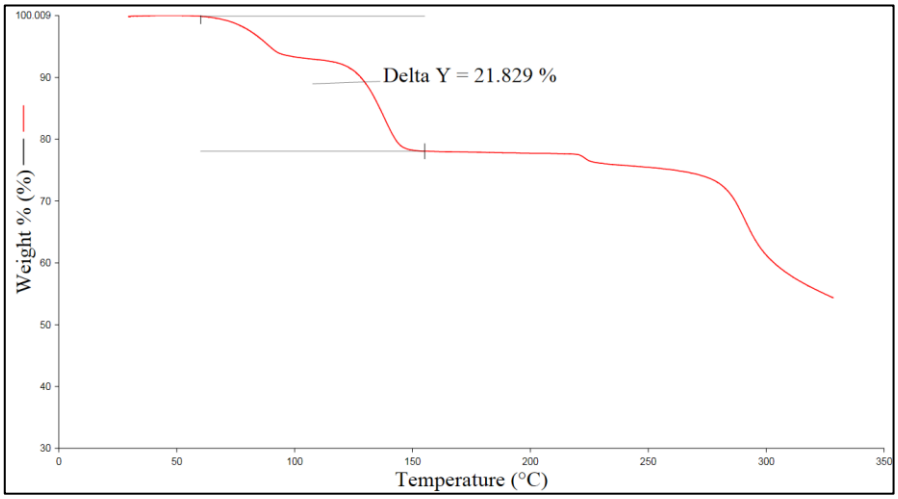

Figure A 5 TGA analysis of FUR·PYRw

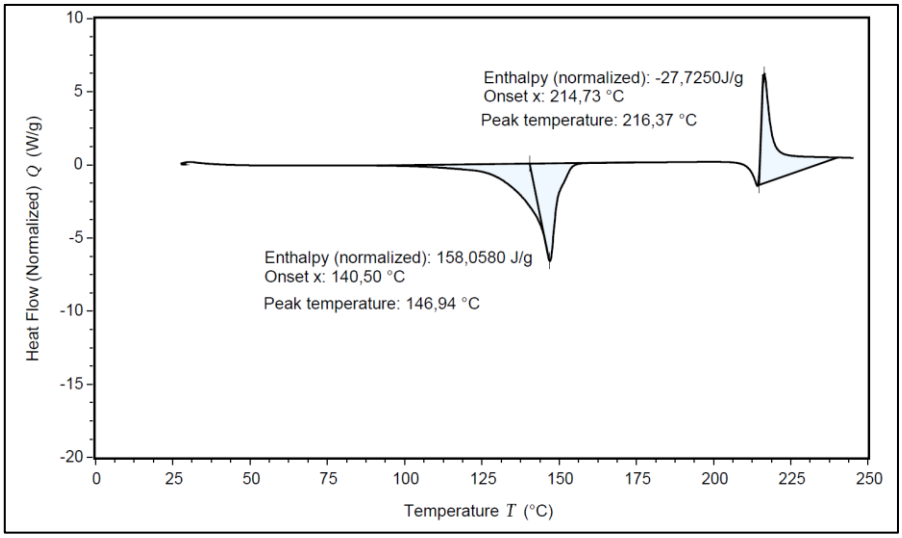

Figure A 6 DSC analysis of FUR·3PIC

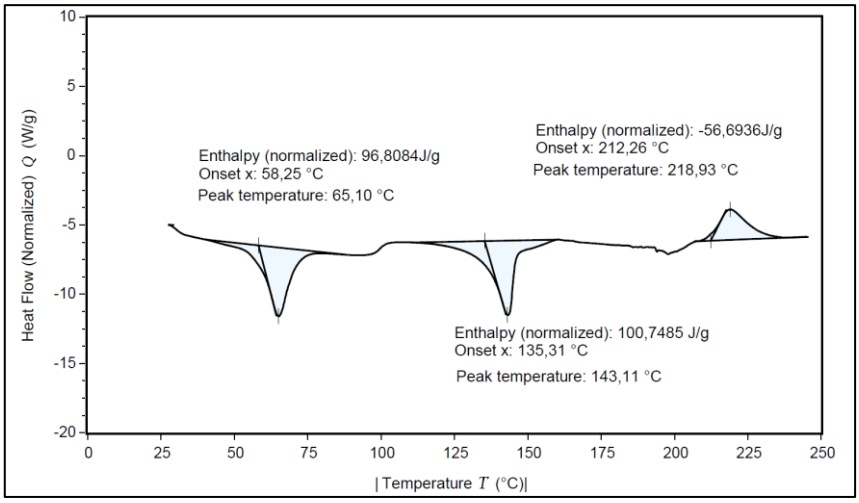

Figure A 7 DSC analysis of FUR·4PIC

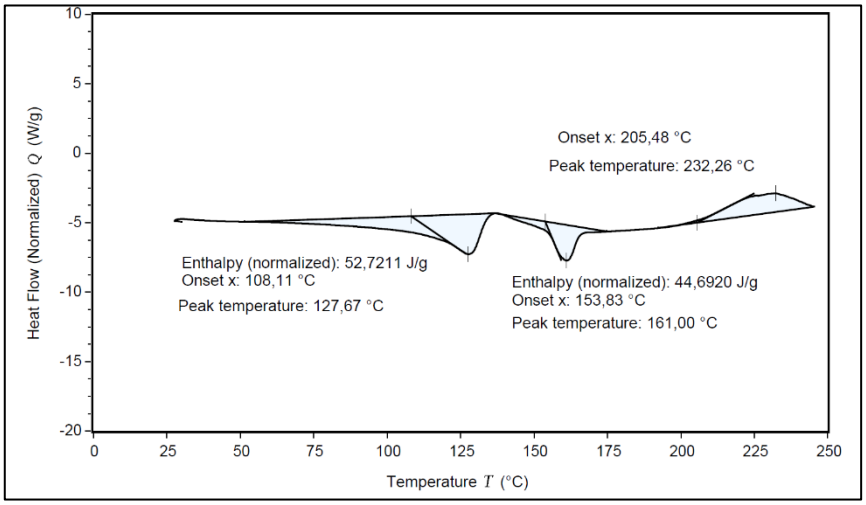

Figure A 8 DSC analysis of FUR·23LUT

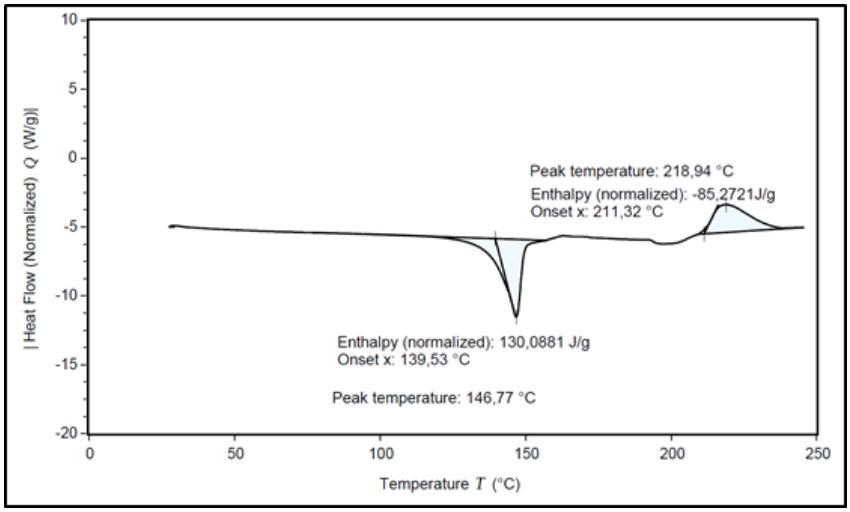

Figure A 9 DSC analysis of FUR·24LUTw

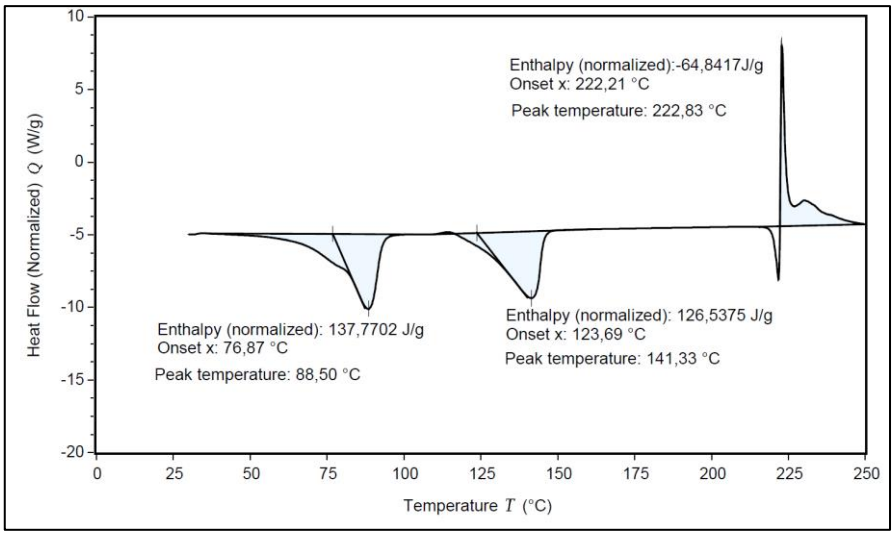

Figure A 10 DSC analysis of FUR·PYRw

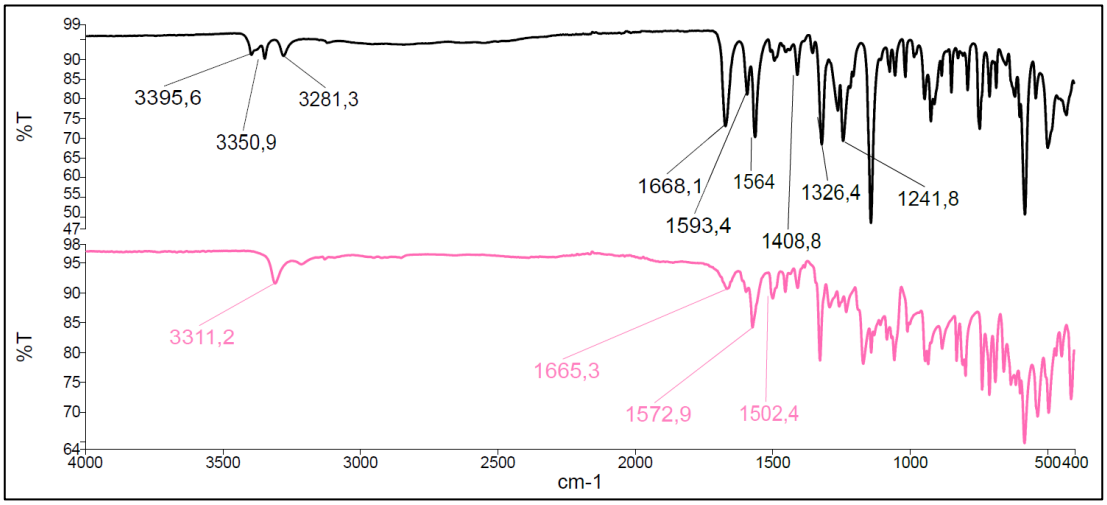

Figure A 11 FTIR spectra of FUR (black) and FUR·3PIC (magenta)

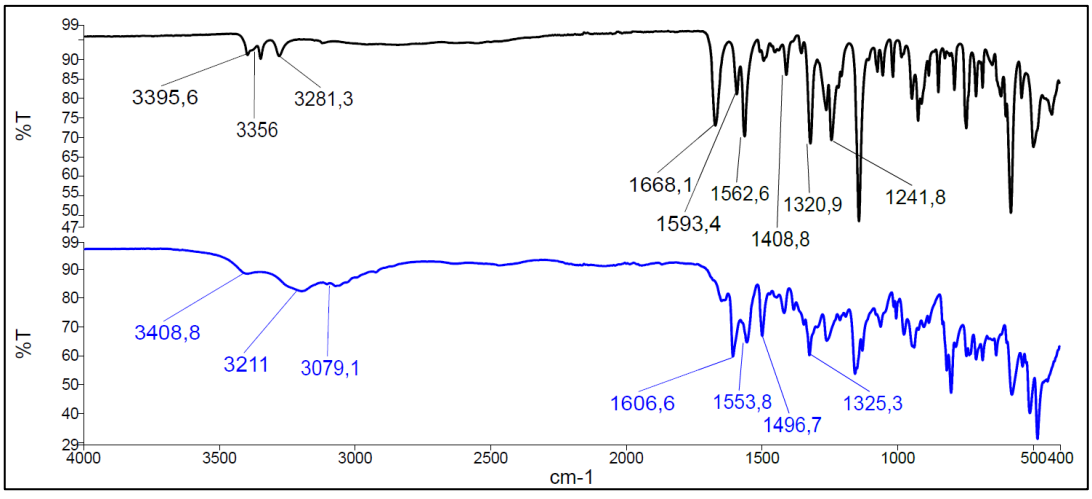

Figure A 12 FTIR spectra of FUR (black) and FUR·4PIC (blue)

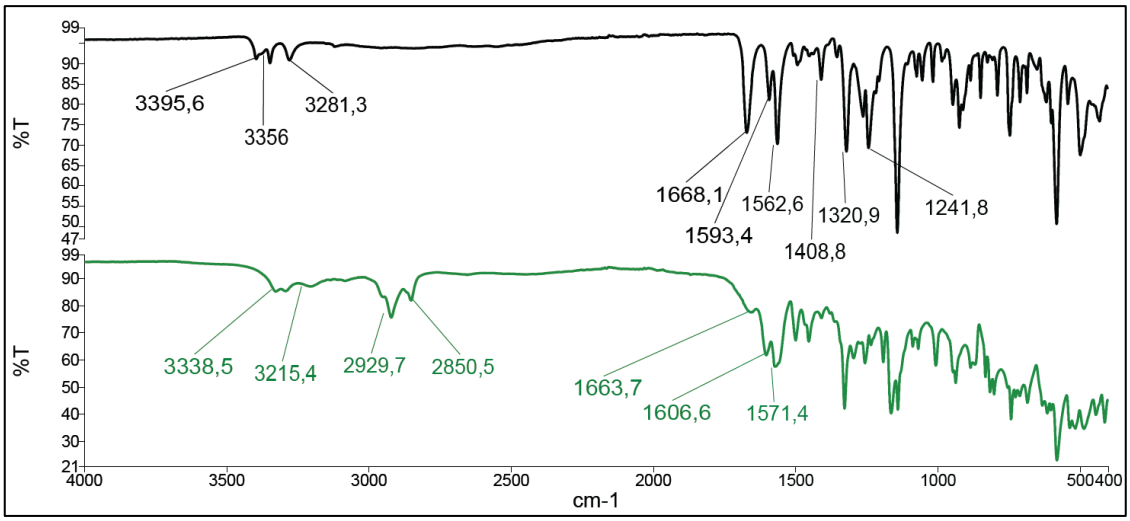

Figure A 13 FTIR spectra of FUR (black) and FUR·23LUT (green)

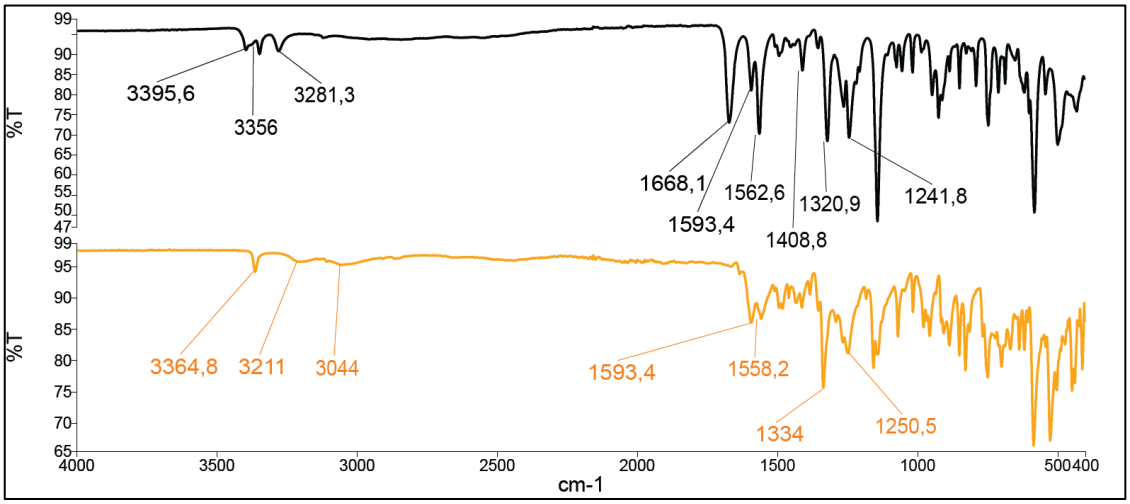

Figure A 14 FTIR spectra of FUR (black) and FUR·24LUT (yellow)

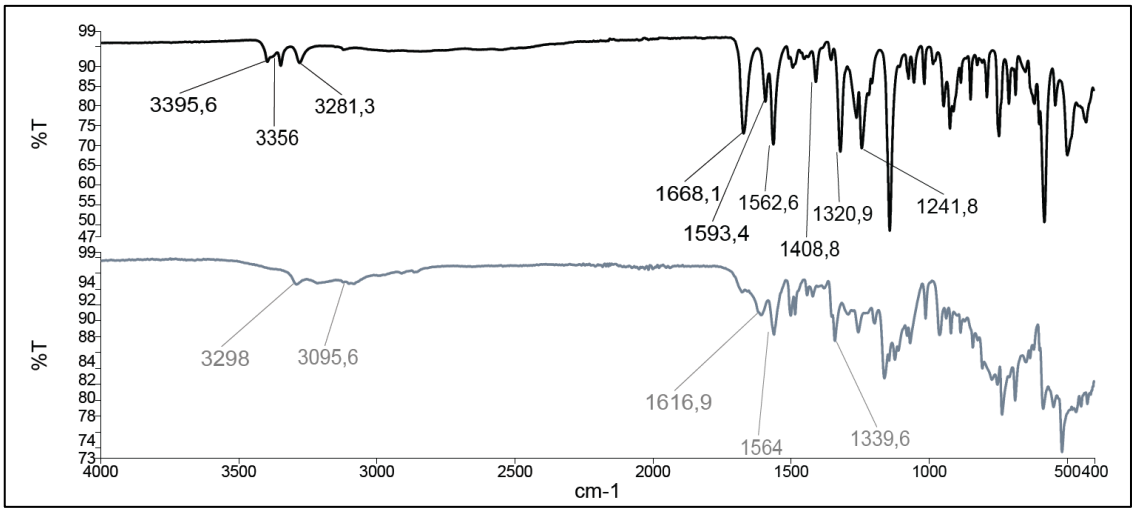

Figure A 15 FTIR spectra of FUR (black) and FUR·PYRw (grey)